

# Updating the Crustal Fault Model for the 2023 National Seismic Hazard Model for Alaska

Peter J Haeussler<sup>1</sup>, Adrian M Bender<sup>1</sup>, Peter M Powers<sup>2</sup>, Rich D Koehler<sup>3</sup>, and Daniel S Brothers<sup>2</sup>

<sup>1</sup>Affiliation not available

<sup>2</sup>U.S. Geological Survey

<sup>3</sup>Nevada Bureau of Mines and Geology, University of Nevada

November 14, 2023

# Updating the Crustal Fault Model for the 2023 National Seismic Hazard Model for Alaska

**Peter J. Haeussler<sup>1</sup>, Adrian M. Bender<sup>1</sup>, Peter M. Powers<sup>2</sup>, Rich D. Koehler<sup>3</sup>, Daniel S. Brothers<sup>4</sup>**

<sup>1</sup>U.S. Geological Survey, Anchorage, Alaska, USA

<sup>2</sup>U.S. Geological Survey, Golden, Colorado, USA

<sup>3</sup>Nevada Bureau of Mines and Geology, University of Nevada, Reno, Nevada, USA

<sup>4</sup>U.S. Geological Survey, Santa Cruz, California, USA

## **Abstract**

We present the crustal fault model for Alaska, based on geologic observations, as a primary input for the 2023 revision of the U.S. Geological Survey National Seismic Hazard Model (NSHM). We update the 2013 Alaska Quaternary fault and fold database (Koehler, 2013) with subsequent findings to produce a simplified model of 105 fault sections and four fault zone polygons with basic geologic parameters including slip sense and rate. Significant updates from prior maps include: 1) A slip rate of ~53 mm/yr on the Queen Charlotte Fault system indicating it accommodates all of the plate boundary motion. 2) Quantified long-term slip rates on megathrust splay faults in the southern Prince William Sound region and near Kodiak Island. 3) Improved details of structures in the Chugach-St. Elias orogen. 4) Revised characterization of Castle Mountain Fault from right-lateral slip to a predominantly reverse fault. 5) Improved Interior Alaska tectonic models that clarify relationships between the Denali Fault, Totschunda Fault, and thrust faults on both sides of the Alaska Range. 6) Identified large earthquake sources in the eastern Brooks Range. 7) Omission of the Chatham Strait section of the Denali Fault. We also describe the growing body of Alaskan lacustrine paleoseismic records of strong shaking, which may offer a test of ground motion recurrence predicted by the 2023 NSHM for crustal, megathrust, and intraslab events. The fault model underscores that the collision of the Yakutat microplate is the dominant driver of active crustal faulting in most of Alaska.

## 1 Introduction

The goal of this paper is to document updates to the crustal fault source model for Alaska in the 2023 National Seismic Hazard Model (NSHM). The previous seismic hazard model of Alaska was published in 2007 (Wesson et al., 2007) after the 2002 M7.9 Denali Fault earthquake (Eberhart-Phillips et al., 2003), and it included substantial improvements in geologic characterization over the prior 1999 model (Wesson et al., 1999) in central interior Alaska, the urban corridor of Anchorage to Fairbanks, and the Cook Inlet region. Since then, Koehler et al. (2012; Koehler, 2013) produced a statewide Quaternary fault and fold database for Alaska, which followed an earlier compilation of Plafker et al. (1994). Koehler & Carver (2018) also published an overview of seismic hazards research in Alaska and pointed to where additional work might be focused. These studies set the stage, and were vital resources, for this paper.

Here, we describe geologically constrained updates to crustal fault parameters that underpin the 2023 NSHM for Alaska. Fault parameters include fault geometry (i.e., length, rake, dip) and slip rate. We use previously published offsets of landforms or strata and geochronology to estimate slip rates and fault characteristics. This paper provides an updated overview of the progress in understanding Alaska's active crustal faults since the last hazard map (Wesson et al., 2007), and in numerous publications including the database of Koehler et al. (2012) and in Koehler and Carver (2018). Research in the last decade has substantially improved the understanding of past earthquakes along major plate bounding faults, including the Alaska-Aleutian megathrust. In this volume, Briggs et al. (2023) address geologic and geodetic inputs that update the megathrust fault parameters in the 2023 NSHM, but do not discuss megathrust forearc or splay faults, intraslab earthquakes, or crustal faults on-land that we discuss in this paper. Moreover, in this paper, we discuss geologic evidence for the frequency of intraslab earthquakes in southcentral Alaska, but they are not explicitly incorporated into the geologic sources.

## 2 Methods

We revised and updated the Alaska Quaternary fault and fold map of Koehler et al. (2012) based on subsequently published research and new fault trace mapping to generate the 2023 NSHM fault model for Alaska. Using available literature and published data, we added 88 mapped faults, updated fault dip and rake, refined geologic slip rates, and improved the location and/or resolution of previously mapped structures. In addition to assimilating independently published data, we also conducted original fault trace mapping where high-resolution digital elevation models (DEMs; the 2016 National Elevation Dataset 5-m IfSAR DEM (USGS, 2016), and the 2018 2-m Arctic DEM (Porter et al., 2018) offered the opportunity to improve the detail of known active faults, or, in some cases, identify previously unrecognized fault traces (Bender and Haeussler, 2021; Figure 1). This work was focused primarily on known active faults in the compilations of Koehler et al. (2012) and Plafker et al. (1994), and was not statewide and systematic. We use the USGS definition of active faults for the Quaternary fault and fold database as those with geologic evidence for coseismic surface deformation in Quaternary time (the past 2,588,000 years). These updates will be incorporated into the U.S. Geological Survey Quaternary fault and fold database of the United States (USGS, 2020) and inform a 2023 source model that includes 105 individual faults compared to 9 crustal faults of the prior source model (Wesson et al., 2007).

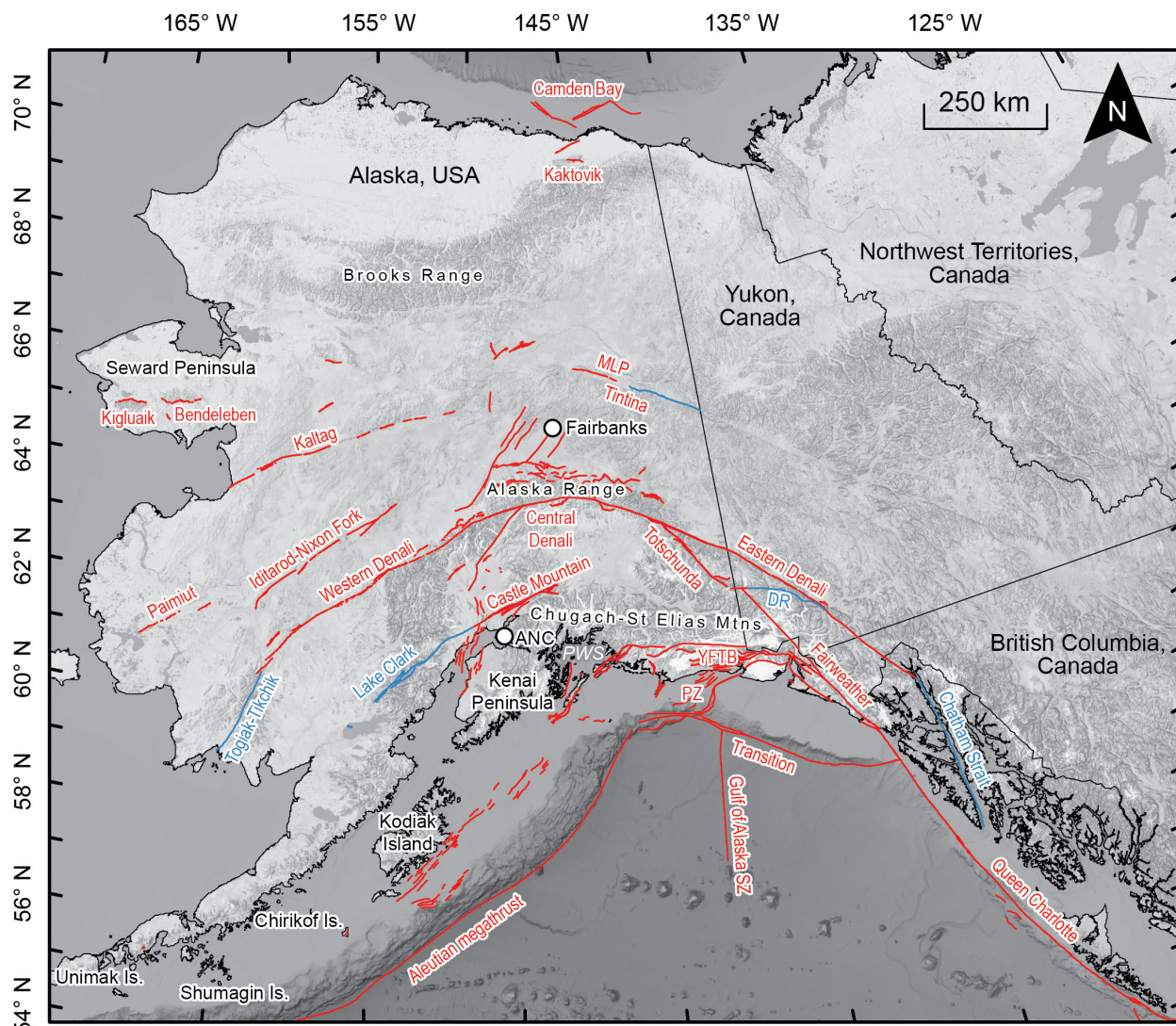


Figure 1: Quaternary faults and folds of Alaska (red lines and fault names) from Koehler et al. (2012) and Bender and Haeussler (2021) and updated based on sources described in this paper. Faults shown with blue lines and labels are those removed from prior compilations of active structures. White dots mark major Alaska cities (ANC—Anchorage). Abbreviated fault names: DR—Duke River, MLP—Medicine Lake-Preacher Fault, PZ—Pamplona deformation zone, YFTB—Yakataga fold-thrust belt, Gulf of Alaska SZ – Gulf of Alaska Seismic Zone. Base topography and bathymetry from GEBCO (2022).

The updated Alaska Quaternary fault and fold database was used to derive the geologic “fault sections” and polygonal “fault zones” developed for the 2023 NSHM (Figure 2; Table 1). The NSHM does not utilize detailed surficial fault traces, but rather simplified faults. We used ESRI ArcMap (version 10.8.1) software to simplify faults longer than 5 kilometers. Simplification involved reducing line vertex spacing to between 1 and 10 kilometers in order to preserve key strike changes while using as few vertices as possible with a maximum spacing approximately equivalent to half the thickness of Earth’s seismogenic crust (e.g., Figure 3). We omitted faults shorter than 5 km, and represented parallel and/or overlapping fault traces within 5 km as single fault traces. For faults and folds with published active deformation rates and

structural information, we attributed the fault section lines with these data. Elsewhere, we attributed the fault sections with categorical rate data in the Alaska Quaternary Fault and Fold Database of Koehler (2013). We assigned nominal rates of 0.01 to 0.1 mm/yr for hypothesized active faults for which there is no rate information. For those faults in the Alaska Quaternary fault and fold database that had a range of categorical slip rates, we chose the lower value as being the most conservative. For faults with otherwise unconstrained dip and rake, we assigned endmember values for thrust, normal, and strike-slip faults (thrust faults – 45° dip; normal faults – 60° dip; strike-slip faults – 90° dip (e.g. Twiss and Moores, 1994)). In four regions, we group seismic sources in “fault zone polygons,” which are zones of diffuse mapped faults or low-rate deformation based on the updated Alaska Quaternary fault and fold database. We decided to use these fault zone polygons where there are numerous active or potentially active and/or poorly characterized faults in a region, and where they were poorly characterized. We do not attach shortening rates or vectors across these regions. Instead, the goal of these is to encompass regions where active deformation is poorly quantified. In the hazard model, the zones can be assigned a moment rate derived from an estimate of the total geologic shortening or slip rates across the fault or faults for which the zone is a proxy or derived from inversion of the GPS velocity field. The fault sections, zones, and all related geologic inputs to the 2023 NSHM for Alaska are also described in Bender et al. (2021), a shortened version is shown in Table 1.

The geologic fault model does not explicitly address uncertainties in, for example, fault location, geometry, or slip rate. The maps on which we base this source model locates fault traces within 10<sup>1</sup>-meter accuracy. Line simplification, related to increased vertex spacing, reduces location accuracy but generally not beyond the 10<sup>1</sup> meter scale. As described above, when fault dip is not independently known from geological or geophysical studies, we assign common end-member fault dips of 90° to strike-slip faults, 60° to normal faults, and 45° to thrust faults.

Uncertainties in slip rates are generally inversely proportional to the slip rate. For example, the average slip rate Haeussler et al. (2017b) reported for 18 sites along the Denali Fault was 7.8 mm/yr and the average error was 1.7 mm/yr, or 21 percent. For 12 sections of the Queen Charlotte Fault, Brothers et al. (2020) data show an average slip rate 54.0 mm/yr and an average error of 7.2 mm/yr, or 13 percent. Another example is Bender et al. (2023) who found a slip rate of  $6.7 \pm 3.2$  mm/yr, or an error of 48 percent on a Northern Foothills thrust fault. However, for slow slip-rate faults where there is an absence of geologic information, we use slip-rate bin values of Koehler et al. (2012). Because we lack direct geologic constraint on these faults' slip rates, epistemic uncertainty prevails and it is not directly quantifiable. Moreover, the inferred low rates are intrinsically more sensitive to small but permissible variations. For example, the lowest rate bin we use (from Koehler et al. 2012, pg. 30) ranges from 0.01 to 0.2 mm/yr. When we use a slip rate derived from a previous rate bin, we arbitrarily use the lowest value. Acknowledging that the bin ranges are somewhat arbitrary for unknown slip rates, the lowest rate bin permits a 20-fold range in slip rates in accord with an equivalent high degree of rate uncertainty. We suggest that future NSHM fault models could be better constrained by fault-specific studies and evaluation of uncertainties.

### 3 Discussion of Active Faults by Region

In the following sections we summarize updates to our understanding of active upper-plate faults throughout the state of Alaska, including significant active offshore faults and folds (Figure 1). We first discuss megathrust splay faults and intraslab earthquakes, then the Queen Charlotte-Fairweather Fault system, faults in the Yakutat region, and the faults of interior Alaska. In some discussions, we estimate earthquake magnitude for a fault using the scaling relations of Shaw (2023). In discussing faults of each region, we aim to contrast geologic rates against modeled geodetic rates, if such data are available. The time span of geodetic models can be strongly influenced by, and reveal, changes during part of a single earthquake cycle, whereas geologic slip rates typically span many thousands to tens of thousands of years and thus reflect surface strain release across numerous earthquake cycles. The first satellite geodetic data for Alaska were acquired in about 1992; hence, the most complete Alaska geodetic time series incorporates ~30 years of data. Where possible, we compare fault section rates against fault rates from the statewide Alaska geodetic block model of Elliott and Freymueller (2020; Figure 4).

#### 3.1 Megathrust splay faults

We define megathrust splay faults as any forearc fault that connects with the subduction megathrust. In contrast, crustal faults may occur in the forearc region but do not connect with the subducting plate interface. Our understanding of splay faults along the Alaskan margin is best within the 1964 earthquake rupture area. Ruptures of the Patton Bay and the related Hanning Bay and Cape Cleare thrust faults (Figs. 1, 2, 5) during the 1964 earthquake are the first recognized examples of megathrust splay faulting (Plafker, 1967; 1969). Recent studies show this fault system has been active for more than 3 million years with rock uplift rates of up to 2 mm/yr (Ferguson et al., 2015). Rupture along the Patton Bay splay fault system appears to be consistent with a persistent asperity beneath Prince William Sound (Liberty et al., 2013; 2019). The fault system is located between two parts of the inner accretionary wedge, which had contrasting thermal histories, with faulting and exhumation driven by underplating along the plate interface (Haeussler et al. 2015). Tsunami modeling, bathymetry, and seismic profiling studies indicate that fault system surface rupture, differential uplift, and tsunami generation extended to the southwest from Montague Island, including rupture offshore the Kenai Peninsula (Figure 5; Plafker, 1969; Suleimani et al., 2010; Suleimani & Freymueller, 2020). Suleimani and Freymueller (2020) concluded the along-strike extent of 1964 splay faulting roughly matched the length of the Prince William Sound asperity.

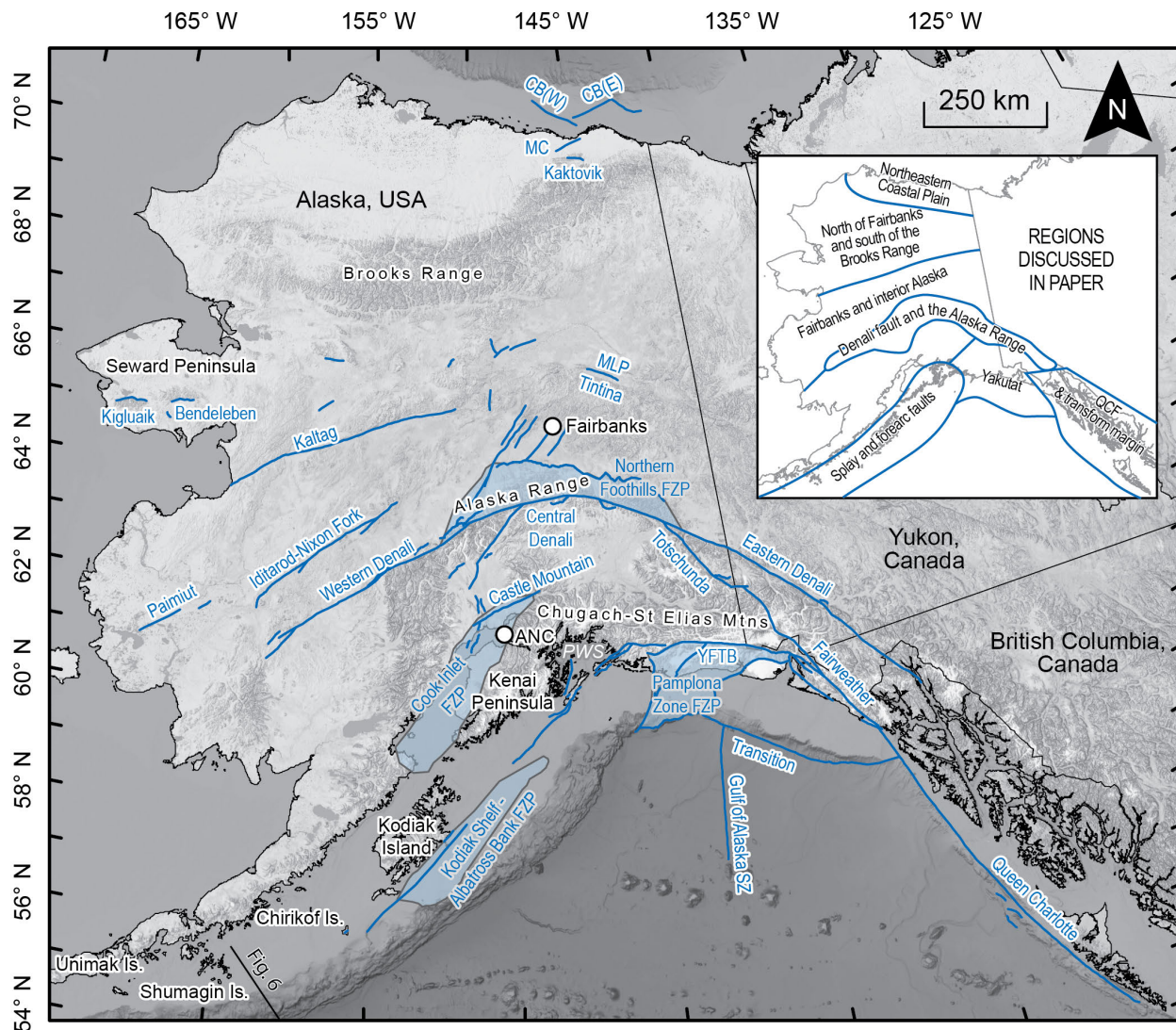


Figure 2: Fault sections and fault zone polygons of the 2023 NSHM update for Alaska. White dots mark major Alaska cities (ANC—Anchorage). FZP—Fault zone polygon. SZ—shear zone. Abbreviated fault names: CB(W,E)—Camden Bay West and East, K—Kaktovik, MC—Marsh Creek, MLP—Medicine Lake-Preacher. Base topography and bathymetry from GEBCO (2022). Inset shows geographic regions discussed in the text.

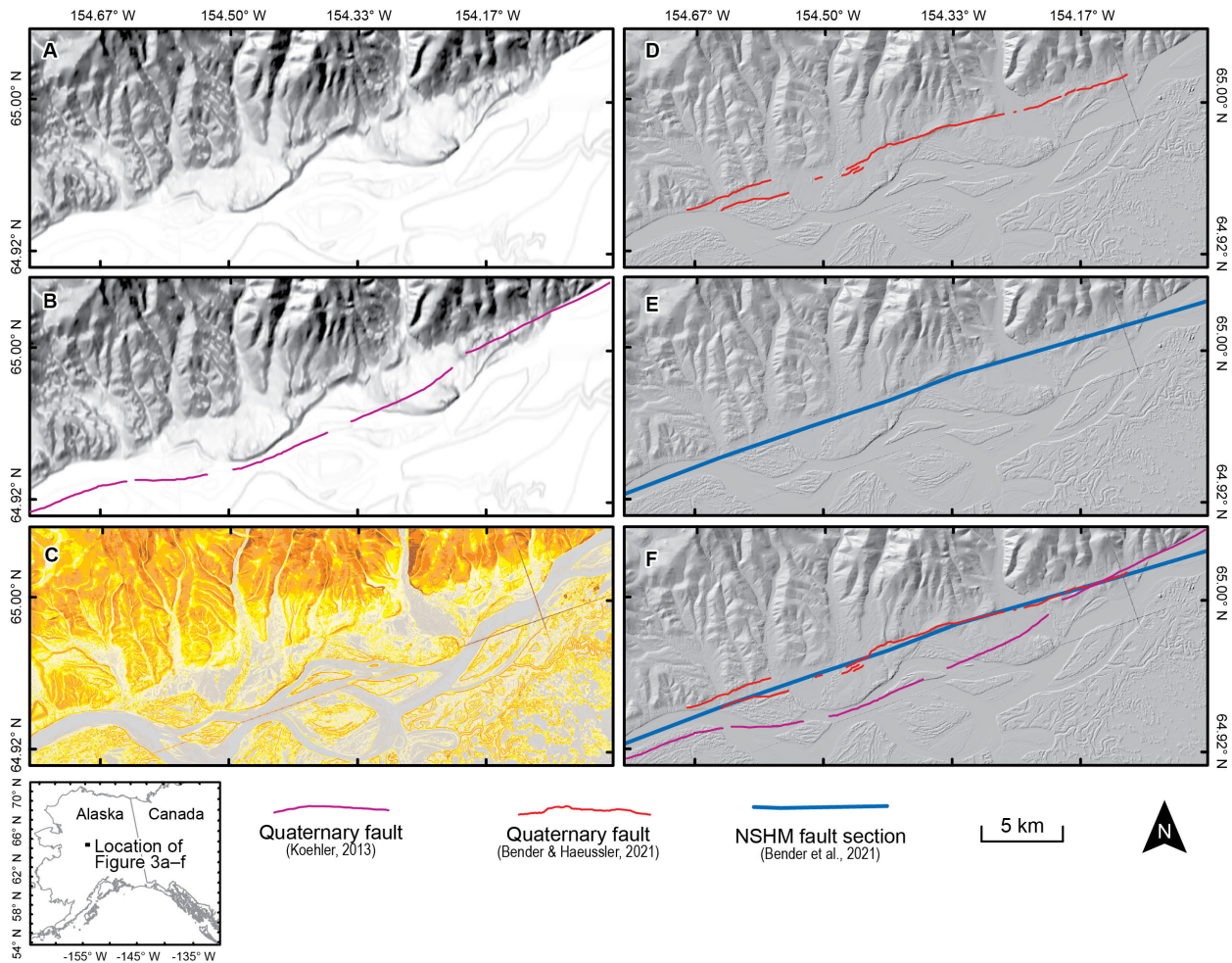


Figure 3. Example of fault mapping comparisons used to derive geologic fault sections for the 2023 NSHM along the Kaltag Fault. (a) Shaded relief rendering of 50-meter resolution National Elevation Dataset digital elevation model, which was the only statewide digital elevation model available for Alaska in 2013. (b) Same as panel (a) but overlain with fault mapping of Koehler (2013). (c) Slope rendering of the ~2 meter resolution ArcticDEM (Porter et al., 2018), which was used by Bender & Haeussler (2021) to refine locations of Alaska fault traces. Note there are some linear and orthogonal grid boundary artifacts in the ArcticDEM that may be mistaken with fault lineaments. (d) Hillshade rendering of the ~2 meter resolution ArcticDEM (Porter et al., 2018), overlain with fault trace mapping of Bender & Haeussler (2021). (e) Hillshade rendering of the ~2 meter resolution ArcticDEM (Porter et al., 2018), overlain with simplified Kaltag Fault section for the NSHM 2023 source model of Bender et al. (2021). (f) Hillshade rendering of the ~2 meter resolution ArcticDEM (Porter et al., 2018) overlain with fault mapping of Koehler (2013; magenta line), fault trace mapping of Bender & Haeussler (2021; red line), and Kaltag fault section for the NSHM 2023 source model of Bender et al. (2021; blue line).

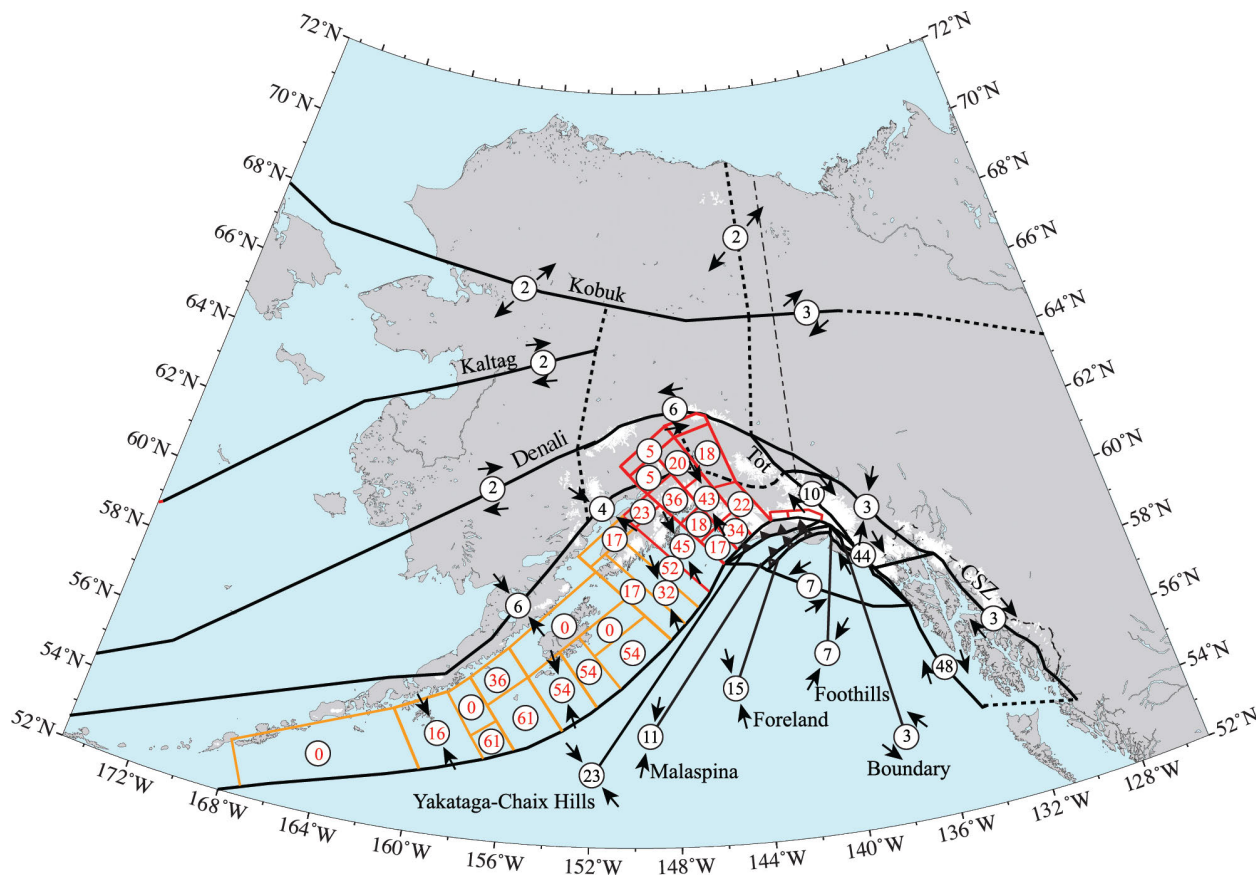


Figure 4. Map from Elliott & Freymueller (2020) showing their geodetic model predictions of relative motions along block bounding faults. Circles show predicted relative motion (mm/yr). Red numbers indicate that coupling ratios have been applied to relative motion estimates for the subduction segments. Arrows indicate overall direction of relative motion. Tot–Totschunda Fault, CSZ–Coast Shear Zone

For the 2023 NSHM we add the Patton Bay, Cape Cleare, Hanning Bay, and Montague Strait megathrust splay faults (Figure 5). For the Patton Bay and Cape Cleare faults, Liberty et al. (2019) estimated near-surface dips between  $40^\circ$  and  $72^\circ$  north from offshore seismic profiles. Given uncertain fault dip between the seafloor and the megathrust, we assign dips of  $45^\circ$  for these structures, and assign slip rates of 2 mm/yr based on the seismic reflection profiling of Liberty et al. (2019). We use the same  $45^\circ$  dip for the 10 km-long Hanning Bay Fault and assign a lower 0.2 mm/yr slip rate. Haeussler et al. (2017) identified the 72-km-long Montague Strait normal fault to the northwest of the Patton Bay Fault system, which dips  $61^\circ$  south in seismic reflection data and appears to facilitate hanging-wall extension associated with rapid exhumation of Montague Island. We assign the  $61^\circ$  dip of Haeussler et al. (2017) and a generic low slip rate of 0.2 mm/yr, which is approximately one tenth the exhumation rate inferred for Montague Island (2 mm/yr; Ferguson et al., 2015). Preliminary paleoseismic work on the Patton Bay splay fault system indicates these splays may not rupture in every megathrust event, but rather in every second or third earthquake (Witter et al., 2022).

The other two faults in the Prince William Sound region that appear to be splay faults are the poorly understood Rude River and Etches Faults (Figure 5A). Winkler and Plafker (1993)

mapped these faults in bedrock and speculated on their continuity in adjacent, strike-parallel valleys floored by active rivers, glaciers, or estuaries that might obscure the geomorphic expression of active or recent faulting. Koehler (2013) designated these northwest-dipping thrusts in the “Class B” age category, defining them as “suspicious features in which the age of the most recent earthquake is unknown but other evidence suggests the possibility that the structure may be active in Quaternary time.” Scarps mapped on the statewide DEMs support these faults’ existence and recent activity (Bender and Haeussler, 2021). The structural position of the faults mimics that of the nearby active Yakutat region faults (see Yakutat Region), which also supports their inclusion as potential seismic sources despite the lack of direct geologic rate or sub-surface geometric constraints. Hence, we incorporate the Cordova, and Etches Faults as 45° northwest-dipping thrusts with nominally low slip rates of 0.01 mm/yr (see Methods) as geologic inputs to the 2023 NSHM for Alaska. We assign a slip rate on the Rude River Fault of 0.2 mm/yr based on its longer length and because it is along strike from the Patton Bay Fault.

There are numerous young and potentially active faults offshore the Kenai Peninsula and Kodiak Island (see Figure 1, Ramos et al., 2022). Of all of these faults, only the on- and near-shore Narrow Cape Fault (Carver et al., 2008) and offshore Ugak Fault (Ramos et al., 2022) have had focused study (Figure 5a). Based on the geologic evidence, we assign a sinistral slip rate of 3.3 mm/yr for the Narrow Cape Fault (Carver et al., 2008) and a reverse fault slip rate of 1.3 mm/yr for the Ugak Fault (Ramos et al., 2022), both having 60°N-dipping fault planes. It is likely there was additional splay faulting in the 1964 earthquake on the Ugak Fault offshore Kodiak Island, or on faults along the Kodiak Shelf Fault Zone as well as near the edge of the shelf on the Albatross bank (see Figure 1; Ramos et al. 2022). Modeling of the 1964 earthquake tsunami by Suleimani and Freymueller (2020) is also consistent with a source on the Albatross bank. Other faults in the region of the Kodiak Shelf and Albatross Bank fault zones offset the sea floor (e.g. Thrasher, 1979), but appear to be lower rate features and are poorly characterized. In recognition of these numerous and poorly defined faults, we include a Kodiak Shelf-Albatross Bank fault zone polygon. A recurring question is, are these faults connected to the megathrust? For the faults that ruptured in the 1964 earthquake, their relationship to the subduction interface is clear. For others, particularly with limited length, the connection is not certain and it seems they have the potential to be independent seismic sources.

The one other known forearc normal fault is on Chirikof Island (Figure 5a). No studies have been undertaken on the fault, but it is about 9-km long, it is oriented parallel to the trench, dips north, and has a south-side-up ~5-m-high scarp, and by regional correlation the offset surface may be about 17,000 yrs old (Misarti et al., 2012), yielding a slip rate of about 0.5 mm/yr. We include this fault in the 2023 NSHM. These fault characteristics are similar to the fault found by Bécél et al. (2017). Additional mapping on Alaska’s shelves would likely lead to the discovery of additional structures.

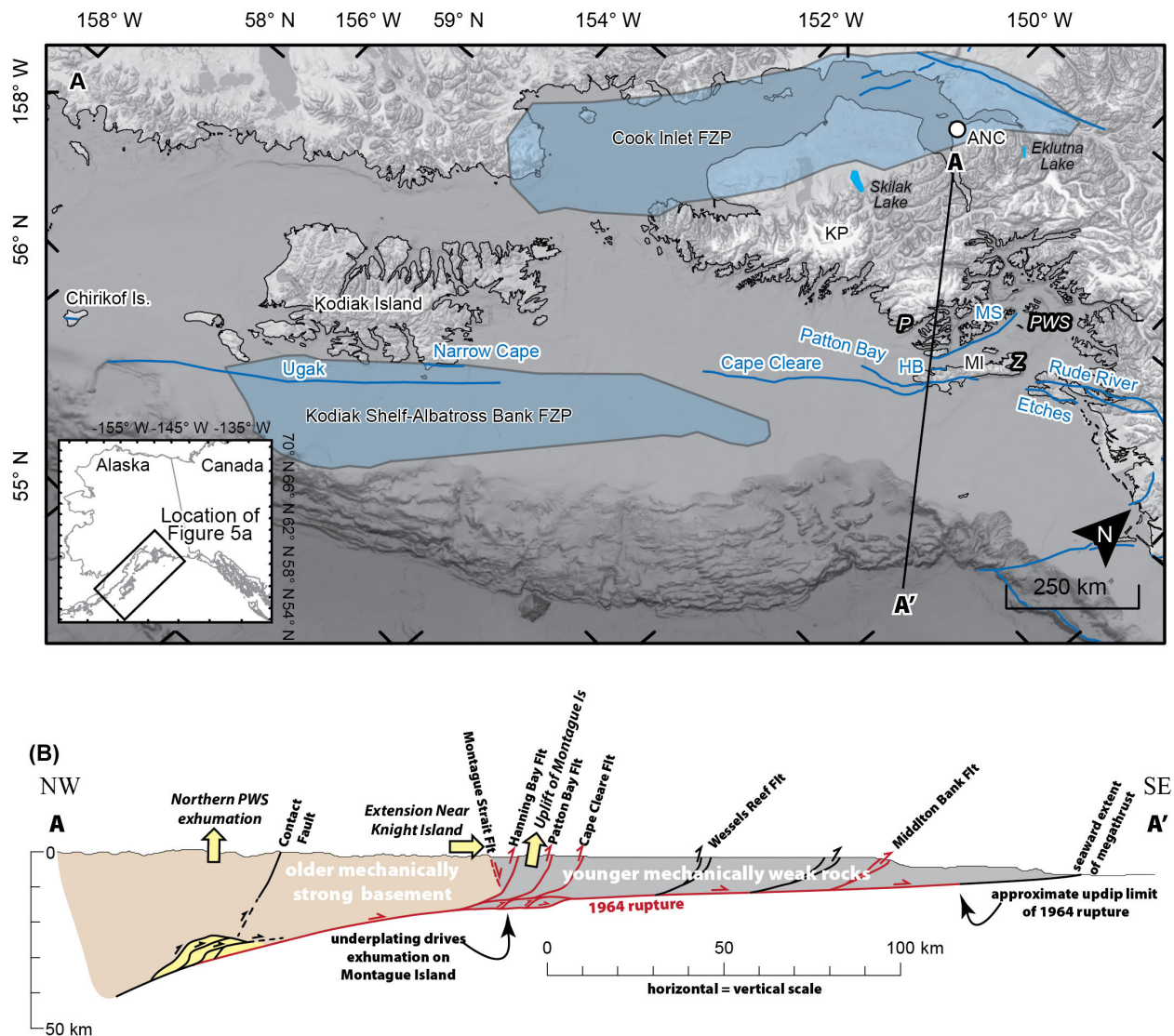


Figure 5. Fault sections, zones, and interpreted upper-plate structure in the greater Prince William Sound (PWS) region. (a) Topography and bathymetry from GEBCO (2022) overlain with fault sections (blue lines) and fault zone polygons of Bender et al. (2021). Fault section abbreviations: HB–Hanning Bay Fault, MS–Montague Strait Fault. Place name abbreviations: ANC–Anchorage (marked by white dot), KP–Kenai Peninsula, MI–Montague Island, PWS–Prince William Sound, P–Puget Bay, Z–Zaikof Bay. (b). Schematic cross section from the Alaska-Aleutian trench to the Kenai Peninsula highlighting splay faulting structures and exhumation, from Haeussler et al. (2015). See location on Figure A. Red lines show inferred extent of rupture in the 1964 earthquake based on aftershocks, surface faulting, geodesy, and Plafker’s (1969) interpretation. Underplated region beneath Montague Island is depicted as much thicker than it likely is for clarity. Note some of these faults are not shown on Figures 1 and 2.

### 3.1.1 Forearc faults not included in the 2023 NSHM

In addition to splay faults activated in the 1964 earthquake, other faults have been recognized in the forearc region, which are not sufficiently characterized for inclusion in the

2023 NSHM. Finn et al. (2015) identified several faults within Prince William Sound with relatively limited lateral extent, small offsets, and thus low slip rates, and the connection with the megathrust is not explicit. These structures were not included in the fault sections database. We identified a new fault trace in the bathymetry of Puget Bay as well as a linear scarp on Montague Island near Zaikof Bay that may be an active reverse fault (Figure 5a; Bender and Haeussler, 2021), but it is also less than 5 km long, and thus not included in the fault sections database.

Bécel et al. (2017) identified splay faults, or out-of-sequence thrust faults in the actively deforming outer wedge in the Shumagin Islands region. Von Huene et al. (2019; 2021) also identified a number of “backstop splay faults”, which are located near the boundary between the inner and outer wedges, and they traced these splay faults along strike for hundreds of kilometers. Given their position near the toe of the megathrust, we infer their rupture is associated with megathrust events, and they should not be considered a “crustal” source. Given their deep-water position, these splays have the potential to be significant tsunami producers, and Von Huene et al. (2019) invoked their rupture in the large tsunami associated with the 1949 Unimak Island earthquake.

Bécel et al. (2017) also discovered a normal splay fault east of the Shumagin Islands (Figure 1). The fault is located near the top of the slope, has two surface-rupturing strands, dips to the northwest, connects with the subduction interface, and bounds a late Cenozoic sedimentary basin. These features led to the interpretation that this normal-motion splay fault is long-lived. The largest of the two sea-bottom scarps has an offset of only 5 m, which indicates to us that this is not a high slip-rate feature. Assuming deglaciation of the region around 17 kya (see summary in Haeussler et al., 2021), this yields a slip rate of 0.3 mm/yr. Seismic profiles show an average dip of 32° through 28 km depth of the crust. Extensional features on convergent margins are common, as pointed out by von Huene et al. (2019; Figure 6). They interpret this normal fault, as well as the backstop splay faults, as being related to trenchward movement of a block at the southernmost part of the outer wedge (Figure 6). However, as the fault has unknown lateral extent, and its contribution to the hazard is likely dwarfed by the megathrust, we do not include it in the 2023 NSHM.

### 3.1.2 Summary of splay faults and forearc faults

Given this scattered state of knowledge of splay faults and forearc faults, we suggest the following for the Alaskan margin. (1) The only splay fault systems in the inner wedge are the Patton Bay Fault system, the Kodiak Shelf fault zone, and the Albatross Bank fault zone (Figure 5A). We include the specific faults in the fault sections database, and the larger Kodiak Shelf and Albatross Bank fault zones as a single fault zone polygon. (2) The backstop splay fault zone offshore and to the southwest of the Shumagin Islands may extend the entire length of the southern Alaskan margin as a system of discontinuous thrust faults in the outer wedge. This fault system should be considered a potential tsunami source, but given the lack of geologic evidence for a hazard and relatively high uncertainty, it appears to be an unlikely seismic source apart from a megathrust earthquake, and it would not change our considerations of ground motions from a megathrust event. We do not consider this as a separate seismic source in the 2023 NSHM. (3) The normal fault splay offshore the Shumagin Islands is likely not a significant tsunami or ground shaking hazard apart from triggering megathrust events, and we do not know its lateral extent, so we do not include it in the 2023 NSHM.

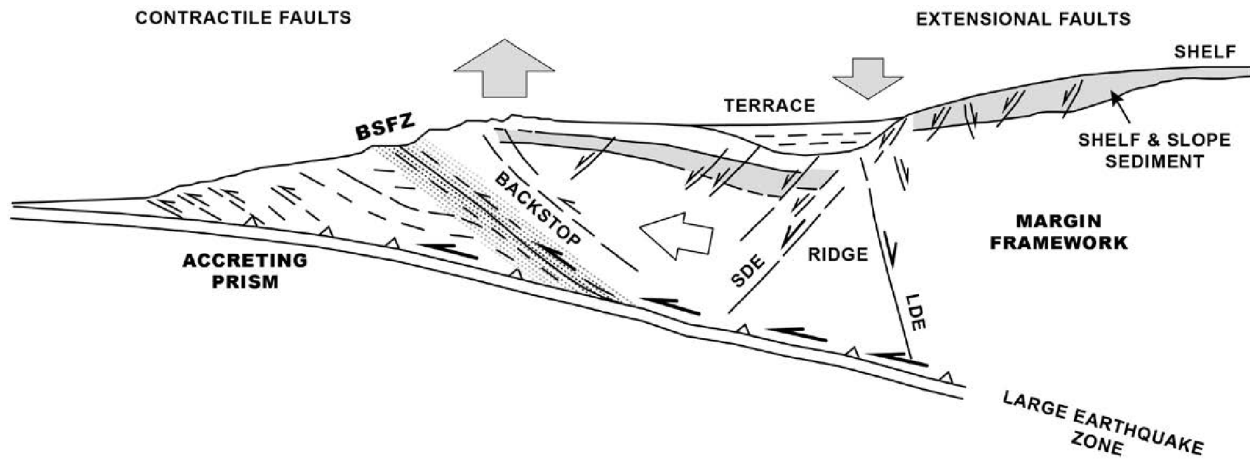


Figure 6. Diagram of structure offshore and southwest of the Shumagin Islands from von Huene et al. (2019). See Figure 2 for approximate location. Abbreviations: BSFZ – backstop splay fault zone; SDE – seaward-dipping extensional fault; LDE – landward-dipping extensional fault. The boundary between the inner and outer wedge here would be roughly at the LDE.

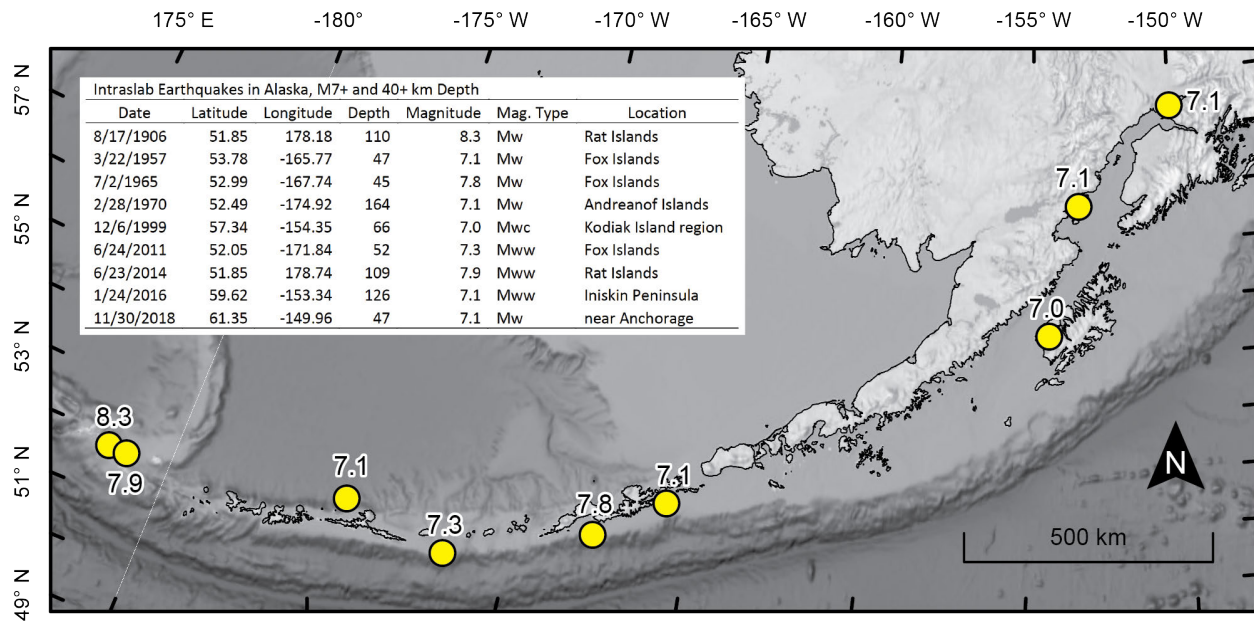


Figure 7. Large (M7+) intraslab earthquakes, deeper than 40 km, in Alaska recorded since 1900. Earthquakes from NEIC ComCat.

### 3.2 Intraslab Earthquakes

Intraslab earthquakes are a significant subduction zone seismic hazard along the southern Alaska margin, the most damaging of which was the 2018 M7.1 Anchorage earthquake (West et al., 2020). These earthquakes, which we loosely define as being within the subducting slab at  $\geq 40$  km depth (that is, below the base of the seismogenic crust), were included in the

2007 hazard model through the gridded and smoothed seismicity model. Since 2007 there have been four M7.0+ intraslab earthquakes in Alaska, and prior to that time there were five M7.0+ events in the earthquake catalog since 1900 (Figure 7).

We do not incorporate intraslab earthquake sources in our ‘crustal’ source model, however, a broader goal of this paper is to describe geologic constraints on earthquake occurrence. The growing field of lacustrine paleoseismology (e.g. Moernaut et al., 2014; De Batiste et al., 2017) is now providing records valuable for interpreting the frequency of intraslab earthquakes in Alaska. Lacustrine paleoseismology utilizes the frequency of distinctive turbidites as a proxy for strong ground shaking, and are sensitive to ground motions triggered by crustal, megathrust, and intraslab events (Vandekerckove et al., 2020; Praet et al., 2020). The 2018 M7.1 Anchorage earthquake provided an ideal case study of the lacustrine record of a large intraslab event. In the region around the epicenter, there was little surficial evidence of the earthquake. A few landslides and some locations with sand blows and liquefaction were observed (West et al., 2020). However, an earthquake-triggered turbidite was deposited at Eklutna Lake in the epicentral region (Figure 5A; Van Daele et al., 2019). Fortuitously, Eklutna Lake had been a focus site for lacustrine paleoseismology research prior to the 2018 earthquake (Praet et al., 2017; Fortin et al., 2019; Vandekerckhove et al., 2020; Praet et al., 2020), and the work suggests an earthquake-triggered deposit occurred every 94 years on average during the last 2250 years (Figure 8). This is far more frequent than the recurrence of the largest megathrust earthquakes, which averages to every ~600 years in intertidal records above the Prince William Sound region (Carver and Plafker, 2008; Shennan et al., 2014). Praet et al. (2022) also described earthquake recurrence based on sediments in Skilak Lake (Figure 5A), on the Kenai Peninsula, and found 18-20 earthquakes in the last 2300 years, indicating an average recurrence of 115-128 years. Singleton et al. (2022) find evidence that Modified Mercalli shaking intensities of at least  $V\frac{1}{2}$  were needed to induce deposition of a turbidite during the 2018 Anchorage earthquake. Therefore, using ground motion intensity conversion equations (Caprio et al., 2015), recurrence rates of intraslab earthquakes in the 2023 NSHM could be checked for consistency with the Eklutna and Skilak lake data. As lacustrine paleoseismic research continues, it may provide useful data to complement and possibly test peak ground acceleration, shaking intensity and recurrence forecasts by future NSHMs.

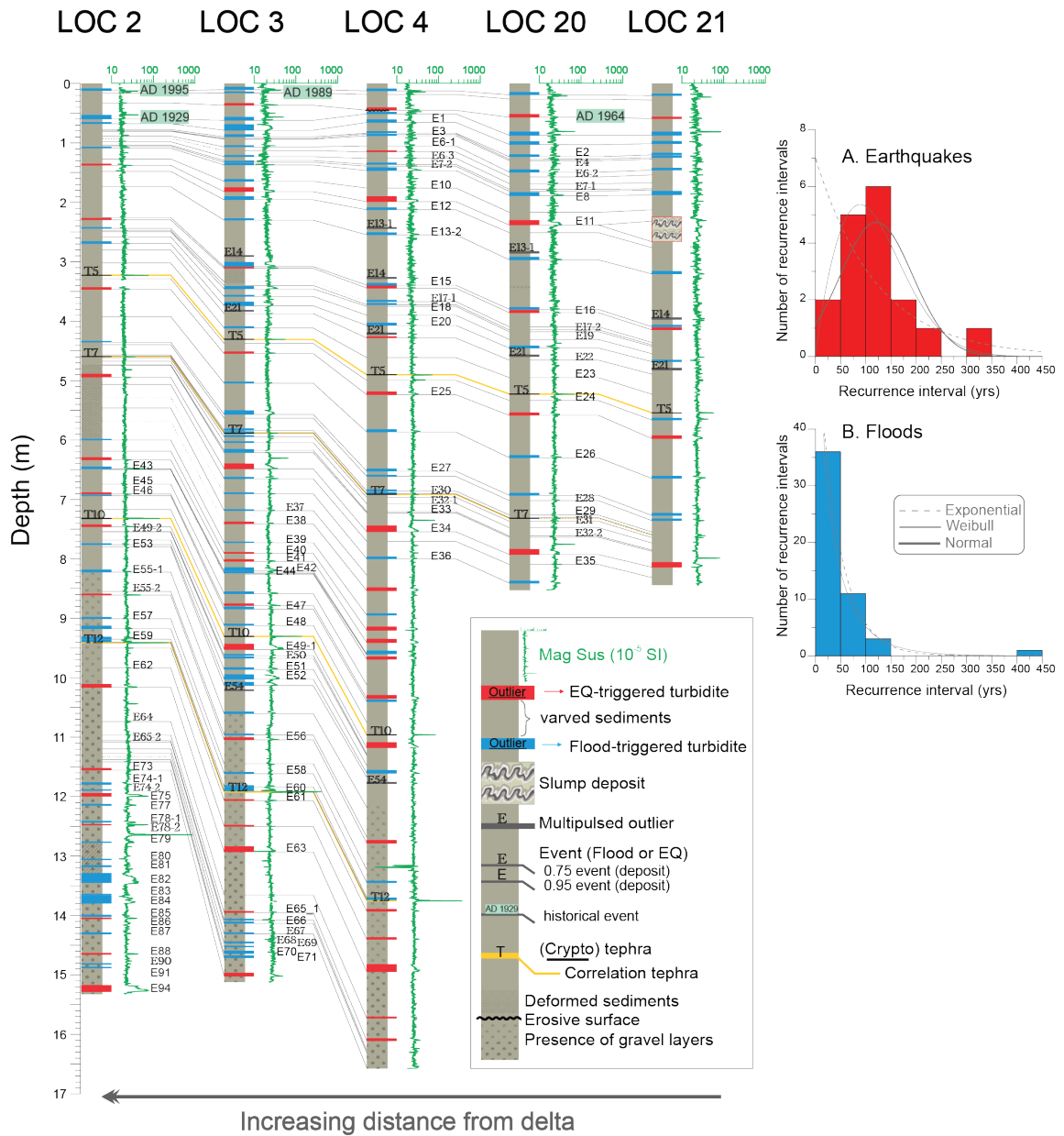


Figure 8. Stratigraphic correlations of turbidites in cores from Eklutna Lake (Figure 5A) from Praet et al. (2020). See their paper for methods of discriminating earthquake and flood turbidites. Core locations shown with increasing distance from a delta (from right to left) and were deposited in the last 2250 years. Turbidites related to historical events in AD 1995, 1989 and 1964 are included in the stratigraphy (Boes et al., 2018; Vandekerkhove et al., 2019). Magnetic susceptibility (MS) peaks pinpoint the presence of (crypto) tephtras T5, T7, T10 and T12 (Fortin et al., 2019). Histograms at right show the frequency of (A) earthquake and (B) floods based on analysis of Praet et al. (2020, figure 11). They note the occurrence of earthquakes fits a Weibull

distribution whereas the occurrence of floods corresponds with an exponential distribution. Part A shows the recurrence for earthquakes recorded in the lake is about 100 years.

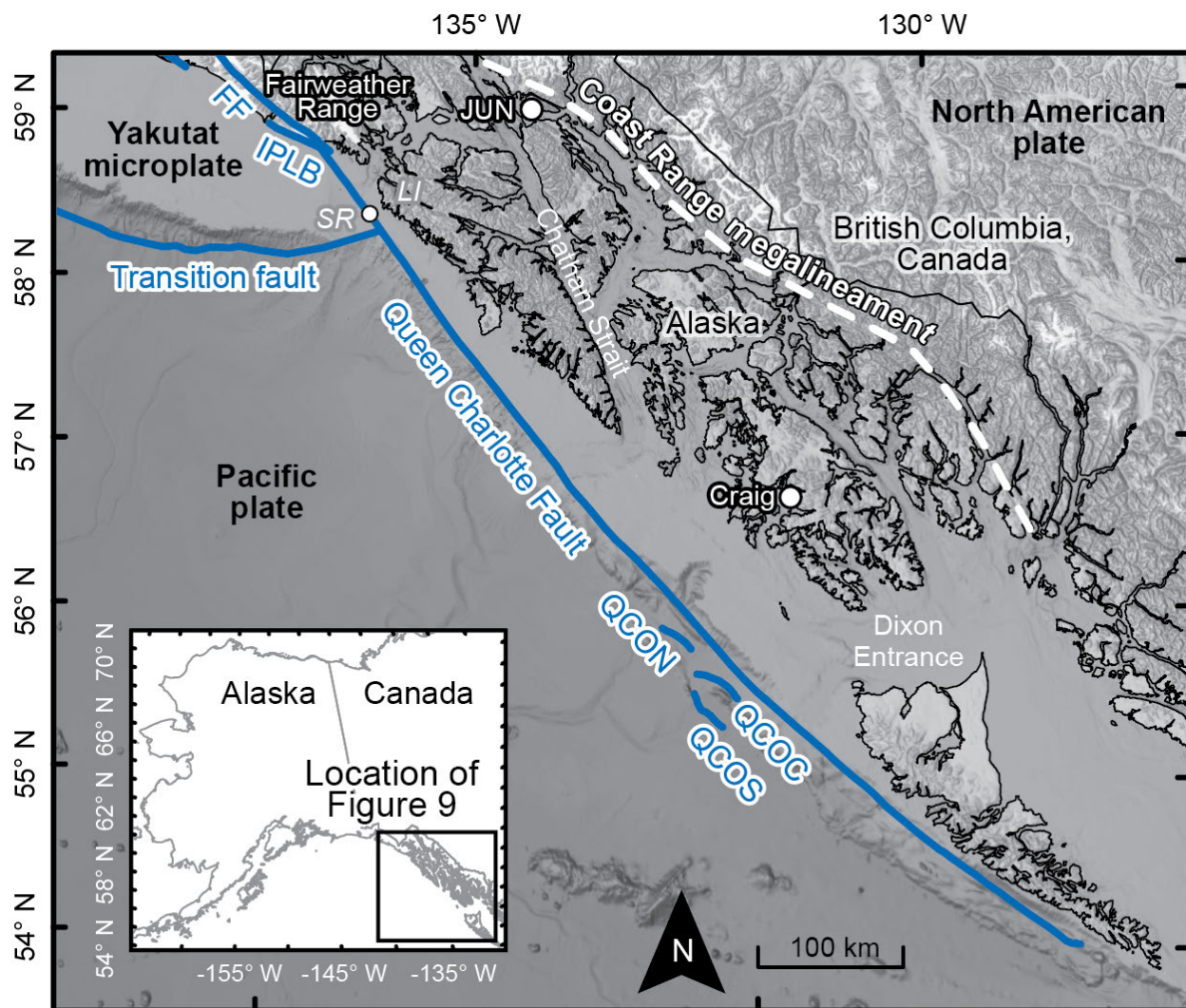


Figure 9. Southeastern Alaska. Blue lines are 2023 NSHM fault sections. White dashed line is the Coast Range megalineament (Brew and Ford, 1978), a vertical fracture zone without apparent Quaternary surface displacement, which could be used as a block boundary in geodetic models (e.g. Elliott & Freymueller, 2020). LI–Lisianski Inlet, FF–Fairweather Fault, IPLB–Icy Point-Lituya Bay Fault, QCON–Queen Charlotte (outboard, north) Fault, QCOC–Queen Charlotte (outboard, center) fault, QCOS–Queen Charlotte (outboard, south) fault, SR–slip rate site. Base topography and bathymetry from GEBCO (2022).

### 3.3 The Queen Charlotte-Fairweather Fault and transform margin

The Queen Charlotte-Fairweather Fault, or QCF, is the transform fault between the North American and Pacific plates, and it is the dominant seismic source in southeastern Alaska (Figs 1, 9). We refer to the offshore part of the fault as the “Queen Charlotte Fault,” and we refer to the onland part as the “Fairweather Fault.” The QCF is a right-lateral fault system and has generated

six M7.1+ earthquakes in the last 100 years (e.g. Doser, 2010). Several recent seagoing expeditions acquired high-resolution multibeam bathymetry data along the entire length of the QCF through southeastern Alaska and northwestern British Columbia (Barrie et al., 2013; Brothers et al., 2020; Andrews et al., 2022). These efforts revealed a simple fault structure comprising a single strand and in places, two parallel, locally overlapping strands with small horsts, graben, and pull-apart basins (Brothers et al., 2020). The remarkable continuity of the fault trace along its entire northern ~500 km, lack of adjacent major fault strands, and the lack of relief across the trace imply a near-vertical fault dip. The geomorphic observations are further supported by historical earthquakes, namely the 1972 M7.6 and 2013 M7.5 strike-slip events that both ruptured along a near-vertical fault plane (Doser and Rodriguez, 2011; Yue et al., 2013). Brothers et al. (2020) determined a QCF slip rate of  $53 \pm 3$  mm/yr based on 181 measured offset seafloor features (eg, scarps, channels, gullies and ridges) that formed during the initial phase of glacial retreat from the continental shelf at ~17 ka, and during the subsequent glacial-interglacial transition that delivered profuse outwash to the continental shelf-edge and slope (Brothers et al. 2020). Other fault splays previously mapped along the continental shelf (e.g., Bruns, 1982 & 1983; Carlson et al., 1988) do not appear to carry significant plate boundary slip and may be largely inactive.

In contrast with the offshore Queen Charlotte Fault, the onshore Fairweather Fault strikes  $17^\circ$  more westerly and expresses subparallel contractional faults to the southwest and high topography to the northeast (i.e., Mt. Fairweather is 4635-m tall and lies in the Fairweather Range that is higher than 3 km; Figs. 9, 10). The change in fault orientation produces a restraining bend where the fault system steps onshore. A thermochronology study of rocks from both sides of the fault indicate rapid exhumation and rock uplift inside the bend (Lease et al., 2021). Tracing the exhumation history along strike also gives an estimate of the fault slip rate of  $54 \pm 6$  mm/yr between 2.5 and 0.5 Mya (Lease et al. 2021). Witter et al. (2021) assessed geologic offsets of correlative age along the southern part of the fault and estimated a  $10^4$ -yr-averaged rate of  $\geq 49$  mm/yr, compatible with the low end of prior estimates by Plafker et al. (1978). The geodetic block modeling of Elliott & Freymueller (2020) yielded slip rates of  $45 \pm 1$  mm/yr and  $36 \pm 1$  mm/yr for the southern and northern parts, respectively, of the Fairweather Fault. Their northern part is in the Yakutat Bay region where additional fault strands are subparallel to the Fairweather Fault, which presumably act to lower the slip rate on the main fault strand.

The Pacific-North America plate rate would usually be considered as the speed limit on the Queen Charlotte-Fairweather transform slip rate. All but two of the 18 plate motion models on the Unavco plate motion calculator (Unavco, 2019) give rates between 47 and 51 mm/yr for a location on the fault offshore Craig, Alaska. More recent and commonly used models have higher rates, such as NNR-MORVEL56 (Argus et al., 2011) and the GEODVEL (Argus et al., 2010), which put that velocity as 51 and 50 mm/yr, respectively. More recently, DeMets and Merkouriev (2016) focused on refining Pacific-North America plate motions for the last 20 million years. They combined sea-floor magnetic anomaly data with a longer and more robust GNSS dataset and found a rate of 49 mm/yr for the QCF at a location offshore Craig. These estimates are all within a millimeter of each other, however, for all these studies the closest GNSS site west of the QCF is in Hawaii, about 4200 km away. Moreover, the DeMets and Merkouriev (2016) pole predicts significant convergence across the entire length of the QCF, which is contrary to the observed submarine tectonic geomorphology (see Brothers et al., 2020). Brothers et al. (2020) discussed uncertainties associated with poles of rotation used in both plate reconstruction and geodetic models, and we concur with their conclusion that the QCF pole of

rotation is distinct from the Pacific-North America pole of rotation and angular velocity defined by the San Andreas transform farther south.

Given all these sources of data, we utilize the geologic slip-rate estimate of  $53 \pm 3$  mm/yr from Brothers et al. (2020) for the QCF for the 2023 NSHM. This rate is based on a submerged glacial scour surface that is offset  $\sim 900$  m since ice receded from the continental shelf at  $\sim 17$  ka. This piercing point is located along the northern section of the QCF where the strike of the fault and plate motion are most closely aligned and deformation is expected to be accommodated by purely strike-slip motion (Figure 10). Thus this estimate is considered to be the most robust. An additional 180 offset features along the fault farther south have higher uncertainties due to limited age control, but all estimates generally range from 45–55 mm/yr (Brothers et al., 2020). A critical assumption in the Brothers et al. (2020) study is the age of the offset features, which are linked to (a) the age of deglaciation on the continental shelf, (b) the onset of glacial outwash sedimentation and morphological modification of submarine canyons, gullies and rills of the continental slope, and (c) the timing of sea level transgression, inundation of the shelf, and shutdown of sediment delivery to the shelf edge and slope. Several constraints on the timing of these events come from both onshore and offshore paleo environmental reconstructions that focused on the glacial-interglacial transition period (e.g., Barrie and Conway, 1999; Davies et al., 2011; Carlson and Baichtal, 2015; Praetorius et al., 2016; Lesnek et al., 2018; Lesnek et al., 2020; Ager et al., 2019; Darvill et al., 2018). If the onset of deglaciation from the shelf occurred closer to 18 ka, the approximate oldest age permissible based on cosmogenic exposure ages in southeastern Alaska (Lesnek et al., 2020), then it would lower Brothers et al. (2020) rate by a couple of millimeters per year, and make their rates within error the same as the Pacific-North America plate rates. Regardless, the slip-rate estimates based on reconstruction of offset submarine geomorphology account for virtually the entire plate boundary slip budget, thus reducing the likelihood for significant motion to be accommodated by faults farther east, e.g. in the vicinity of Juneau.

Plate motion, geodesy, and geologic estimates of the slip rate on the Fairweather Fault are all high, and differ by  $< 10$  mm/yr. The rate for the time interval of 2.5-0.5 Mya obtained using thermochronology (Lease et al., 2021) is  $54 \pm 6$  mm/yr, and the late Holocene geologic rate calculated by Witter et al. (2020) was  $\geq 49$  mm/yr. However, the evidence for a contractional Icy Point-Lituya Bay Fault to the southwest of the Fairweather Fault (see below), and the high topography of the Fairweather Range (Figure 9, 10) both indicate contraction across the region and that the fault slip rate should be lower than the rate on the Queen Charlotte Fault to the south. Elliott and Freymueller (2020) modeled a slip rate of 45 mm/yr on the Fairweather Fault from GNSS data. Elliott et al. (2010) also found a north-northeasterly orientation of velocities (relative to stable North America) for sites in the region between the Fairweather and the eastern Denali Faults. These vectors provide evidence of shortening across that region. The higher Lease et al. (2021) rate appears robust for the interval from 2.5 to 0.5 Ma, but it is possible the fault has slowed in the last 500,000 yrs as the Yakutat microplate collision has progressed. Taking these considerations together, we utilize the minimum rate from Witter et al. (2021) of 49 mm/yr for the Fairweather Fault slip rate for the 2023 NSHM.

Brothers et al. (2018) searched for, but did not find, evidence for other young and active faults in southeastern Alaska east of the QCF (Figure 9). In particular, they looked for evidence of active faulting on the Lisianski Inlet Fault, the Chatham Strait Fault, and the Coast Shear Zone (see also discussion below regarding this term), but seismic reflection profiles did not produce

evidence for offset strata emplaced since ~13 ka. We note a discrepancy between geologic evidence of active faults and geodetic models in southeastern Alaska. The geodetic data indicate north-northwestward motion of all the communities in southeast Alaska relative to geodetic sites more than 200 km to the east in British Columbia (Elliott & Freymueller, 2020). Elliott and Freymueller (2020) infer  $2.8 \pm 0.2$  mm/yr dextral slip occurs across the region. They model this motion along the Coast Shear Zone, the largest geologic structure in the region (Figure 4). However, Brothers et al. (2018) collected high-resolution seismic profiles across the trace of this feature in Berners Bay, north of Juneau, but saw no evidence for young deformation. We are unaware of other evidence for geologically recent deformation along the Coast Shear Zone. We note the geologic evidence indicates the Coast Shear Zone was a contractional structure that was active prior to 57-53 Ma, when Juneau gold belt mineralization occurred (Miller et al., 2000; Karl et al., 2023). A vertical subparallel feature with brittle Cenozoic deformation that postdates the Coast Shear Zone, is the Coast Range megalineament (Twenhofel and Sainsbury, 1958; Brew and Ford, 1978; Figure 9), which is a more likely candidate for active faulting. The exact location, or perhaps the zone of distributed deformation, of low-rate dextral shear inferred by Elliott and Freymueller (2020) is not clear and may be a target for future work.

Several active slow slip-rate contractional or strike-slip faults occur to the west of Dixon Entrance and the Queen Charlotte Fault in the deep ocean (Walton et al., 2015; Tréhu et al., 2015). At least some of these structures are likely reactivated spreading-ridge normal faults but now have a component of transpression. These structures are likely insignificant for producing consequential ground motions, but the structures do have the potential to generate significant tsunami as they lie at abyssal depths. For the 2023 NSHM, we use a dip of  $45^\circ\text{E}$  and a nominal slip rate of 0.01 mm/yr on these three structures.

### 3.4 Yakutat Region

The Yakutat region is located where the Yakutat microplate (e.g., Chapman et al., 2012; Pavlis et al., 2019 and references therein) collides with and subducts beneath Alaska's southern margin between the dextral Fairweather Fault and the northeastern corner of the Alaska-Aleutian megathrust (Figures 1, 2, 10). There, faults and related folds of the St. Elias orogen collectively accommodate ~75 percent of the 53 mm/yr Yakutat-North America plate convergence (Elliott & Freymueller, 2020) and all the dextral Pacific-Yakutat plate motion, with the remainder transmitted hundreds of kilometers into the continental interior (Haeussler et al., 2000; Haeussler et al., 2017b; Koehler & Carver, 2018; Elliott & Freymueller, 2020). Constraints on numerous details of the locations, geometries, and rates of Yakutat-region faults improved significantly after completion of the 2007 NSHM for Alaska (Wesson et al., 2007; Shumway, 2019) principally as a result of multidisciplinary research supported by the National Science Foundation under the St. Elias Erosion and Tectonics Project (e.g., Gulick et al., 2015; Enkelmann et al., 2015a, b; Pavlis et al., 2019; Walton et al., 2021). We utilized contributions from this large body of work to increase the number of Yakutat region faults to 19 in the 2023 NSHM for Alaska (compared to one fault—the Transition Fault—in the 2007 model) and describe these changes in this section. Onshore, the east-west striking faults have been referred to as the Yakataga fold and thrust belt (e.g. Wallace et al., 2008), and offshore the zone of deformation trends more northeasterly and has been referred to as the Pamplona zone (e.g. Lahr and Plafker, 1980). The smaller presumably active faults, in the Yakataga fold and thrust belt and the larger offshore Pamplona zone shown in red on Figure 10 are not specifically included in the 2023 NSHM, but rather are included within a single larger Pamplona fault zone polygon.

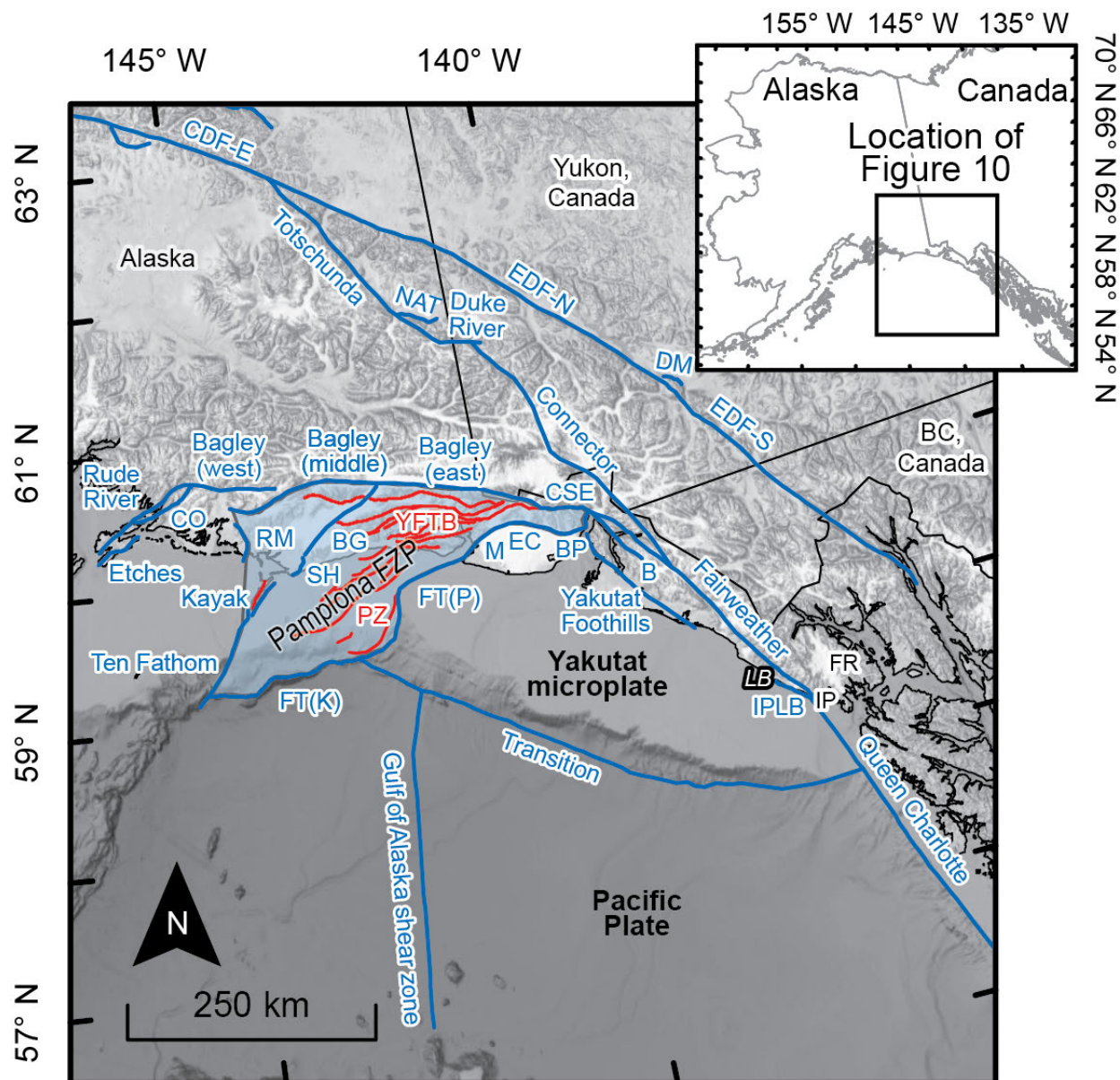


Figure 10. Fault sections (blue lines) and the Pamplona fault zone polygon (blue shading) of the greater Yakutat region in the 2023 NSHM for Alaska source model (Bender et al., 2021). Fault sections are labeled by name, including abbreviations: CO–Cordova, RM– Ragged Mountain, SH–Suckling Hills, FT(K)–Foreland thrust (Khitrov), FT(P)–Foreland thrust (Pamplona), M–Malaspina, EC–Esker Creek, BP–Bancas Point, YF–Yakutat Foothills, B–Boundary, CSE–Chugach-St. Elias, CDF-E–Central Denali Fault (east), EDF-S–Eastern Denali (south), DM–Decoeli Mountain, EDF-N–Eastern Denali (north), NAT–Natashat. Red lines are Quaternary active faults (USGS, 2020) of the Yakataga fold-thrust belt (YFTB) and Pamplona deformation zone (PZ). FZP–fault zone polygon. Place name abbreviations: IP–Icy Point, LB–Lituya Bay, FR–Fairweather Range, IPLB–Icy Point-Lituya Bay. Base topography and bathymetry from GEBCO (2022).

### 3.4.1 Transition Fault

The submarine Transition Fault appears to accommodate a small amount of dextral motion between the Yakutat microplate and the Pacific plate (Figure 10; Gulick et al., 2007, 2013; Reece et al., 2013). We assign the Transition Fault a vertical dip (Christeson et al., 2010), and a right-lateral slip rate of 4 mm/yr, which is consistent with modest expectations of Transition Fault dextral slip (Christeson et al., 2010; Reece et al., 2013; Gulick et al., 2013). In particular, Christeson et al. (2010) showed the crustal structure of the fault is consistent with a transform fault – there is no geologic evidence for significant underthrusting. Geophysical profiles across the western part of the fault show evidence of dominantly strike-slip deformation with contractional deformation on some adjacent structures (Gulick et al., 2013). Geodetic models indicate some contraction across the fault (Elliott et al., 2013; Elliott & Freymueller, 2020). Assuming the Transition Fault takes up the entire difference between the Queen Charlotte Fault (53 mm/yr) and the Fairweather Fault (49 mm/yr) yields a slip rate of ~4 mm/yr. The geodetic block model of Elliott and Freymueller (2020) implies a Transition Fault slip rate of 4 mm/yr, but in a left-lateral sense that we deem unlikely based on regional seismotectonics (Doser and Lomas, 2000). Lahr and Plafker (1980) inferred a dextral slip rate of 4 mm/yr for a block model of the region. Doser and Lomas (2000) calculated a convergence rate of 3 mm/yr for the southern part of the fault. Our assigned dextral slip rate of 4 mm/yr compares well with the rate range from these prior tectonic and geodetic models.

### 3.4.2 Icy Point-Lituya Bay, Boundary, Yakutat Foothills

There is strong evidence of a thrust or reverse fault to the southwest of the Fairweather Fault, from offshore Icy Point to the region of Lituya Bay (Miller, 1961; Carlson et al., 1988; Plafker et al., 1994; Lease et al., 2021; Witter et al., 2023), the “Icy Point-Lituya Bay Fault” (Figure 10). Seismic reflection profiles across this fault at Icy Point show significant young (post Last Glacial Maximum (LGM)) contractional deformation in this region (Witter et al., 2023), bedrock mapping by Miller et al. (1961) showed Miocene-age sediments with near vertical dips. Miller et al. (1961) proposed a fault-cored fold that parallels the shoreline and lies just offshore. Recent LiDAR data collected by the Glacier Bay NPS (National Park Service) show evidence of bedding-parallel slip planes offsetting alluvial terraces, indicating distributed deformation resulting from flexural-slip folding, rather than focused deformation on a single structure. It seems likely this fault-cored fold is connected with the Fairweather Fault at depth, and it constitutes a separate seismic source (Witter et al., 2023). For the 2023 NSHM, we use the dip of 50°E and slip rate of 5 mm/yr constrained by low-temperature thermochronometry (Lease et al., 2021). We note that Witter et al. (2023) find a rate of 9 mm/yr and a fault dip of 30-45° for this structure, but these results came out after the release of the Bender et al. (2021) NSHM data release, and they are not incorporated into this hazard map update.

The region east and north of Yakutat Bay occupies the leading edge of the Yakutat microplate collision, and it is consequently one of the most complex structural settings in Alaska. Between Yakutat Bay and the Fairweather Fault, lie the right-transpressive Boundary Fault and the reverse Yakutat Foothills Fault (Figure 10). The Boundary and Yakutat Foothills Faults deform the eastern margin of the Yakutat microplate at Pliocene- and late-Pleistocene-average hanging-wall exhumation rates of  $\leq 1.5$  and 3 mm/yr, respectively, as derived from thermochronology (Enkelmann et al., 2015b). Vertical rates of hanging-wall exhumation should closely approximate long-term slip rates on these steeply dipping faults (70–85°, Walton et al.,

2021), and map patterns of 106-year exhumation rates across these faults mimic the spatial distribution of coseismic surface uplift during the 1899 Yakutat Bay earthquakes (M8.1 and M8.2; Plafker and Thatcher, 2008; Enkelmann et al., 2015a).

Lateral slip rates on these faults remain unconstrained. Given their proximity to the Fairweather Fault, and the fact that the Boundary Fault lies in a linear valley comparable to the dextral Fairweather Fault indicates there is likely a significant strike-slip component. The Elliott and Freymueller (2020) geodetic model estimates a right-lateral strike slip rate of 3 mm/yr on the Boundary Fault and a 4 mm/yr right-lateral strike-slip rate, along with a 5 mm/yr contractional slip rate, on a vertical Yakutat Foothills Fault (Elliott & Freymueller, 2020). We combine the lateral geodetic component with the vertical thermochronology-constrained component for the slip rates, although it seems an imperfect solution in that it combines disparate data types. This gives a rate of 3 mm/yr for the Boundary Fault and 5 mm/yr for the Yakutat Foothills Fault, which are the rates we use for the 2023 NSHM.

### 3.4.3 Malaspina, Esker Creek, Bancas Point

The north-dipping and contiguous Foreland, Malaspina, Esker Creek, and Bancas Point thrust faults define the front of active Pamplona fold-and-thrust belt deformation and sole into a ~12–16 km-deep, 5–10° north-dipping detachment that may be the contact between Yakutat microplate basement and overlying sedimentary rock (Figure 10; Berger et al., 2008a; Worthington et al., 2010; Chapman et al., 2012; Elliott et al., 2013). The Malaspina Glacier conceals the surface trace of the Malaspina Fault (Figure 10), but structural geology, borehole data, and earthquake relocations collectively confirm the presence of this gently north-dipping structure (10–30°, Chapman et al., 2012 and references therein). The Malaspina Fault adjoins the Esker Creek Fault to the east across a prominent change in structural trend, from northeast to northwest, respectively. Dip estimates for the Esker Creek Fault range from 30° (Plafker & Thatcher, 2008) to 45–60° northeast (Bruhn et al., 2012; Chapman et al., 2012). Low-temperature (apatite-Helium) thermochronology constrains Esker Creek Fault vertical exhumation rates to 3–5 mm/yr since ~1 Ma, consistent with a 3–9 mm/yr slip rate on a 45±15°-dipping fault (Enkelmann et al., 2015a). The Esker Creek Fault adjoins the Bancas Point Fault to the east across another along-strike change in trend, from northwest back to northeast. Slip on the northwest-dipping Bancas Point Fault and the Esker Creek Faults produced >14 m of coseismic hanging wall uplift during a single M8.1 event in the 1899 Yakutat Bay earthquake sequence (Plafker & Thatcher, 2008; Walton et al., 2022). The broad map pattern of surface uplift sustained during this event defines a maximum on the Esker Creek-Bancas Point Fault intersection (Plafker & Thatcher, 2008) where late-Pleistocene apatite-Helium exhumation rates of 2–3 mm/yr imply moderate rates of long-term slip (Enkelmann et al., 2015a). We assign 45° dip angles to all three faults, and we adopt the exhumation rates of Enkelmann et al. (2015a) as slip rates of 5 mm/yr for the Malaspina and Esker Creek Faults, and 3 mm/yr for the Bancas Point Fault. We reiterate that all these faults appear to join the regional decollement at ~12 km depth as shown, for example, in the cross sections of Worthington et al., (2010) and Pavlis et al. (2012, 2019).

### 3.4.5 Foreland Thrust

The Pamplona zone represents the offshore equivalent of the Yakataga fold-and-thrust belt (Figure 10), comprising a thin-skinned belt of imbricate thrust faults and fault-cored folds

that deform Miocene–present-aged sediments of the Yakataga Formation, sole into a sub-horizontal detachment, and young to the south (Worthington et al., 2008; 2010; 2012; 2018; Gulick et al., 2013). Like the Yakataga belt, the Pamplona system and its basal detachment may take up a substantial fraction of late-Pleistocene Yakutat convergence (e.g., Pavlis et al., 2004; Worthington et al., 2010), with the remainder driving faulting tens of kilometers onshore in the St. Elias mountains (e.g., Bruhn et al., 2004; Berger et al., 2008a), and hundreds of kilometers inland on the Denali Fault system (e.g., Haeussler et al., 2000; 2017b). Whether earthquakes rupture Pamplona zone faults independent of the detachment remains unclear, but geophysical data and drill records imply that late Pleistocene Pamplona zone seafloor deformation is focused on a frontal fault, termed the Foreland thrust, expressed as a laterally near-continuous southeast-facing seafloor escarpment above a southeast-vergent reverse fault (Worthington et al., 2010; 2012; Gulick et al., 2013).

We simplified the Pamplona fold-and-thrust zone into two contiguous lines representing the Foreland thrust, divided at the intersection with the northwestern end of the Transition Fault, and refer to these as the Pamplona (FT(P)) and Khitrov (FT(K)) sections (Figure 10; e.g., Gulick et al., 2007; 2013). We assigned a dip of 45° north to both Foreland thrust sections after the geophysical interpretations of Worthington et al. (2010; 2012). Prevalent interpretations of geologic and geophysical data place <17 percent of the total Yakutat plate convergence on the Foreland thrust (Worthington et al., 2010). A larger but unknown amount of Yakutat convergence is taken up by slip on a sub-horizontal detachment between Yakutat basement and overlying Yakataga sediments at ~8–12 km depth, into which the Foreland thrust and overlying faults sole (Worthington et al., 2010 and references therein). For our purposes, the Foreland thrust section rates represent slip on both the deformation front and the detachment and are consistent with higher Pleistocene estimates of the total Pamplona zone shortening rate (30–40 mm/yr, Pavlis et al., 2004; Worthington et al., 2010).

The Pamplona section of the Foreland Thrust (FT(P)) represents the deformation front where the Yakutat microplate underthrusts Yakataga Formation sediments north of the dextral Transition Fault (Figure 10; e.g., Worthington et al., 2008; 2010; 2012; 2018). We assigned the Foreland thrust a slip rate of 32 mm/yr. This rate represents the difference between the southern Fairweather Fault slip rate (49 mm/yr; Witter et al., 2020), which dextrally accommodates Yakutat-North America motion to the south and east, and slip rates of structures that take up Yakutat convergence to the north: the Denali Fault (13 mm/yr; Haeussler et al., 2017b) and the eastern Bagley Fault (4 mm/yr; Berger et al., 2008). This slip rate is essentially the same as the slip rate from geodesy. In our simplification, the Foreland thrust is a combination of the Foreland and Malaspina thrusts in the block model of Elliott and Freymueller (2020). Combining their rates (15 mm/yr and 11 mm/yr, respectively) yields 26 mm/yr, which is slightly less than our geologic rate. Considering the different approaches taken to arrive at this number, and the similar values provides us some confidence in the result.

The Khitrov Fault section is the westernmost part of the Foreland Thrust (FT(K)) and is the leading edge of the internally deforming corner of the Yakutat microplate and overlying sediments, west of the dextral Transition Fault and underthrust by the Pacific plate (Figure 10; Worthington et al., 2008; Gulick et al., 2013). The section name refers to Khitrov Ridge, a fault-cored seafloor high that likely reflects the bathymetric expression of ongoing deformation on this fault section. Seismic images imply a fault configuration within Khitrov Ridge consistent with seaward-younging transpressive “flower structure” type faulting (Worthington et al., 2008;

Gulick et al., 2013), which we greatly simplify as a north-dipping thrust for the hazard model of Alaska. We assigned the Khitrov thrust a slip rate of 34 mm/yr. This rate represents the difference between the Pacific-North America plate rate (51 mm/yr; Elliott & Freymueller, 2020) and slip rates of structures that accommodate Yakutat convergence to the north, including the Kayak Fault (3.5 mm/yr; Chapman et al., 2012), expected low cumulative rates of thrust faults further north (0.5 mm/yr), and the maximum Denali Fault rate (13 mm/yr; Haeussler et al., 2107b). There is no geodetic estimate for the slip rate on this fault.

#### 3.4.6 Suckling Hills, Bering Glacier, Ten Fathom, Kayak Faults

North and west of the Pamplona zone at the leading edge of the Yakutat microplate, a laterally discontinuous system of colinear northeast-striking thrust faults absorb some of Yakutat-North America convergence, deforming Eocene to Pleistocene-aged sedimentary rocks and giving rise to the Suckling Hills onshore and Kayak Island offshore (Figure 10; Chapman et al., 2011). Onshore, the Suckling Hills preserve remnants of a northwest-sloping, low-relief, loess-draped upland surface of unknown origin and uncertain age, which Chapman et al. (2011) used to constrain back-limb tilt in a geometric model of listric thrust faulting. According to their model, the Suckling Hills Fault dips  $60\pm 10^\circ$  northwest and slips at a late-Pleistocene-average rate of  $4.7\pm 1.2$  mm/yr, assuming an age of  $55\pm 5$  ka consistent with surface formation via glacial erosion during the penultimate glacial maximum. This rapid geologic slip rate is consistent with observations of anomalously high local uplift during the 1964 M9.2 Great Alaska earthquake (Plafker, 1969), where  $\sim 3$  meters of coseismic slip occurred on the Suckling Hills thrust (Chapman et al., 2014). The Suckling Hills Fault may therefore be a megathrust splay fault at the easternmost end of the 1964 rupture.

We delineate the offshore Kayak Island deformation zone front in two sections: the Ten Fathom Fault beneath Kayak Island, and the Kayak Fault to the southwest (e.g., Worthington et al., 2008; Chapman et al., 2011). A seafloor seismic profile constrains the Ten Fathom Fault dip at  $60\pm 10^\circ$  northwest. Worthington et al. (2008) identified a northwest-sloping horizon above the fault on this profile, later interpreted as a tilted and growth strata-mantled erosional surface of LGM-age ( $14.5\pm 1.1$  ka; Chapman et al., 2011) comparable to the Suckling Hills upland surface. The listric thrust fault model, constrained by the tilt and hypothesized age of the buried LGM surface, implies a late-Pleistocene average slip rate of  $3.5\pm 1.0$  mm/yr. For our purposes, we adopted the rates and geometries of the Suckling Hills Fault and Kayak Island deformation zone faults reported by Chapman et al. (2011).

Given the high deformation rates along the Suckling Hills, Kayak, and Ten Fathom Faults, it has been inferred these faults link and extend to the northeast beneath the Bering Glacier (Richter et al., 2006, Bruhn et al., 2012; Chapman et al., 2008.). Although the fault cannot be directly observed, we adopt a subglacial Bering Glacier Fault with similar parameters to the Suckling Hills thrust Fault: a slip rate of 4.6 mm/yr based on the estimate of Elliott and Freymueller (2013) and a dip of  $60^\circ$ N.

Geodetic data do not clarify the slip rates on all these faults. The only detailed geodetic model for this region is by Elliott et al. (2013), which was incorporated into Elliott and Freymueller (2020). They infer a larger “St. Elias block” defines the velocities of this region northwest of the Malaspina and Foreland thrusts (Figure 3), except for a  $\sim 40$ -km-wide northeast-trending strip within the block that includes the Suckling Hills, Ten Fathom, and Kayak Faults. The southeast edge of the St. Elias block is essentially at the Foreland, Malaspina, and Esker

Creek Faults in our model. In order to explain more westerly velocity vectors, Elliott et al. (2013) define a Bering Deformation Zone as a fully creeping region within the St. Elias block. Evidence for coseismic uplift of the Suckling Hills in the 1964 earthquake (Chapman et al., 2014) seem to violate the inference of a fully creeping region. As mentioned by Elliott et al. (2013), one way to reconcile their model with a rigid block model is to have a region deforming at a low rate extend to the northeast edge of the St. Elias block, such that there is an additional smaller block that is part of the St. Elias block. To our view, this geometry seems most likely. Our model also includes a Pamplona fault zone polygon in recognition of numerous faults in the region apart from the major players (Bruns, 1982, 1983).

#### 3.4.7 Ragged Mountain Fault

Northwest of the Suckling Hills, Ragged Mountain is the hanging wall topography above the Ragged Mountain thrust (Figure 10; Heinlein et al., 2018; McCalpin et al., 2020). Along the east flank of Ragged Mountain, the primary surface expression of faulting is a set of uphill-facing extensional scarps within a hanging-wall graben above a sinuous east-facing thrust scarp (McCalpin et al., 2020). McCalpin et al. (2020) propose that this geomorphic configuration fits a model of thrusting in which the fault dips  $\sim 30^\circ$  west at depth but is less steep near the surface such that the hanging wall collapses as it is thrust over the fault bend. These researchers did not explicitly compute a late-Pleistocene slip rate, but a trench across the thrust scarp reveals evidence for three surface-rupturing earthquakes since  $\sim 45$  ka, including 0.77 m of displacement during the most recent event at  $\sim 4$ –5.8 ka (McCalpin et al., 2020). We adopt the dip of  $30^\circ$  west favored by McCalpin et al. (2020) and use a geologic slip rate of 1 mm/yr after the compilation of Koehler (2013) as geologic inputs for the Ragged Mountain Fault in the 2023 NSHM for Alaska.

Geodetic data do not constrain the slip rate on the Ragged Mountain Fault. Elliott et al. (2013), in their assessment of the geodetic data for the region, lump the region of the Ragged Mountain Fault into their 40-km-wide “Bering Deformation Zone,” which accommodates internal deformation within their “Elias Block.” From a geologic perspective, the Ragged Mountain Fault is in the position of being the principle western fault of the Yakutat microplate collision zone, with Paleocene-Eocene Orca Group rocks in the hanging wall and Eocene Stillwater Formation rocks of the Yakutat microplate in the footwall. This relationship is similar to the Himalayan Frontal Thrust in that it juxtaposes the exotic rocks of the colliding block beneath the rocks of the backstop. However, from the geodetic perspective, the Ragged Mountain Fault is not acting as if it is a major plate boundary. Rather, it is a zone of internal deformation within the upper plate.

#### 3.4.8 Chugach-St. Elias, Bagley Faults

Structures representing the orogenic “backstop” for Yakutat-North America convergence include the Chugach-St. Elias and Bagley thrust faults (Figure 10; e.g., Pavlis et al., 2012). Based on the geologic relationship of Orca Group basement rocks thrust over poorly lithified Cenozoic sediments, the Chugach-St. Elias Fault is a fundamental fault in the St. Elias orogen. However, Apatite-He thermochronology data constrain the cooling history of the St. Elias orogen and reveal minimal rates of differential exhumation across the Chugach-St. Elias Fault (Berger et al., 2008a, b) indicating the juxtaposition of the rock units occurred prior to Quaternary time. In contrast, the hypothesized Bagley Fault of Berger et al. (2008a), which is a south-dipping back

thrust concealed by the Bagley icefield, drives differential exhumation rates equivalent to a Pleistocene-average slip rate of 3–4 mm/yr, assuming a dip of 45° south. We adopt the 4 mm/yr slip rate and 45° south dip for the Bagley Fault, and we assign the Chugach-St. Elias Fault a dip of 45° north and a slip rate of 0.1 mm/yr after the compilation of Koehler (2013). Geodetic models do not require the presence of either the Chugach-St. Elias or the Bagley Faults, nor do they have the ability to resolve the faults with our preferred parameters (Elliott et al., 2013; Elliott & Freymueller, 2020). However, the models do require a significant change in the fault geometry at depth. From the Bering Glacier region and westward, the geodetic data are best fit by an underthrusting or subduction model where the western part of the Bagley Fault connects to a regional decollement, which is 80-100 percent locked and is essentially the easternmost part of the Alaska-Aleutian subduction zone.

### 3.4.9 Gulf of Alaska shear zone

The Gulf of Alaska shear zone accommodates dextral slip within the Pacific Plate associated with the spatial partitioning of Yakutat-North America collision and subduction (Figure 10; Reece et al., 2013). A prominent and persistent seismic source, the Gulf of Alaska shear zone hosted four large dextral strike-slip earthquakes up to M7.8 from 1987–1992 (Pegler and Das, 1996), and historical seismicity continues to illuminate the linear, >200 km-long, north-south-oriented structure (e.g., Gulick et al., 2007; Reece et al., 2014). Although the shear zone lacks a seafloor trace, geophysical imaging confirms the presence of a several-km-wide zone of shallowly buried near-vertical faults (Reece et al., 2013). In the 2023 NSHM for Alaska, we represent the Gulf of Alaska shear zone as a single feature with a slip rate of 0.1 mm/yr and a vertical dip in keeping with steep faults observed by Reece et al. (2013).

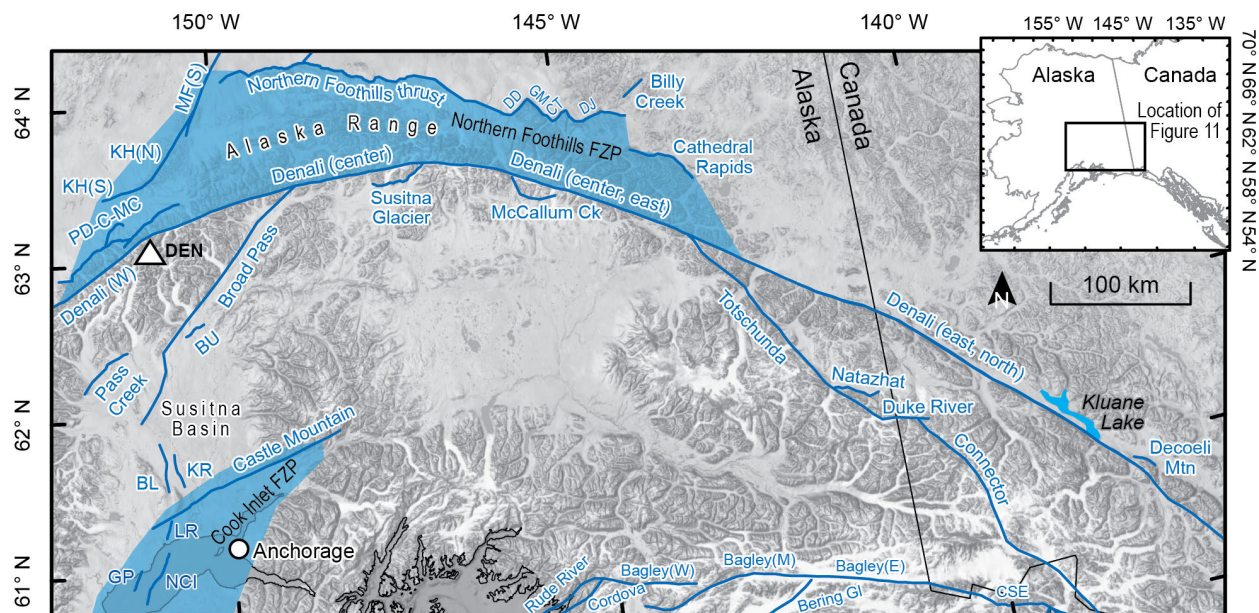


Figure 11. Fault sections (blue lines) of the central, south-central, eastern Alaska and western Canada regions in the 2023 NSHM source model (Bender et al., 2021). Fault sections labeled by name, including abbreviations: BU–Bunco Lake, BL–Bulchitna Lake, CT–Canteen, CSE–Chugach-St. Elias, Denali(W) – Denali (west), DD–Donnelly Dome, DJ–Dot “T” Johnson, GM–

Granite Mountain, , GP–Granite Point, KH(N)–Kantishna Hills (north), KH(S)–Kantishna Hills (south), KR–Kahiltna River, LR–Lewis River, MF(S)–Minto Flats (south), NCI–North Cook Inlet-SRS, PD-C-MC–Peters Dome-Chedotlatna-Mcleod Creek thrusts, FZP–fault zone polygon. Triangle marks the Denali (DEN) massif.

### 3.4.10 Connector Fault

Residual Yakutat-North America motion exceeding 10 mm/yr drives active deformation of interior Alaska (e.g., Haeussler et al., 2000; Haeussler et al., 2017b). Seismicity (Doser, 2014) and a prominent geodetic velocity gradient (Elliott & Freymueller, 2020) support the presence of a structure, termed the Connector Fault by Elliott et al. (2010; Figs. 10, 11) that transmits this motion as right-lateral slip from the Fairweather Fault system to the Totschunda-Denali Fault system. Despite rapid rates, the geologic expression of the Connector Fault remains ambiguous due at least in part to the remote glacier-mantled terrain of the Saint Elias Mountains that it traverses near international borders. We delineate the Connector Fault as a single fault contiguous with the Fairweather and Totschunda Faults, in a position consistent with locations of earthquakes analyzed by Doser (2014) and with previously mapped bedrock fault contacts (see compilations of Wilson et al., 2015; Yukon Geological Survey, 2020). There is a possible eastern alternative trace for the fault beneath glaciers (Doser, 2014), but for simplicity, and because it is in a remote region, we use a single trace consistent with the bedrock geology. We assign a vertical dip to the Connector Fault and the maximum late-Pleistocene average right-lateral slip rate of the Denali Fault (13 mm/yr; Haeussler et al., 2017b) to the west of its junction with the eastern Denali and Totschunda Faults.

Geodetic data support a dextral Connector Fault slip rate of 10 mm/yr (Elliott & Freymueller, 2020). Our preferred rate of 13 mm/yr is at the high end of the range of possible fault perpendicular geodetic velocities. We favor our geologic rate over the geodetic rate as there are multiple sites along the Denali Fault with slip rates greater than 10 mm/yr, and because there were limited GPS observations along the Denali Fault prior to the 2002 Denali Fault earthquake (e.g. Freymueller et al., 2008).

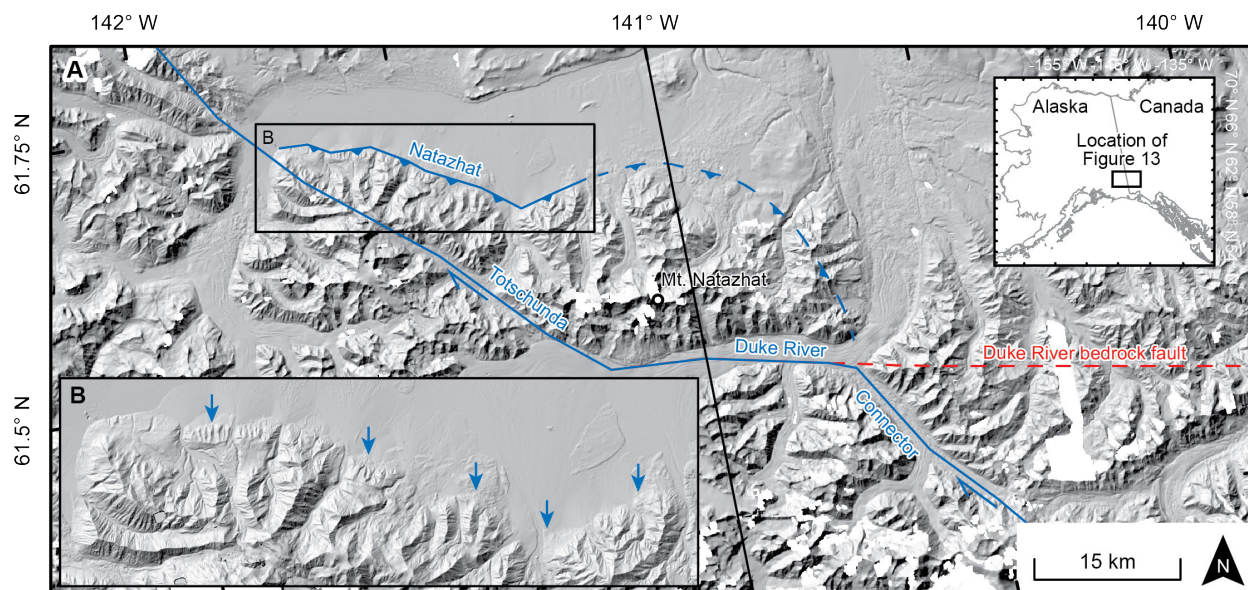


Figure 12. A) The Natazhath thrust and Duke River Faults as a restraining bend in the Totschunda and Connector Fault system. Mt. Natazhath is anomalously tall for the region at 4095 m. Fault sections shown in blue line, dashed where interpreted. There is no evidence of activity on the Duke River Fault where it lies in bedrock. B) Detail view of range-front thrust shown by Marechal et al. (2018).

#### 3.4.11 The Duke River Fault and the Natazhath Thrust

The connection between the Totschunda Fault and the Connector Fault lies along the Alaska and Yukon boarder and is the Duke River Fault (Figure 12). It lies east of the southern end of the Totschunda Fault and strikes east or southeast. To the east of this area in bedrock, it thrusts Triassic and older rocks over the Wrangell Lava (Cobbett et al., 2016). Along strike in eastern Alaska, some of these lavas have ages as young as 1 Ma, indicating the fault may have Quaternary activity. There is no evidence of activity along the Duke River Fault on ArcticDEM images, although it lies beneath glacial ice at its western end. Marechal et al. (2018) interpret a sinuous scarp on the DEMs as being a thrust fault scarp associated with the Duke River Fault. They interpret offset surfaces of up to 82 m, and given the glacial history of the region, they infer a maximum slip rate of up to 3 mm/yr and a fault dip of 30° to the south. Their identification of this fault trace, and its activity is compelling, but we note their location of what they termed the Duke River Fault is not the same as the location of the fault in bedrock, which is about 20 km to the south (see Cobbett et al., 2016). We suggest a more appropriate name for the fault trace they identified is the “Natazhath thrust fault” as it lies on the north side of Mt. Natazhath (Figure 12). Moreover, when considering the position and length of this scarp, it appears the Natazhath thrust fault is in a restraining bend between the Connector and Totschunda fault systems, which resulted in the high topography of Mt. Natazhath (4095 m). Thus, we use the parameters of Marechal et al. (2018) for the Natazhath thrust for the 2023 NSHM. We infer a 25 km length of the Duke River Fault is active beneath glacier ice and its slip is the difference between the Connector Fault slip rate (13 mm/yr) and the Natazhath thrust slip rate (3 mm/yr), thus it is 10 mm/yr. We do not include the eastern part of the Duke River Fault in our compilation of active structures.

### 3.5 The Denali Fault and the Alaska Range

In the two decades since the 2002 M7.9 Denali Fault earthquake, significant work focused on refining geologic slip rates on the Denali, Totschunda, and contractional faults flanking the Alaska Range (Figures 1, 2, 11). We first examine the Totschunda and Denali Faults and faults flanking the Alaska Range. We then discuss structures south and north of the Alaska Range.

#### 3.5.1 The Denali and Totschunda Faults

By all accounts, the Denali Fault is the most significant active fault in central interior Alaska (e.g. Haeussler, 2008; Elliott & Freymueller, 2020). It is a right-lateral strike-slip fault with a slip rate of about 13 mm/yr just west of where it intersects the Totschunda and eastern Denali Faults, based on cosmogenic dating of offset surfaces (Figure 11; Haeussler et al., 2017b). The slip rate decreases to the west along the fault, down to about 7 mm/yr near Denali (formerly Mt. McKinley), to about 3 mm/yr 200 km southwest of that and then westward to low rates, perhaps 1-2 mm/yr west of the Alaska Range. In considering the slip rate along the Denali Fault,

kinematics require the slip rates on the eastern Denali and Totschunda Faults just east of the fault junction to sum to the 13 mm/yr slip rate just west of the fault junction. Geologic estimates of the slip rates on all these faults are based on  $^{10}\text{Be}$  dating of offset landforms (Haeussler et al., 2017b). The slip rate on the eastern Denali Fault decreases to the southeast (Haeussler et al., 2017b) and the fault trace disappears to the southeast of Kluane Lake in the Yukon, indicating the slip rate is essentially zero. The geologically estimated slip rates on the Totschunda Fault are 6 to 9 mm/yr. For the 2023 NSHM, we use a slip rate of 5 mm/y for the northwestern part of the eastern Denali Fault, a slip rate of 2 mm/yr for the southeastern part, and a vertical dip for both, and a rate of 7 mm/yr for the Totschunda Fault. We use a slip rate of 0.1 mm/yr for the southeasternmost eastern Denali Fault where there is no surface trace. For the central Denali Fault, we use the cosmogenically determined slip rates for fault sections determined by Haeussler et al. (2017b) and a vertical dip.

The Boss Creek section of the western Denali Fault lies in the lowlands between the Alaska Range and the Kuskokwim Mountains (Figure 13). The 2-m ArcticDEM shows the fault trace continuously across the entire region as a linear trace with small welts of locally uplifted topography along both sides of the fault. The fault has almost no geologic constraints on the age and slip rate, except that the scarp is absent from modern river floodplains. The scarp cuts Quaternary-age surficial deposits, but the region was ice free at LGM time, and the age of the Quaternary deposits is unconstrained. Koehler et al. (2012) classify the displacement as “mid-Quaternary.” Elliott and Freymueller (2020) estimate a rate of 2 mm/yr for this part of the Denali Fault system, which seems plausible with the locally prominent, but likely old fault scarp. We suggest a maximum slip rate of 1 mm/yr for the 2023 NSHM, which would be in the range of error of the geodetic data and models.

We make several changes to the westernmost part of the Denali Fault system in the 2023 NSHM source model (Figure 13). In particular, the only two faults with surface scarps on modern DEMs (Bender and Haeussler, 2021) are the main Boss Creek and Holitna segments, and a fault subparallel to the Holitna segment, but located about 20 km to the northwest of it, called the Atsakovluk Fault (St. Amand, 1957; Koehler & Carver, 2018). We remove the Togiak-Tikchik segment that has appeared on prior compilations of potentially active faults (Figs. 1, 13). The Togiak-Tikchik segment is an important fault in bedrock (e.g. Hoare, 1961), and it follows a series of linear valleys, which suggested to others that it may be active (W. Coonrad in Plafker et al., 1994). However, we are unaware of scarps that disrupt Quaternary landforms along any valleys (Bender and Haeussler, 2021). Much of the fault was covered by glaciers until around 12 kya (Briner et al., 2017), and there is no evidence for surface faulting along the fault since that time. In prior maps of active faults of western Alaska, coming from the east, the Farewell segment of the Denali Fault takes a slight bend and turns into the Holitna segment, which then turns into the Togiak-Tikchik segment. In previous depictions, the Farewell segment has a ‘tail’ that extends to the southwest beyond the branchpoint with the Holitna segment. We shorten this tail to be only 66 km long as there is no evidence of faulting to the southwest.

We note an unresolved conflict between the geodesy and geology of this region. Elliott and Freymueller (2020) place the boundary between their “Kuskokwim” block, to the north, and their “Naknek” block, to the south, along the trace of the Holitna segment of the Denali Fault, which fits the geologic observations (Figs. 4, 13). However, their block boundary diverges from the Denali Fault trace, in the region of the Tikchik Lakes, and they extend it linearly westward to the coast across the Kilbuck Mountains where bedrock geologic mapping appears to preclude a

single fault trace crossing that region – active or not. However, the modeled velocity differences at sites between their blocks are significant and their model residuals are low. Perhaps there is distributed deformation over a large region that obfuscates active faulting. Future studies are needed to further evaluate active faulting and deformation in the Kilbuck Mountains region.

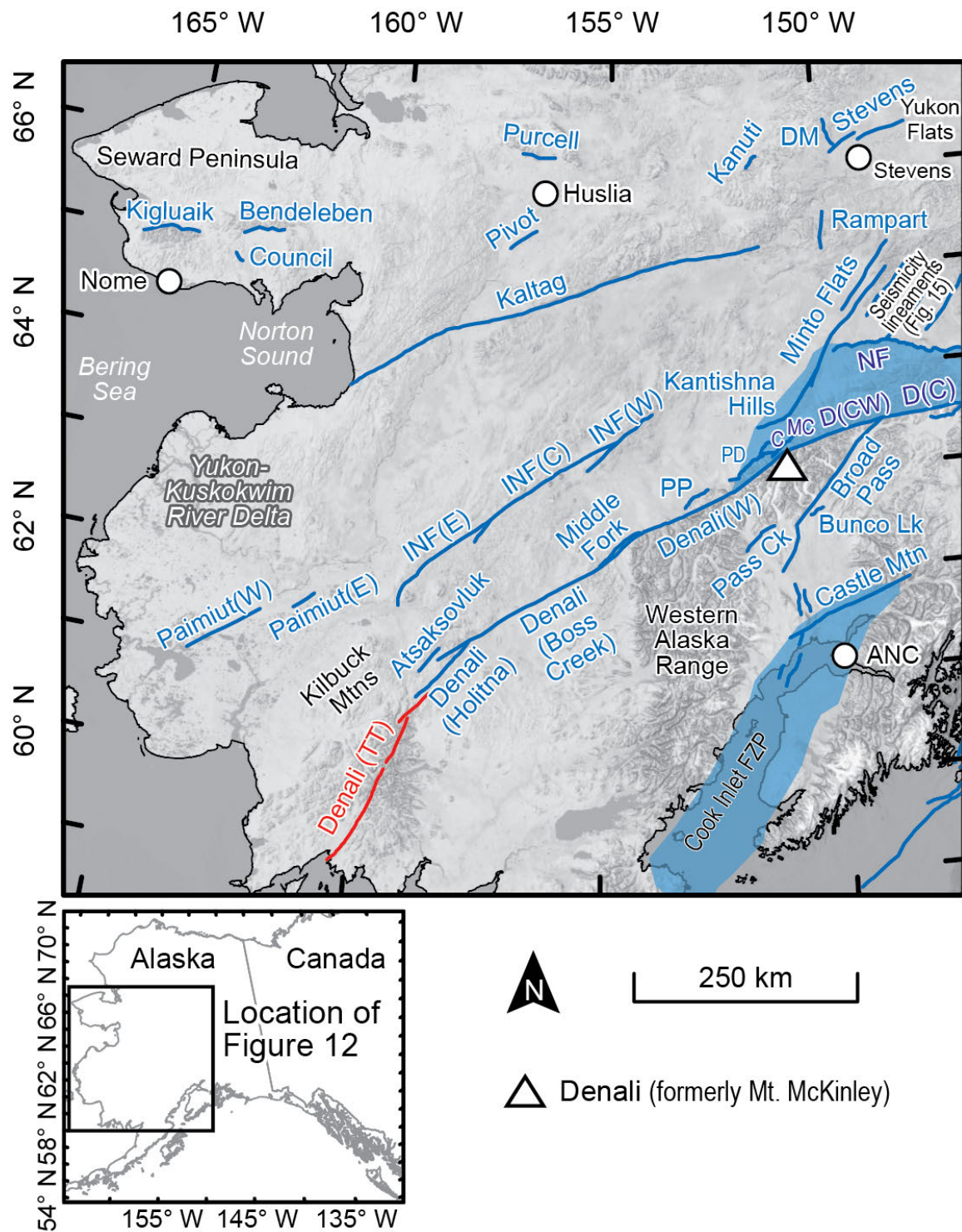


Figure 13. Fault sections (blue lines) and fault zones (blue-shaded polygons) of the western Alaska region in the 2023 NSHM for Alaska source model. Fault sections are labeled by name, including abbreviations: C–Chedotlohtna, DM–Dall Mountain, D(CW) Denali (center west), D(C) Denali (center), INF(E)–Iditarod-Nixon Fork (east), INF(C)–Iditarod-Nixon Fork (center), INF(W)–Iditarod-Nixon Fork (west), MC–McLeod Creek, PD–Peters Dome, PP–Purkeypile. Red lines represent the Togiak-Tikchik section of the Denali (Denali TT) in the Quaternary fault database (USGS, 2020), which we do not include as a fault section in the 2023 NSHM update for Alaska due to a lack of evidence for geologically recent surface-rupturing earthquakes (see text). ANC–Anchorage. Base topography and bathymetry from GEBCO (2022).

### 3.5.2 North of the Alaska Range – the Northern Foothills Fold and Thrust Belt

Numerous thrust faults flank the Denali Fault and the Alaska Range (Figs. 11, 13). Identification of specific faults and folds is clearer on the north side of the mountain range, where many young and active faults have been mapped and are collectively referred to as the Northern Foothills fold-and-thrust belt (NFFTB; Bemis et al., 2012). This fold-and-thrust belt extends laterally about 500 km and deforms Pliocene-Pleistocene Nenana Gravel (Bemis et al., 2012; Bemis, 2004, 2010; Bemis and Wallace, 2007; Athey et al., 2006; Nørgaard et al., 2022) and younger deposits across a series of anticlines and synclines. Identified active faults include the Billy Creek, Canteen, Cathedral Rapids, Ditch Creek, Donnelly Dome, Dot “T” Johnson, East Fork, Eva Creek, Glacier Creek, Gold King, Granite Mountain, Healy Creek, Healy, Hunter, Kansas Creek, Macomb Plateau, McGinnis Glacier, Molybdenum Ridge, Mystic Mountain, Panoramic, Park Road, Potts, Red Mountain, Rex, Stampede, Trident, and Trident Glacier Faults, as well as the Kantishna Hills anticline and the Northern Foothills thrust (Bemis et al., 2012).

Little information constrains the rates of deformation or the timing of prehistoric earthquakes on these NFFTB faults. Exceptions are the Healy Fault (Thorson, 1979; Bemis et al., 2010), the Northern Foothills thrust and associated Stampede backthrust (Bemis, 2010; Devore et al., 2012; Koehler et al., 2016), the Dot “T” Johnson Fault (Carver et al., 2008, 2010), and the Cathedral Rapids Fault (Koehler and Woods, 2013). Paleoseismic studies of these faults indicate infrequent earthquakes along individual structures, with events occurring thousands to tens-of-thousands of years apart, which seems consistent with all of these active faults being low slip-rate structures. The oft-cited 1–3 mm/yr estimate of total contraction across the NFFTB (e.g., Bemis et al., 2015; Haeussler et al., 2017) is derived from elevation profiles of landforms and deposits deformed and offset across the Northern Foothills thrust and the Stampede backthrust (Bemis, 2010), and relies on assumed fault dips and untested correlative ages of offset landforms. We cautiously adopt the high end of this rate range given its lack of age or structural control and integration of only two of many mapped faults.

None of the faults have been directly imaged at depth, however the Kantishna Hills structure deserves a special mention. The Kantishna Hills are an actively growing fold at the western edge of Northern Foothills fold-and-thrust belt structures (Bender et al., 2019). There is persistent seismicity concentrated along a gently south-dipping zone at ~10 km depth beneath the Kantishna Hills. A lack of other nearby contractional structures indicates this western edge of the NFFTB localizes strain entirely onto the Kantishna Hills anticline. Bender et al. (2019) dated incised river terraces warped across the fold and interpreted the dates and structure to indicate a total of 1.2 mm/yr of shortening across the structure since ~22 ka. This represents the only direct

geologic constraint on Pleistocene NFFTB deformation rate and is consistent with 1-3 mm/yr rates inferred by Bemis et al. (2015) across the entire NFFTB to the east.

Whether and how these structures connect at depth remain important questions for earthquake hazards. Bemis and Wallace (2007) interpreted structural data and the northward slope of the NFFTB topography to show the thrusts merge into a regional decollement, which dips southward and joins the Cenozoic Hines Creek Fault at ~10 km depth. This hypothesized fault configuration could produce a large earthquake during rupture of the decollement and faults that ramp to the surface. Alternatively, if these contractional faults extend below the brittle-ductile transition and are not connected at depth within the seismogenic zone, then the maximum earthquake magnitude would be significantly lower. The largest historical earthquake attributed to the Northern Foothills thrust was the 1947  $M_w$  7.1 blind thrusting event (St. Amand, 1948; Ruppert et al., 2008), which occurred 10–20 km south of the range front thrust at depths estimated between 6 km (Fletcher & Christensen, 1996) and 26 km (Bondár et al., 2015). The deeper estimate places the source below the Moho in this region (e.g., Miller et al., 2018). In contrast, the shallower depth estimate is broadly consistent with the depth of the hypothesized detachment (cf. Bemis and Wallace, 2007), but cannot independently rule out other fault configurations. Hence, the presence of a regionally extensive decollement that NFFTB faults sole into, possibly linked to the Hines Creek Fault in the seismogenic zone at depth, cannot be ruled out but requires more data to test.

Given limited knowledge of NFFTB deformation rate and structure, we provide two representations of this system in the 2023 NSHM source model to represent epistemic uncertainty (Figure 11). One option places all fault slip on the range-bounding Northern Foothills thrust fault section at the northernmost edge of the fault system at a rate of 3 mm/yr and a fault dip of 45° to the south onto the Foothills fault. Alternatively, we aggregate all of the structures north of the Alaska Range into a single NFFTB fault zone polygon. Although the several hundred km-long range front Northern Foothills thrust is more continuous than NFFTB faults mapped to the south, there is little information to distinguish the activity of one fault from another. Hence, the Northern Foothills fault zone polygon represents the NFFTB as a single region of diffuse deformation (Figure 11) with a net slip rate of 3 mm/yr consistent with total inferred contraction rate of 1-3 mm/yr (Bemis et al. 2015).

In addition to the NFFTB faults, in the Yukon Territory, we are aware of one active fault trace to the north of the Denali Fault – the Decoeli Mountain Fault (Haeussler et al., 2013). This 17-km-long fault lies along a mountain front about 20 km to the northwest of the easternmost part of the Denali Fault and is associated with a ~6-m-tall scarp (Figure 11). Relative motion on the fault is not clear, although evidence suggests an oblique reverse fault. Given the scarp height and deglaciation in the region around 13,000 years ago (Bond and Lipovsky, 2009), slip on this fault could approach 0.5 mm/yr, assuming a 45° dip to the south. This constitutes a local seismic source with a length that could produce a  $M_w$ 6.5 earthquake.

### 3.5.3 North of the Western Alaska Range Thrusts

Between the Kantishna Hills and Denali, the character of the thrusts on the north side of the Denali Fault and the Alaska Range changes significantly (Figure 13). The thrusts are close to the Denali Fault trace, and lie within 4-14 km, whereas the NFFTB thrust front is ~42-85 km from the Denali Fault trace. These ‘North of the Western Alaska Range’ thrusts include: McLeod Creek, Chedotlothna, Peters Dome, Purkeypile, and West Fork of the Kuskokwim thrust faults.

Given the proximity of the thrusts to the Denali Fault, it is reasonable to infer these thrusts likely connect with the Denali Fault near the base of the seismogenic crust. For the 2023 NSHM, we assign a dip of  $45^\circ$  south for these faults and a slip rate of 1 mm/yr, except the Chedotlothna, which we infer a rate of 0.01 mm/yr as its geomorphic expression is much less pronounced.

### 3.5.4 South side of the Alaska Range

The westward-decreasing slip rate along the Denali Fault system (e.g. Haeussler et al., 2017b) implies there are structures on the south side of the Alaska Range that accommodate strain. Perhaps most notable among these is the Susitna Glacier Fault that was discovered after its surface rupture in the M7.9 2002 Denali Fault earthquake (Figure 11; Eberhart-Phillips et al., 2003; Crone et al., 2004). As this fault splays southwesterly off the Denali Fault, it is oriented so that slip along the Denali Fault system should be reduced to the west. Riccio et al. (2014) demonstrated the fault has been active since middle Miocene time using thermochronology data. From paleoseismic trenching, Personius et al. (2017) find a single-earthquake offset of 4.8 m, and infer a slip rate of 1.8 mm/yr from an earthquake recurrence interval of 2270 years. A geometrically similar fault that splays off the Denali Fault is the Broad Pass Fault (Haeussler et al., 2017b). This feature lacks Holocene fault scarps, but geological, structural and geophysical evidence imply its presence, location, and at least Quaternary activity. The presence of the active Pass Creek normal fault to the north of the Broad Pass Fault, was interpreted by Haeussler et al. (2017b) as being related to hanging wall extension associated with thrusting, indicating these two structures are related. They constrained the dip of the Broad Pass Fault to be  $38^\circ$  to the north from where the fault crosses a large river valley. They estimate the slip rate on the Broad Pass Fault to be no higher than 3 mm/yr, and we use their parameters for the 2023 NSHM.

The McCallum Creek thrust fault is the only other contractional structure to the south of the Alaska Range that also appears to splay off the Denali Fault (Waldien et al., 2018). This fault appears to have been active for the last  $\sim 6$  Ma, accommodates contraction perpendicular to the Denali Fault, and Waldien et al. (2018) estimate a slip rate of 0.5-0.6 mm/yr since 3.8 Ma and a dip of  $38^\circ$  to the north, and we use these parameters for the 2023 NSHM.

To summarize, the McCallum Creek, the Susitna Glacier, and the Broad Pass thrust faults splay off, or connect with, the Denali Fault on the south side of the Alaska Range, and they all have low slip rates. Although the westward-decreasing slip rate on the Denali Fault is clear, it seems that additional unidentified structures are likely present on the south side of the range to accommodate and thereby decrease slip of the Denali Fault system. Although we recognize the issue, we do not include additional structures in the 2023 NSHM fault model.

The Susitna basin lies between the Alaska Range and the Castle Mountain Fault, and it has a few low-rate active structures related to contractional deformation (Haeussler et al., 2017a; Figure 11). The longest of these is the Bulchitna Lake Fault that has a 34-km-long north-south striking 3-4 m tall fault scarp. The scarp is adjacent to a 55-km-long feature imaged in seismic reflection data and dips about  $80^\circ$  east (Lewis et al., 2015). Thus, based on moment magnitude scaling relationships, this could produce a  $M_w 6.9-7.1$  rupture. The nearby Kahiltna River Fault is similar in orientation and subsurface length, but has a slightly lower dip of about  $70^\circ$  (Lewis et al., 2015). Other faults with a Holocene scarp in the Susitna basin are significantly shorter, and presumably would be involved in smaller magnitude events (Haeussler et al., 2017b). The only one of these that meets the 5 km minimum length for the 2023 NSHM is the Bunco Lake Fault at the north end of the basin. We infer it is a reverse fault based on its sinuous south-side-up scarp.

None of the faults appear to have a slip rate greater than 0.4 mm/yr based on scarp height and timing of deglaciation.

### 3.6 The Castle Mountain Fault and the Cook Inlet basin

The Castle Mountain Fault is perhaps the most significant crustal fault near Alaska's largest population centers between Anchorage and adjacent communities to the north (Figure 11). We now recognize that Holocene activity on the Castle Mountain Fault is predominantly reverse faulting, not strike-slip, as previously understood and we reduce the slip rate significantly. Aspects of the fault's character are enigmatic. The fault's linear trace (Haeussler, 1998), historical seismicity (Lahr et al., 1986), Riedel shears imaged on LiDAR (Koehler et al., 2014), and long-term geologic history (Trop, 2008) all indicate right-lateral strike slip motion on the Castle Mountain Fault. However, contractional deformation across the fault is indicated by the consistent north-side-up fault scarp, offsets in some paleoseismic trenches, a 4-km-wide anticline adjacent to, and north of, the fault trace identified on seismic reflection profiles. The previous National Seismic Hazard model for Alaska (Wesson et al., 2007) used a slip rate of 3 mm/yr for the Castle Mountain Fault, based on the apparent dextral offset of a post-glacial stream channel (Willis et al., 2007). Koehler et al. (2014) acquired LiDAR over the Castle Mountain Fault and showed that the feature Willis et al. (2007) identified as a channel could not be verified on the LiDAR or in the field. The LiDAR analysis of Koehler et al. (2014) also found no lateral offset of terminal end moraines along the fault. The mapping and trenching of Koehler et al. (2014; 2016) indicates that the fault displaces glacial and Holocene deposits dated to 13.7 kya (Kopczynski et al., 2017) along its entire length with across vertical scarps of 0.5-5 m, from which a vertical slip rate of 0.03-0.4 mm/yr can be inferred. Koehler & Carver (2018) use a rate of 0.5 mm/yr, which is the value we use for the 2023 NSHM. Ziwu et al. (2020) analyzed magnetic and gravity potential field data across the Castle Mountain Fault to demonstrate a dip of 85°–87° north.

In bedrock, the western extension of the Castle Mountain Fault is the Lake Clark Fault (Figure 1). Some prior studies suggested the Lake Clark Fault may have Quaternary activity (see Plafker et al., 1994). Koehler and Reger (2011) reassessed the evidence and re-examined the fault trace, and they concluded there is no evidence for offset of moraines in the last ~70 kya. Haeussler and Waythomas (2011) also examined evidence for surficial offset of a feature along the fault system and found no evidence for Holocene offset. Thus, we remove the Lake Clark Fault from the fault sections for the 2023 NSHM (Figure 2).

The understanding of seismic sources in the Cook Inlet basin has not changed much since the 2007 NSHM (Figures 2, 11). As outlined by Haeussler et al. (2000) and Haeussler and Saltus (2011), a number of fault-cored folds lie beneath the Cook Inlet basin. Some of these appear to be active, have produced historical earthquakes, and could produce up to an M7 earthquake (Haeussler et al. 2000). Given the inferred low slip rates on most structures, for the 2023 NSHM we utilize a fault zone polygon to define the hazard in this region. Three structures at the northeastern end of the basin (Figure 11; Lewis River, Granite Point, North Cook Inlet-SRS) likely have significantly higher slip rates than those elsewhere in the basin, and for the 2023 NSHM we retain these as fault sections and utilize the fault parameters from Haeussler and Saltus (2011).

### 3.7 Fairbanks and North Central Interior Alaska

The bedrock Tintina-Kaltag Fault system (Figs. 1, 2, 13) is analogous to the Denali Fault system in that both dextral fault systems have a similar arcuate trace on a map, both had an important Mesozoic displacement history, and they both were originally more linear fault systems that were subjected to oroclinal bending in earliest Cenozoic time (e.g. Coe et al., 1989; Saltus, 2007; Murphy, 2019 Figure 13). However, the Denali Fault system has relatively high slip rates in Holocene time, and the Kaltag and Tintina Faults show limited and variable evidence for Quaternary faulting at low slip rates. Quaternary fault scarps along the Kaltag and Tintina are separated by about 275 km, and thus we treat these as separate features. The Tintina Fault has weak geomorphic expression and the best available geologic slip rate estimate is  $<0.2$  mm/yr assigned by Koehler et al. (2013) based on the fault's subdued surface expression. We identified some additional scarps along the Medicine Lake-Preacher Fault (Plafker et al., 1994; Bender and Haeussler, 2021), which we ascribe to, and label as, the Tintina Fault system on Figures 1 and 2. This fault is 66-km-long and has scarps  $\leq 5$  m up-to-the-north. The identified scarps cross a surface likely underlain by loess deposited from 19 to 12 kya (Muhs et al., 2018), indicative of a maximum vertical slip rate of 0.3 mm/yr on a vertical fault. There is also seismicity along this section of the fault (e.g. Leonard et al., 2008). We find no evidence for a Quaternary scarp along the southeastern and main part of the Tintina Fault (see also Plafker et al., 1994), nor is there seismicity along this section, and it is not resolved in the geodetic model of Elliott and Freymueller (2020) so we remove it from our compilation. Leonard et al. (2008) estimate a slip rate of 0.5 mm/yr from earthquake catalog statistics from within the Yukon, which is the value we use for the 2023 NSHM.

West of the Tintina Fault, clear scarps delineate the Kaltag Fault (Koehler & Carver, 2018). Using recent high-resolution digital topography, we improved on the mapping of the Kaltag Fault (Figure 3; Bender and Haeussler, 2021), but no firm geologic constraints on the Kaltag Fault slip rate yet exist. The Koehler (2013) Quaternary fault and fold database assigned a rate of  $< 0.2$  mm/yr. As described, our practice for the 2023 NSHM is to use the lowest value of a rate bin for the slip rate, which in this case is 0.01 mm/yr, and is the rate we use in the 2023 NSHM. Despite this conservative estimate, we suspect a higher slip rate based on prominent fault scarps (Figure 3). Moreover, Elliott and Freymueller (2020) utilized geodetic data for a block model, which describes the fault as having 2.1 mm/yr dextral slip on the fault as well as 0.6 mm/yr of normal motion. A prominent south-side-up Kaltag Fault scarp east of Norton Sound (Figure 13; Plafker et al., 1994) is consistent with the component of normal motion implied by geodesy. Additional work is needed to clarify the Quaternary slip rate of this important and poorly understood fault.

The last of the major bedrock right-lateral strike slip faults is the Iditarod-Nixon Fork Fault system of western Alaska (Figure 13), which shares similarities with Kaltag or western Denali Faults in orientation and parts of its bedrock history (e.g. Murphy, 2019). Tape et al. (2017) argue a 1904  $M_s 7.3$  earthquake occurred along this fault zone. The fault is shown to be about 355-km long in our model, but only a 113-km-long stretch of the Iditarod-Nixon Fork Fault system has a clear scarp on the ArcticDEM that cuts Quaternary sediments (Bender and Haeussler, 2021). Given the relatively weak expression of the scarp in older Quaternary sediments, the fault likely has a very low slip rate. For the 2023 NSHM, we use the lowest slip rate bound from Koehler et al. (2012) of 0.01 mm/yr. Two additional fault strands occur southwest of the Iditarod-Nixon Fork Fault (Bender and Haeussler, 2021). We refer to the

northeastern scarp as the Paimiut-east Fault, which is about 29 km long, and the southwest scarp as the Paimiut-west Fault, which is about 92 km long. Both scarps persistently express north-side-up throw of several meters where they cross-cut the Yukon-Kuskokwim River delta. The continuous bedrock geology between these scarps and the Iditarod-Nixon Fork Fault (see compilation of Wilson, 2006) does not support a simple linkage. Rather, they appear to be right step overs in a larger dextral shear system. The apparent lack of fault connection also implies the total amount of strain is low. GNSS geodetic data do not indicate measurable dextral shear across this fault system (see Elliott & Freymueller, 2020).

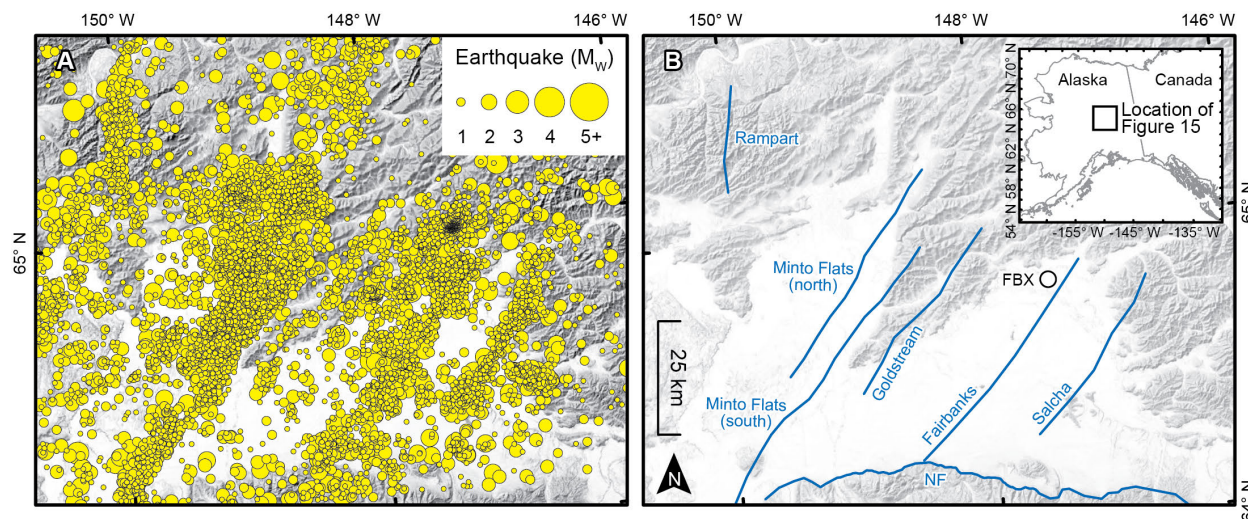


Figure 14. Seismicity lineaments of the Rampart, Minto Flats, Goldstream, Fairbanks, and Salcha seismic zones, near Fairbanks (FBX). A) shows earthquakes with yellow dots, B) shows inferred structures along which the seismicity occurs with blue lines. NF—Northern Foothills Fault.

The Rampart, Minto Flats, Fairbanks, and Salcha seismic zones all lie in central Alaska and north of the Alaska Range in the region near Fairbanks (Figs. 1, 2, 14). These seismic zones are all defined by northeast-trending belts of seismicity, and all have earthquake focal mechanisms indicating left-lateral strike-slip faulting (Figure 14; Ratchkovski and Hanson, 2002). These four seismic zones are well-documented (e.g. Ruppert et al., 2008), and we include an additional one defined by a parallel linear band of seismicity – the Goldstream seismic zone (Figure 14). Four M6.0+ earthquakes have occurred along these features: the 1937 M7.3 Salcha earthquake, the 1968 M7.1 Rampart earthquake, the 1985 M6.1 Dall City earthquake, and the 1995 M6.0 Minto Flats earthquake. Despite the abundance of seismicity and the certainty that there must be causative faults for the earthquakes, there are no identified surface traces for any of these features, except possibly along the Salcha seismic zone. In the epicentral region of the 1937 M7.3 earthquake along the Salcha seismic zone, there is a northeast trending line of more than 11 aligned and elongate mounds (Koehler & Carver, 2018). The mounds' origin seems related to periglacial processes, however their linear arrangement is unusual and indicative of an underlying structure consistent with a sinistral strike-slip fault trace. Of the five features, the Minto Flats seismic zone has been the focus of the most research. The seismic zone consists of two fault strands separated by 10 km. The deepest part of the Nenana sedimentary basin lies between these two fault strands and is up to 8-km-deep as delineated from seismic reflection

profiling (Tape et al., 2013, 2015). The basin appears to be the product of ongoing left-transensional tectonics. Tape et al. (2015) infer the zone is capable of producing M7.0-7.5 earthquakes, and we use their fault parameters of an 80° west dip and slip rate of 2 mm/yr for the 2023 NSHM. Due to the abundance of seismicity, we include the other seismic zones (Rampart, Fairbanks, Salcha, and Goldstream) in the 2023 NSHM as linear features. With no geological information other than their inferred length from the seismicity, we assign a nominal slip rate of 0.01 mm/yr indicating they are active, but we have no geologic information on slip rate. We infer the hazard of these seismic zones should be incorporated through the regional seismicity catalog.

The overall tectonic setting of these northeast-trending left-lateral seismic zones (Minto Flats, Rampart, Fairbanks, Salcha, Goldstream) is well explained by the tectonic model of Page et al. (1995), in which there is right shear between the Denali Fault and the Kaltag-Tintina Fault system (Figure 15). As discussed above, the Kaltag, Tintina, and Denali are some of the most important dextral faults in the history of the region (e.g. Murphy, 2019), and there is some evidence for Holocene faulting on both fault systems. The Kaltag and Tintina have diffuse seismicity indicative of dextral strike-slip faulting and each has produced one historical M5+ earthquake. Expansion of seismic monitoring in the last decade better delineates the seismicity along the Tintina Fault in particular (Buurman, 2018). Although both faults have Quaternary fault scarps, there is not a clear connection between the two as the scarps are 280 km apart (Koehler & Carver, 2018; Reifentstahl et al. 1997; Weber and others, 1992). Regardless of these details, the northeast-trending left-lateral seismic zones (and their faults) likely result from large-scale block rotation and right-shear between the Denali and the Tintina-Kaltag Faults (Figure 15). The north-side-up Medicine Lake-Preacher scarp implies local extension along the Tintina Fault, perhaps due to the extension predicted by the ‘bookshelf’ model of faulting to the south. Given the low modern slip rates on the Tintina (0.3 mm/yr) and Kaltag Faults (0.01 mm/yr), the rate of significant earthquakes (M7+) should be small.

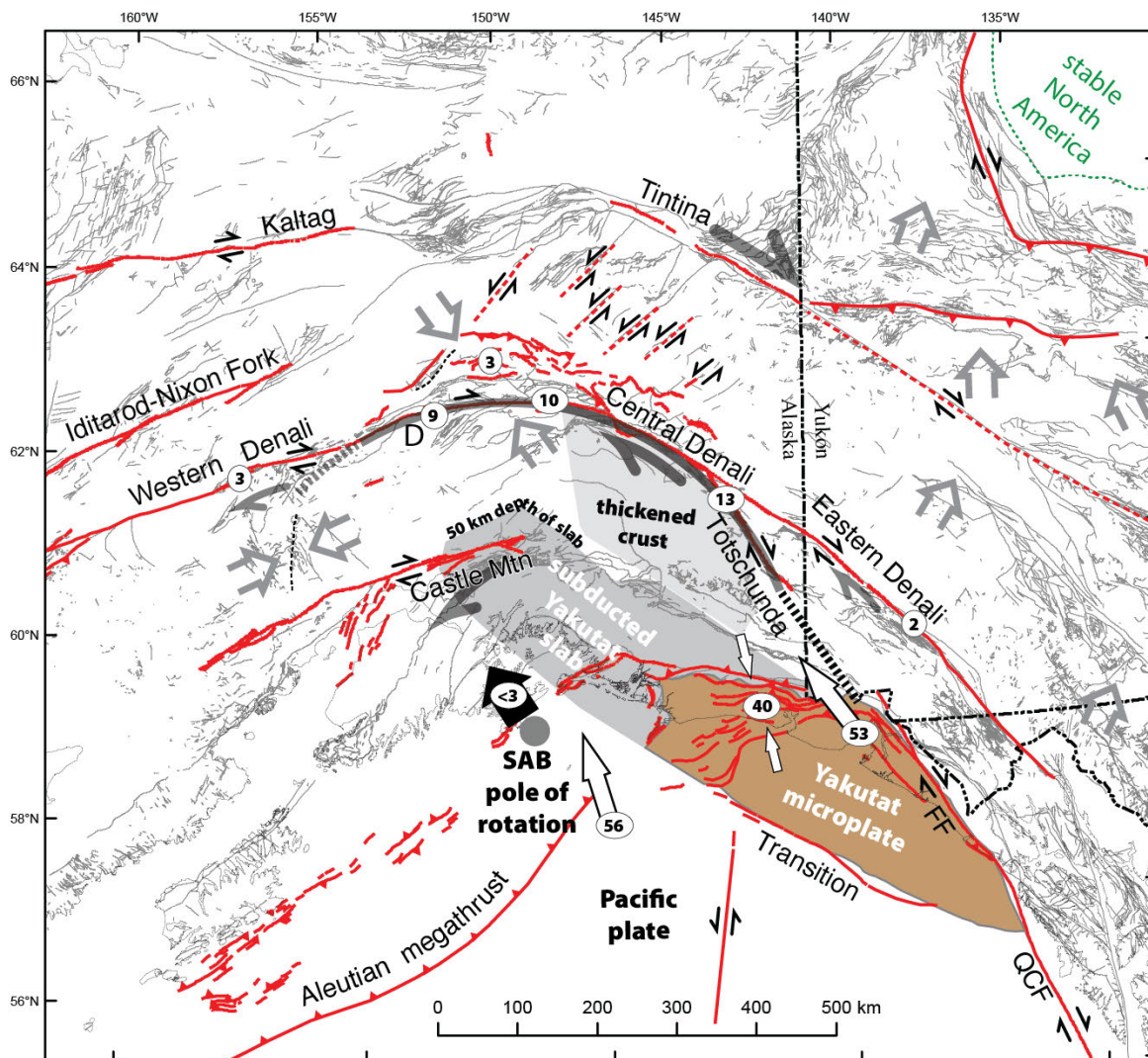


Figure 15. Preferred tectonic model for southern Alaska modified from Haeussler et al. (2017b, Figure 8D). The region south of the Denali Fault is referred to as the southern Alaska block (SAB), and this model has a combination rotation and indentation and extrusion as indicated by the arrows. The base map shows active faults with red lines (modified from Koehler, 2013). All known bedrock faults are shown as thin grey lines. The Yakutat microplate is brown, the subducted part is shaded dark grey. Grey arrows show the inferred movement directions. Active, or proposed active, faults in the Yukon are shown and come from Leonard et al. (2007). Abbreviations: D – Denali (the mountain); FF - Fairweather Fault; QCF - Queen Charlotte Fault. Circles with numbers inside are velocities (mm/yr) from GPS geodesy (Elliott et al. 2013; Marechal et al. 2015), or strike-slip rates along the Denali Fault from Haeussler (2017b). White arrows give GPS velocity (mm/yr) with respect to North America, or where two arrows point toward a white circle with a number, it indicates the amount of contraction. Open grey arrows show schematic motion; directions in Yukon from Leonard et al. (2008). Blue lines show  $\sigma_1$  orientation from GPS model of Marechal et al. (2015).

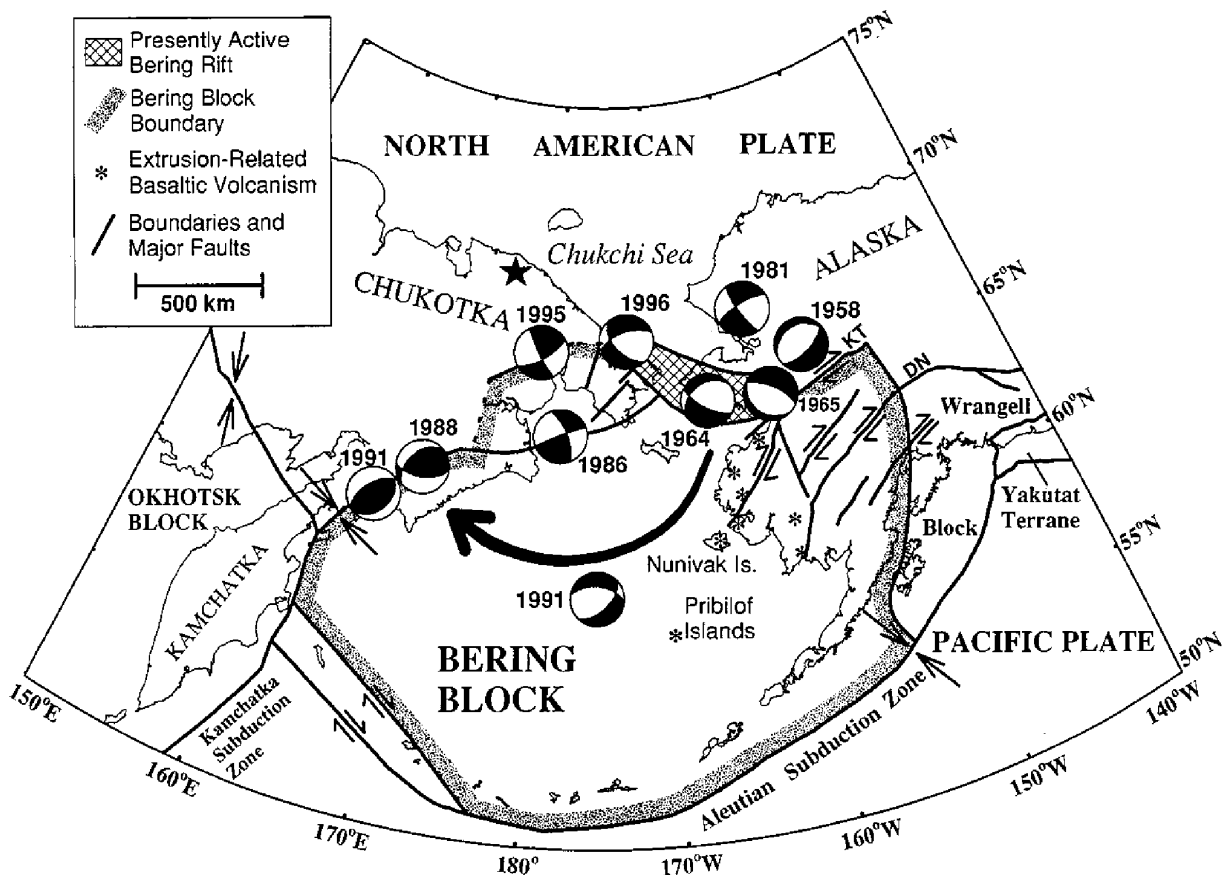


Figure 16. Tectonics of the Bering Sea region from Mackey et al. (1997). Representative focal mechanisms are shown in lower-hemisphere projections with compressional quadrants colored black with year of earthquake. Relative motion between Bering block and North America is shown by large arrow, with star representing Euler pole. DN is Denali Fault.

### 3.8 South of the Brooks Range and North of the Kaltag-Tintina Faults

A few scattered fault scarps have been found south of the Brooks Range in a region that is about the size of California (Figs 1, 2). Starting from the west, the Kigluaik and Bendeleben Faults on the Seward Peninsula (Figure 13) are located almost along strike from each other, both are normal faults, and they accommodate regional north-south extension also indicated by regional seismicity (Figure 16; Mackey et al., 1997). The 62-km-long Kigluaik Fault dips south and is located on the north side of the Kigluaik Mountains, and the 45-km-long Bendeleben Fault dips north and is located on the south side of the Bendeleben Mountains. Koehler et al. (2012) estimate the slip rate from published data as 0.2 to 1 mm/yr. As described in the methods section, we use the lower rate for the 2023 NSHM when we are using a rate from a rate bin.

The Pivot Fault lies east of the Kigluaik and Bendeleben Faults, and southwest of the village of Huslia (Figure 13). The fault was identified on the Plafker et al. (1994) active fault map, but was not identified on Koehler et al.'s (2012) map of active folds and faults. The new ArcticDEM images convinces us that this is likely an active fault, because there is a linear south-

side-up 34-km-long scarp, which displaces ponded periglacial lowland surfaces. The scarp is parallel to bedrock structure to the northeast and southwest, but there is no indication of bedrock outcrops in the region of the scarp. The scarp is also subparallel to the Kaltag Fault that lies about 75 km to the south. The age of the affected surfaces is unclear, but we assume it is Quaternary. The consistent sense of offset suggests it is a normal fault, like the Seward Peninsula faults and the Purcell Mountains Fault (described next). We ascribe the lowest slip-rate category for this fault for the 2023 NSHM.

The Purcell Mountain Fault is located on the south flank of the Purcell Mountains and lies about 45 km north of the village of Huslia (Figure 13). We recognized this fault scarp using the Arctic DEM during the 2019-2020 Purcell Mountain swarm (<https://earthquake.alaska.edu/event/0192zumrhu/aftershocks>, last accessed 11 July 2022) in which 29 earthquakes greater than magnitude 4 were measured. The scarp is 32-km long and is somewhat sinuous with the appearance of a typical normal fault. Offsets are south-side-down and offset the Quaternary-age surface except for alluvium in stream drainages. There was an M7.3 earthquake in the region in 1958 (Fletcher and Christensen, 1996), and it is conceivable that it occurred on, or in the region of this fault. For the 2023 NSHM, we infer a slip rate of 0.2 mm/yr, given the uncertainties in the age of the offset surface. We are unaware of any evidence that the 2019-2020 earthquake swarm resulted in surface offset on this fault.

The Kanuti Fault was first identified by Brogan et al. (1975) as a 40-km-long north-side-down normal fault (Figure 13). ArcticDEM hillshade images show a scarp along about a 20-km length of the feature, which offset the Quaternary hillslope deposits and some older alluvial deposits, but not the youngest alluvium. Brogan et al. (1975) report scarp heights of 3-10 m. Given the similarity in appearance to the Purcell Mountain and Dall Mountain Fault, we infer a slip rate of 0.2 mm/yr for the 2023 NSHM.

The Dall Mountain Fault is located at the western side of the Yukon Flats (Figure 13). The scarp strikes north-south, is on the west side of Dall Mountain, is about 30-km long, and offsets the bedrock or thin colluvium with west-side-down normal offsets (Koehler and Carver, 2018). Koehler et al. (2012) ascribed a slip rate of less than 0.2 mm/yr, which is the value we use for the 2023 NSHM.

East of the Dall Mountain Fault, in the northwestern part of the Yukon Flats are 7 east-northeast trending scarps that are 6 to 30-km-long that offset river alluvium or Quaternary surficial deposits (Figure 13; Bender and Haeussler, 2021). We refer to these as the Stevens Faults as these are located near the village of Stevens. These scarps have not appeared in prior active fault compilations, and only became apparent to us through examination of the ArcticDEM images. Together, the scarps have a horst-and-graben appearance, indicating north-south extension across this region, and that these are normal faults. We observe that an older generation of Yukon River meanders incises the uplifted blocks between scarps, which is consistent with Quaternary faulting. We infer a slip rate of 0.01 mm/yr for the 2023 NSHM, based on the lowest slip rate category in Koehler et al. (2012).

### 3.9 Northeastern Arctic Coastal Plain

A map of seismicity of Alaska shows a band of small earthquakes in the northeastern Brooks Range, which had been thought to present a relatively minor earthquake hazard. However, no previous active fault compilations included any structures in the region, with the

exception of Marsh Creek anticline, discussed below (Figs. 1, 2). The 2018 Kaktovik earthquake sequence provides evidence that this region can have significant earthquakes. A  $M_w$ 6.4 and  $M_w$ 6.0 earthquake occurred 6 hours apart on August 12<sup>th</sup>, and these are the two largest earthquakes ever recorded in the Brooks Range. A combination of earthquake aftershocks and InSAR and Sentinel-1 SAR data shows that the main rupture was right-lateral strike-slip on an east-west fault that had previously been a thrust or reverse fault (Gaudreau et al., 2019; Xu et al., 2020). We use these geophysical constraints on the underlying geologic fault. For the 2023 NSHM, we utilize the fault parameters from Xu et al. (2020; their two fault model), which defines the fault as having a dip of  $69^\circ$  to the south and a slip rate of 0.1 mm/yr. The right-lateral strike slip on this east-west striking fault plane was not expected by any tectonic model (e.g. Mazzotti et al. 2008), showing us we have more to learn about this region. Prior interpretation of moment tensor solutions suggested there would be left-lateral slip on a north-northeast-south-southwest striking fault plane. Given the presence of a north-south belt of seismicity in the region, the east-west striking Kaktovik Fault plane appears to be evidence of sinistral wrench faulting (see Gaudreau et al., 2019) rather than faulting along a north-south striking sinistral fault system.

Several other features north of the northeastern Arctic Coastal Plain have been identified as potential earthquake sources. These include the Marsh Creek anticline and the Camden Bay faults and folds (Figure 2). The Marsh Creek anticline has long been identified as a northeast-plunging fold, and late Neogene to Quaternary motion on the structure is indicated by steep dips in Pliocene rocks and warped Pleistocene river terraces, and interpretations of drainage patterns (see Burbank et al., 1996). For the 2023 NSHM, we utilize the fault geometry of a  $65^\circ$  south dip from Leiggi (1987) and for the slip rate, the lowest slip rate bin from Koehler et al. (2012).

The Camden Bay Faults and anticlines lie offshore in the Beaufort Sea (Figures 1, 2). Using seismic reflection data, Grantz et al. (1994) noted a region 60 km long and 30 km wide in the nearshore region of the Beaufort Sea that is unusually devoid of Holocene sediment, and which correlates with a region of sparse seismicity. They interpret this uplifted region as the Camden Bay anticline, which appears as an uplifted block of Tertiary and Quaternary sediment on top of a basement high. Faults in the anticline dip steeply north and have normal offsets. Grantz et al. (1994) also find some of these faults cut Holocene sediments and may be driven by gravity. For the 2023 NSHM, we use the fault parameters in Koehler et al. (2012).

#### **4 Discussion and conclusions**

This active crustal fault model for the 2023 National Seismic Hazard Model for Alaska has considerably more resolution and refinement from the 2007 hazard map (Figure 2). This fault model has 105 (vs 17 previously) fault sections. Some significant differences from the prior map are: (1) improved mapping of megathrust splay faults at the eastern end of the Alaska-Aleutian subduction zone, (2) a higher (53 mm/yr) slip rate on the Queen Charlotte Fault indicating this transform fault takes up virtually all of the plate boundary deformation in southeastern Alaska, (3) improvements in the mapping and characterization of active structures in the Chugach-St. Elias orogen, (4) recognition of the Castle Mountain Fault as a dominantly contractional low slip-rate reverse fault, (5) evidence for significant earthquakes in the eastern Brooks Range, (6) removal of the easternmost (Chatham Strait) Denali Fault system, and (7) addition of a Connector Fault between the Fairweather Fault system and the Totschunda Fault.

Our crustal model corroborates the existing paradigm that the collision of the Yakutat microplate into the southern Alaska margin, along with the accompanying flat slab subduction, drives most of the crustal faulting in Alaska (Haeussler et al., 2000, 2008, Finzel et al., 2011; Jadamec et al., 2013). There are some details of this understanding that have changed, which we outline below.

The lack of any recognized active structures east of the Queen Charlotte Fault system (Figure 9) is consistent with the idea that essentially all of the Pacific-North America plate motion is on the Queen Charlotte Fault. This is also consistent with the lack of evidence for activity on the Chatham Strait Fault, which we removed from the active fault list. As mentioned, geodetic vectors in British Columbia differ from those in southeastern Alaska, indicating some deformation between the two regions. However, it is unresolved as to where that deformation is taking place and on what structures.

The Yakutat microplate collision drives the deformation on the Denali Fault system and into interior Alaska (Figs. 10, 15, 17). As the Denali Fault is the principal active structure in central interior Alaska along which this occurs, the region south of the Denali Fault has been referred to as the southern Alaska block. Haeussler et al. (2017b) explored several end-member tectonic models for the neotectonics of southern Alaska, which include rotation, indentation, and extrusion of the southern Alaska block. However, none of the end-member models explain the location, rates, and types of faulting. They concluded that a combination of different amounts of all three mechanisms are operating concurrently (Figure 15).

We find no evidence for activity on the Togiak-Tikchik segment of the Denali Fault system, and we remove it from the active fault database (Figs. 1, 13). The orientation of the Togiak-Tikchik segment is also not consistent with other active faults in southwestern Alaska. However, we note the presence of the Atsakovluk Fault at the western end of the Denali Fault system (Figure 13), which appears to be a stepover. This and other nearby low-slip-rate faults on the western part of the Denali Fault system indicate strain is dissipating westward on the Denali Fault system. An unresolved issue is the geodetic evidence for motion along a westward extension of the Denali Fault system through the Kilbuck mountains. No geologic evidence has yet been found to support such a feature.

Deformation in western Alaska seems to be explained well by the tectonic model of Mackey et al. (1997) with a clockwise-rotating “Bering Block” (Figure 16). Diffuse seismicity with a mixture of strike-slip and normal focal mechanisms initially led to the development of this idea, but it is also consistent with the geodetic data (Cross and Freymueller, 2008; Freymueller et al., 2008; Elliott and Freymueller, 2020), and the mixture of southwest-striking dextral fault scarps with shorter and variable orientation normal fault scarps discussed in this paper. There is no evidence for crustal shortening in western Alaska.

We highlight the presence of the Paimiut scarps in the Yukon-Kuskokwim (YK) River delta, which lie along the general trend of the Iditarod-Nixon Fork Fault (Figure 13). These faults support the idea that dextral shear is propagated into the YK river delta region. As these faults do not directly connect to the Iditarod-Nixon Fork Fault, but appear to be stepovers, strain does not appear to be high. Thus, the Iditarod-Nixon Fork Fault system, as well as the Denali Fault system, does propagate strain into western Alaska. These observations support the idea of limited far field deformation of the region driven by the Yakutat microplate collision, but it does not support the idea of large-scale extrusion of western Alaska.

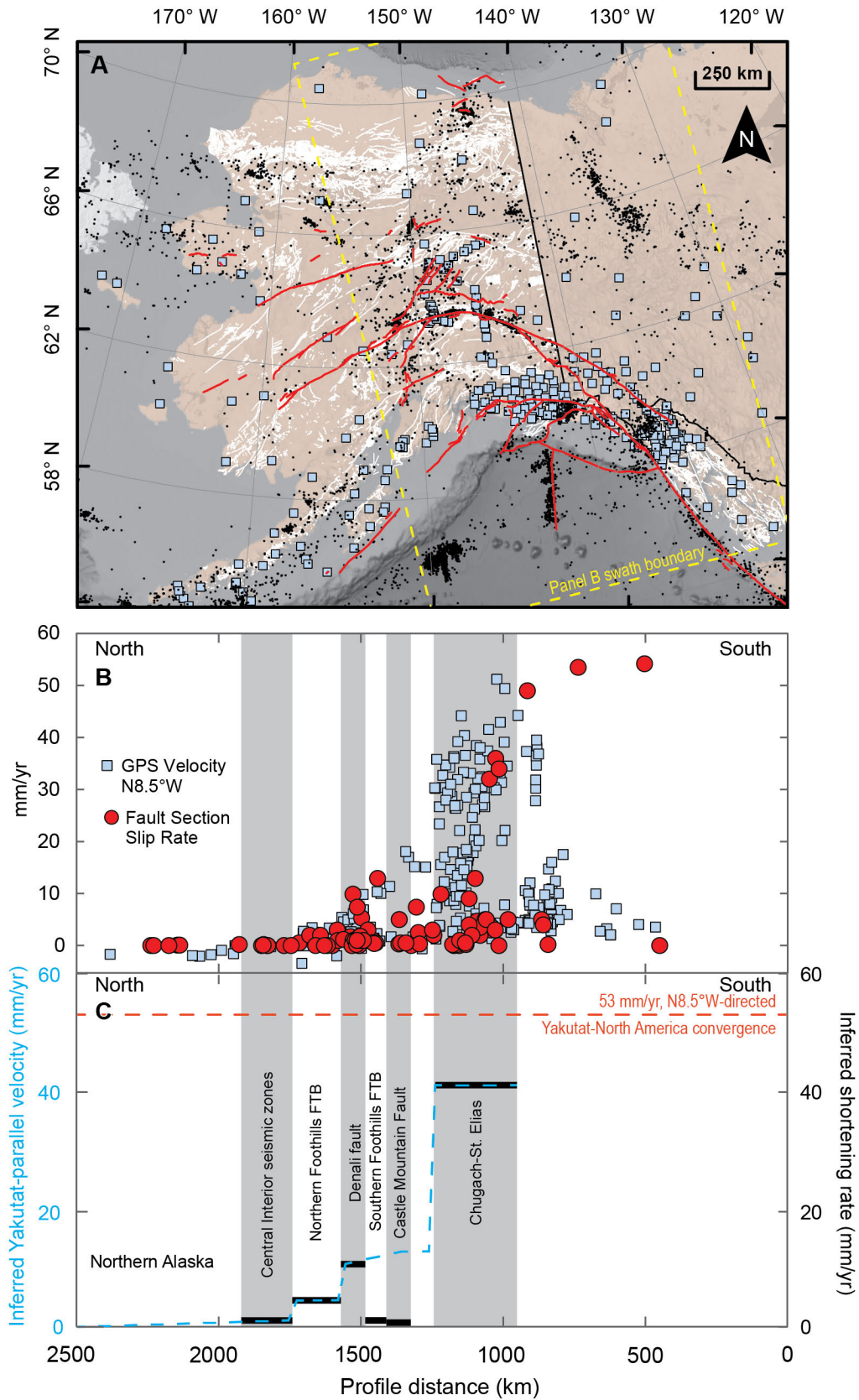


Figure 17. Map and active crustal deformation rate profiles from the Yakutat microplate to the north slope of Alaska. A) Fault sections of Alaska and Yukon are shown in red (Bender et al., 2021), bedrock faults are shown in white (Wilson et al., 2015), GNSS stations are shown with light blue squares (Elliott and Freymueller, 2020), and earthquake epicenters are black dots (<https://earthquake.alaska.edu/>). B) Swath profile of fault section slip rates (red dots, Bender et al., 2021) and geodetic velocities (light blue squares; Elliott and Freymueller, 2020) within the yellow dashed box in (A), with south on the right and north on the left. C) Inferred shortening and crustal velocity rates parallel to Yakutat microplate convergence direction across the deforming zones of Alaska. This plot is adapted and modified from Koehler and Carver (2018, Figure 20) with values from this paper.

Future refinements to an active fault map of Alaska that can be integrated into improved seismic hazard maps will undoubtedly reduce the uncertainty in hazard maps for Alaska. The seismic hazard of the state is dominated by the plate boundary faults – the subduction megathrust and the Queen Charlotte-Fairweather transform fault. However, the greatest uncertainties in our understanding of the neotectonics are where slip rates are low, fault systems are diffuse, and where distributed deformation may mask our abilities to see surface deformation. The work to characterize the seismic hazard of Alaska is far from complete.

This compilation of active structures in Alaska reinforces the idea that the collision of the Yakutat microplate into the southern Alaska margin is distributed over more than a thousand kilometers into the northeastern Brooks Range (Figure 17). Our work agrees with the conclusions of Koehler and Carver (2018) in showing that most of the 53 mm/yr rate of the Yakutat collision is accommodated within the St. Elias orogen, and by the Denali Fault system (Figure 15) with the remainder distributed across a 1000-km-wide region across the state. Most of the population of Alaska is along the Pacific margin, as is most of the seismic hazard of the state.

## Acknowledgements

This paper would not have come to fruition without the productive conversations and collaborations with numerous people, including, but not limited to: Rob Witter, David Schwartz, Ari Matmon, Lee Liberty, Phil Armstrong, Richard Lease, George Plafker, Gary Carver, Jeff Freymueller, Julie Elliott, Natalia Ruppert, Diane Doser, Terry Pavlis, Eva Enklemann, Ron Bruhn, Sean Bemis, Sean Gulick, Maureen Walton, Nathan Miller, Nore Praet, Maarten Van Daele, Gordon Seitz, Rob Wesson, and many others. Excellent reviews by Rob Witter, Mike West, and Chris DuRoss substantially improved the manuscript – we are very grateful. Any use of trade, firm, or product names is for descriptive purposes only and does not imply endorsement by the U.S. Government.

## Availability Statement

All data used for this paper are publicly available, and the data are referenced in the paper. Topographic data for the ArcticDEM are from Porter et al. (2018). The Alaska Quaternary fault and fold database is from Koehler et al. (2012) and Koehler (2013). New fault trace mapping is in Bender & Haeussler (2021). The derived fault sections and fault zone polygons and their attributes are in Bender et al. (2021).

Table 1.

*Table of Fault Sections and Attributes for the 2023 NSHM*

Name	State	Rate [mm/yr]	Rate reference or source	Fault type	Dip [°]	Dip direction	Lower depth [km]	Depth reference
Atsakovluk	AK	0.01	nominal assigned value	dextral?	90	V	15	nominal assigned value
Bagley (east)	AK	4	Berger et al. (2008a)	reverse	45	N	15	nominal assigned value
Bagley (middle)	AK	1	nominal assigned value	reverse	45	N	15	nominal assigned value
Bagley (west)	AK	0.2	QFFD slip rate bin lower bound	reverse	45	V	15	nominal assigned value
Bancas Point	AK	3	QFFD slip rate bin lower bound	reverse	45	N	15	nominal assigned value
Bendeleben	AK	0.2	QFFD slip rate bin lower bound	normal	60	S	15	nominal assigned value
Bering Glacier	AK	9	see Bender et al. (2021)	reverse	45	NW	15	nominal assigned value
Billy Creek	AK	0.01	QFFD slip rate bin lower bound	reverse	60	W	15	nominal assigned value
Boundary	AK	3	Enkelmann et al. (2015a)	reverse	85	NE	15	nominal assigned value
Broad Pass Thrust	AK	3	Haeussler et al. (2017a)	reverse	60	NW	20	Haeussler et al. (2017a)
Bulchitna Lake	AK	0.3	Haeussler et al. (2017a)	reverse	45	W	15	nominal assigned value
Bunco Lake	AK	0.4	QFFD slip rate bin lower bound	reverse	45	S	15	nominal assigned value
Camden Bay (east)	AK	0.01	QFFD slip rate bin lower bound	reverse	45	S	15	nominal assigned value
Camden Bay (west)	AK	0.01	QFFD slip rate bin lower bound	reverse	45	S	15	nominal assigned value
Canteen	AK	1.6	Bemis et al. (2012)	dextral	90	V	15	nominal assigned value
Cape Cleare	AK	2	Liberty et al. (2019)	reverse	45	NW	15	nominal assigned value
Castle Mountain	AK	0.5	Koehler & Carver (2018)	reverse	85	NE	14	Ziwu et al. (2020)
Cathedral Rapids	AK	1	QFFD slip rate bin lower bound	reverse	45	S	15	nominal assigned value
Chedotlothna	AK	0.01	QFFD slip rate bin lower bound	reverse	45	S	15	nominal assigned value
Chirikof	AK	0.5	nominal assigned rate	normal	60	SE	15	nominal assigned value
Chugach - St.Elias	AK	4	Chapman et al. (2012)	reverse	45	NW	15	nominal assigned value
Connector (inferred)	AK	12.9	see Bender et al. (2021)	dextral	85	V	15	nominal assigned value

Cordova	AK	0.01	QFFD slip rate bin lower bound	reverse	45	SE	15	nominal assigned value
Council	AK	0.01	nominal assigned value	normal	60	W	15	nominal assigned value
Dall Mountain	AK	0.2	QFFD slip rate bin lower bound	normal	60	W	15	nominal assigned value
Decoeli Mountain	YT	0.5	nominal assigned value	reverse?	45	SW	15	nominal assigned value
Denali (Boss Creek)	AK	0.2	QFFD slip rate bin lower bound	dextral	90	V	15	nominal assigned value
Denali (center, east)	AK	12.9	Haeussler et al. (2017b)	dextral	90	V	15	nominal assigned value
Denali (center, middle)	AK	7.4	Haeussler et al. (2017b)	dextral	90	V	15	nominal assigned value
Denali (center, west)	AK	9.9	Haeussler et al. (2017b)	dextral	90	V	15	nominal assigned value
Denali (east, middle)	YT	2	Haeussler et al. (2017b)	dextral	90	V	15	nominal assigned value
Denali (east, north)	YT	5	QFFD slip rate bin lower bound	dextral	90	V	15	nominal assigned value
Denali (east, south)	YT	0.01	nominal assigned value	dextral	90	V	15	nominal assigned value
Denali (Holitna)	AK	0.2	QFFD slip rate bin lower bound	dextral	90	V	15	nominal assigned value
Denali (west)	AK	5.3	Haeussler et al. (2017b)	dextral	90	V	15	nominal assigned value
Donnelly Dome	AK	1	QFFD slip rate bin lower bound	reverse	45	S	15	nominal assigned value
DOT T Johnson	AK	1	QFFD slip rate bin lower bound	reverse	45	S	15	nominal assigned value
Duke River	YT	9.9	see Bender et al. (2021)	reverse	45	S	15	nominal assigned value
Esker Creek	AK	5	Enkelmann et al. (2015a)	reverse	45	NE	14	Chapman et al. (2012)
Etches	AK	0.01	QFFD slip rate bin lower bound	reverse	45	N	15	nominal assigned value
Fairbanks (seismicity)	AK	0.01	nominal assigned rate	sinistral	90	V	15	nominal assigned value
Fairweather (north)	AK	36	Brothers et al. (2020)	dextral	88	V	15	nominal assigned value
Fairweather (south)	AK	49	Brothers et al. (2020)	dextral	85	W	15	nominal assigned value
Foreland Thrust (Khitrov)	AK	34	see Bender et al. (2021)	reverse	45	N	15	nominal assigned value

Foreland Thrust (Pamplona)	AK	32	see Bender et al. (2021)	reverse	45	N	12	nominal assigned value
Goldstream (seismicity)	AK	0.01	nominal assigned rate	sinistral	90	V	15	nominal assigned value
Granite Mountain (east)	AK	0.2	QFFD slip rate bin lower bound	reverse	45	SW	15	nominal assigned value
Granite Mountain (west)	AK	0.2	QFFD slip rate bin lower bound	reverse	60	SE	15	nominal assigned value
Granite Point	AK	2.5	Haeussler & Saltus (2011)	reverse	45	SE	15	nominal assigned value
Gulf of Alaska	AK	0.2	Enkelmann et al. (2015a)	dextral	90	NE	15	nominal assigned value
Hanning Bay	AK	0.2	QFFD slip rate bin lower bound	reverse	45	N	15	nominal assigned value
Icy Point-Lituya Bay	AK	5	Lease et al. (2021)	reverse	50	N	15	nominal assigned value
Iditarod - Nixon Fork (center)	AK	0.01	QFFD slip rate bin lower bound	dextral	90	V	15	nominal assigned value
Iditarod - Nixon Fork (east)	AK	0.01	QFFD slip rate bin lower bound	dextral	90	V	15	nominal assigned value
Iditarod - Nixon Fork (west)	AK	0.01	QFFD slip rate bin lower bound	dextral	90	V	15	nominal assigned value
Kahiltna River	AK	0.5	Haeussler et al. (2017a)	reverse	45	W	15	nominal assigned value
Kaktovik (east)	AK	0.1	Xu et al. (2020)	reverse	32	W	15	nominal assigned value
Kaktovik (west)	AK	0.1	Xu et al. (2020)	dextral	69	S	15	nominal assigned value
Kaltag	AK	0.01	QFFD slip rate bin lower bound	dextral	90	V	15	nominal assigned value
Kantishna Hills (north)	AK	1	QFFD slip rate bin lower bound	thrust	5	S	10	nominal assigned value
Kantishna Hills (south)	AK	1.2	Bender et al. (2019)	thrust	5	S	10	nominal assigned value
Kanutu	AK	0.1	nominal assigned rate	normal	60	NW	15	nominal assigned value
Kayak	AK	3.5	QFFD slip rate bin lower bound	reverse	60	NW	15	nominal assigned value
Kigluaik	AK	0.2	QFFD slip rate bin lower bound	normal	60	N	15	nominal assigned value
Lewis River	AK	0.01	QFFD slip rate bin lower bound	reverse	45	W	15	nominal assigned value
Malaspina	AK	5	Enkelmann et al. (2015a)	thrust	20	N	15	nominal assigned value

Marsh Creek	AK	0.01	nominal assigned rate	reverse	65	S	15	nominal assigned value
McCallum Creek	AK	0.6	Waldien et al. (2018)	thrust	35	N	15	nominal assigned value
McLeod Creek	AK	1.7	Burkett et al. (2016)	reverse	45	S	15	nominal assigned value
Middle Fork	AK	1	nominal assigned value	reverse	45	SE	15	nominal assigned value
Minto Flats (north)	AK	2	Tape et al. (2015)	sinistral	80	W	19	Tape et al. (2015)
Minto Flats (south)	AK	2	Tape et al. (2015)	sinistral	80	W	14	Tape et al. (2015)
Montague Strait	AK	0.2	Haeussler et al. (2015)	reverse	61	E	15	nominal assigned value
Narrow Cape	AK	3.3	QFFD slip rate bin lower bound	reverse	60	NW	15	nominal assigned value
Natazhat	AK	3	Marechal et al. (2018)	reverse	45	S	15	nominal assigned value
North Cook Inlet - SRS	AK	0.3	Haeussler & Saltus (2011)	reverse	45	NW	15	nominal assigned value
Northern Foothills	AK	3	Bemis et al. (2015)	reverse	45	S	15	nominal assigned value
Paiumiut (east)	AK	0.01	nominal assigned rate	dextral?	90	V	15	nominal assigned value
Paiumiut (west)	AK	0.01	nominal assigned rate	dextral?	90	V	15	nominal assigned value
Pass Creek	AK	0.5	Haeussler et al. (2017a)	normal	38	NW	15	nominal assigned value
Patton Bay	AK	2	Liberty et al. (2019)	reverse	45	N	15	nominal assigned value
Peters Dome	AK	1	QFFD slip rate bin lower bound	reverse	45	S	15	nominal assigned value
Pivot	AK	0.01	QFFD slip rate bin lower bound	normal	90	V	15	nominal assigned value
Purcell Mountains	AK	0.2	QFFD slip rate bin lower bound	normal	60	S	15	nominal assigned value
Purkeypile	AK	1	nominal assigned rate	reverse	45	SE	15	nominal assigned value
Queen Charlotte (center)	AK	54.2	Brothers et al. (2020)	dextral	90	V	15	nominal assigned value
Queen Charlotte (north)	AK	53.5	Brothers et al. (2020)	dextral	88	V	15	nominal assigned value
Queen Charlotte (outboard, center)	AK	0.01	nominal assigned rate	reverse	45	NE	15	nominal assigned value
Queen Charlotte	AK	0.01	nominal assigned rate	reverse	45	NE	15	nominal assigned value

(outboard, north)								
Queen Charlotte (outboard, south)	AK	0.01	nominal assigned rate	reverse	45	NE	15	nominal assigned value
Queen Charlotte (south)	AK	54.4	Brothers et al. (2020)	dextral	90	V	15	nominal assigned value
Ragged Mountain	AK	1	QFFD slip rate bin lower bound	thrust	30	W	15	nominal assigned value
Rampart (seismicity)	AK	0.01	nominal assigned rate	sinistral	90	V	15	nominal assigned value
Rude River	AK	0.2	QFFD slip rate bin lower bound	reverse	45	N	15	nominal assigned value
Salcha (seismicity)	AK	0.01	nominal assigned rate	sinistral	90	V	15	nominal assigned value
Stevens (east)	AK	0.01	nominal assigned value	normal?	90	V	15	nominal assigned value
Stevens (west)	AK	0.01	nominal assigned value	normal?	90	V	15	nominal assigned value
Suckling Hills	AK	4.7	Chapman et al. (2011)	reverse	60	NE	15	nominal assigned value
Susitna Glacier	AK	1.8	Personius et al. (2017)	reverse	45	N	15	nominal assigned value
Ten Fathom	AK	3.5	Carver et al. (2008)	reverse	60	N	15	nominal assigned value
Tintina (Medicine Lake-Preacher)	AK	0.5	Leonard et al. (2008)	dextral	90	V	15	nominal assigned value
Totschunda	AK	7.4	Haeussler et al. (2017b)	dextral	90	V	15	nominal assigned value
Transition	AK	4	see Bender et al. (2021)	dextral	90	V	15	nominal assigned value
Ugak	AK	1.3	Ramos et al. (2022)	reverse	45	NW	15	nominal assigned value
Yakutat Foothills	AK	5	Berger et al. (2008a)	reverse	70	S	15	nominal assigned value

*Notes:* See Bender et al. (2021) for all attributes for each fault section. Some fault rates inferred from logic presented in Bender et al. (2021) and in this paper. Dip direction listed as cardinal

values except “V” is vertical. QFFD is the Alaska Quaternary fault and fold database from Koehler et al. (2012).

## References

- Abers, G. A., Adams, A. N., Haeussler, P. J., Roland, R., Shore, P. J., Wiens, D. A., Schwartz, S. Y., Sheehan, A. F., Shillington, D. J., Webb, S., & Worthington, L. L. (2019). Examining Alaska’s earthquakes on land and sea. *Eos*, *100*, <https://doi.org/10.1029/2019EO117621>.
- Ager, T. A. (2019). Late Quaternary vegetation development following deglaciation of northwestern Alexander Archipelago, Alaska. *Frontiers in Earth Science*, *7*, 104.
- Argus, D. F., Gordon, R. G. & DeMets, C. (2011). Geologically current motion of 56 plates relative to the no-net-rotation reference frame. *Geochemistry, Geophysics, Geosystems*, *12*(11). Q11001, doi:10.1029/2011GC003751.
- Argus, D. F., Gordon, R. G., Heflin, M. B., Ma, C., Eanes, R. J., Willis, P., Peltier, W. R. & Owen, S. E. (2010). The angular velocities of the plates and the velocity of Earth’s centre from space geodesy. *Geophysical Journal International*, *180*(3), p.913-960. <https://doi.org/10.1111/j.1365-246X.2009.04463.x>
- Athey, J., Newberry, R., Werden, M., Freeman, L., Smith, R., & Szumigala, D. (2006). Bedrock geologic map of the Liberty Bell area, Fairbanks A-4 Quadrangle, Bonfield mining district, Alaska. *Alaska Division of Geological & Geophysical Surveys Report of Investigation RI2006: Vol. 1.0.1*. <https://doi.org/https://doi.org/10.14509/15026>
- Barrie, J. V., & Conway, K. W. (1999). Late Quaternary glaciation and postglacial stratigraphy of the northern Pacific margin of Canada. *Quaternary Research*, *51*(2), 113-123.
- Barrie, J. V., Conway, K. W., & Harris, P. T. (2013). The Queen Charlotte fault, British Columbia: Seafloor anatomy of a transform fault and its influence on sediment processes. *Geo-Marine Letters*, *33*(4), 311-318.
- Bécel, A., Shillington, D. J., Delescluse, M., Nedimović, M. R., Abers, G. A., Saffer, D. M., Webb, S. C., Keranen, K. M., Roche, P. -H., Li, J., & Kuehn, H. (2017). Tsunamigenic structures in a creeping section of the Alaska subduction zone. *Nature Geoscience*, *10*(8), 609–613, <https://doi.org/10.1038/ngeo2990>
- Bemis, S. P. (2004). Neotectonic framework of the north-central Brooks Range foothills, (master’s thesis), Fairbanks, AK: University of Alaska Fairbanks.
- Bemis, S. P. (2010). Moletrack scarps to mountains—Quaternary tectonics of the central Alaska Range, (Doctoral dissertation) Eugene, OR: University of Oregon.
- Bemis, S. P., Carver, G. A., & Koehler, R. D. (2012). The Quaternary thrust system of the northern Alaska Range. *Geosphere*, *8*(1), 1-10. <http://doi.org/10.1130/GES00695.1>
- Bemis, S. P., & Wallace, W. K. (2007). Neotectonic framework of the north-central Alaska Range foothills. in K. D. Ridgway, J. M. Trop, J. M. G. Glen, and J. M. O’Neill (Eds.), *Tectonic Growth of a Collisional Continental Margin—Crustal Evolution of Southern Alaska, Geological Society of America Special Paper*, (Vol. 431, pp. 549–572). Washington, DC: American Geophysical Union. [http://doi.org/10.1130/2007.2431\(21\)](http://doi.org/10.1130/2007.2431(21))

- Bemis, S. P., Weldon, R. J., & Carver, G. A. (2015). Slip partitioning along a continuously curved fault: Quaternary geologic controls on Denali fault system slip partitioning, growth of the Alaska Range, and the tectonics of south-central Alaska. *Lithosphere*, 7(3), 235-246.
- Bender, A. M. & Haeussler, P. J. (2021). Alaska fault trace mapping, 2021. *U.S. Geological Survey data release*. <https://doi.org/10.5066/P9H02FXB>.
- Bender, A. M., Haeussler, P. J. & Powers, P. M. (2021). Geologic inputs for the 2023 Alaska update to the U.S. National Seismic Hazard Model (NSHM). U.S. Geological Survey data release. <https://doi.org/10.5066/P97NRR0F>.
- Bender, A. M., Lease, R. O., Haeussler, P. J., Rittenour, T., Corbett, L. B., Bierman, P. R. and Caffee, M. W. (2019). Pace and process of active folding and fluvial incision across the Kantishna Hills anticline, central Alaska. *Geophysical Research Letters*, 46(6), pp.3235-3244.
- Bender, A. M., Lease, R. O., Rittenour, T., & Jones, J. V. (2023). Rapid active thrust faulting at the northern Alaska Range front. *Geology*, 51, 527–531. <https://doi.org/10.1130/G51049.1>
- Berger, A. L., Gulick, S. P., Spotila, J. A., Upton, P., Jaeger, J. M., Chapman, J. B., Worthington, L. A., Pavlis, T. L., Ridgway, K. D., Willems, B. A. & McAleer, R. J. (2008b). Quaternary tectonic response to intensified glacial erosion in an orogenic wedge. *Nature Geoscience*, 1(11), 793-799. doi:10.1038/ngeo334
- Berger, A. L., Spotila, J. A., Chapman, J. B., Pavlis, T. L., Enkelmann, E., Ruppert, N. A. & Buscher, J. T. (2008a). Architecture, kinematics, and exhumation of a convergent orogenic wedge: A thermochronological investigation of tectonic–climatic interactions within the central St. Elias orogen, Alaska. *Earth and Planetary Science Letters*, 270(1-2), 13-24. doi:10.1016/j.epsl.2008.02.034
- Biggs, J., Wright, T., Lu, Z., & Parsons, B. (2007). Multi-interferogram method for measuring interseismic deformation: Denali fault, Alaska. *Geophysical Journal International*, 170, 1165-1179. doi: 10.1111/j.1365-246X.2007.03415.x
- Boes, E., Van Daele, M., Moernaut, J., Schmidt, S., Jensen, B. J., Praet, N., Kaufman, D., Haeussler, P., Loso, M.G. & De Batist, M. (2018). Varve formation during the past three centuries in three large proglacial lakes in south-central Alaska. *GSA Bulletin*, 130(5-6), 757-774.
- Bondár, I., Engdahl, E. R., Villaseñor, A., Harris, J., & Storchak, D. (2015). ISC-GEM: Global Instrumental Earthquake Catalogue (1900-2009), II. Location and seismicity patterns. *Physics of the Earth and Planetary Interiors*, 239, 2-13. <https://doi.org/10.1016/j.pepi.2014.06.002>
- Briggs, R., Witter, R., Freymueller, J., Powers, P. (2023, submitted). An Alaska-Aleutian subduction zone interface recurrence model from geology and geodesy. In N. A. Ruppert, M. Jadamec, and J. T. Freymueller (Eds.), *Tectonics and seismicity of Alaska and western Canada: Earthscope and beyond*. American Geophysical Union Geophysical Monograph Series (Vol. XXX, pp. XX-XX). Washington, DC: American Geophysical Union

- Briner, J. P., Tulenko, J. P., Kaufman, D. S., Young, N. E., Baichtal, J. F., & Lesnek, A. (2017). The last deglaciation of Alaska. *Cuadernos de Investigacion Geographica*, 43(2), 429-448.
- Brogan, G. E., Cluff, L. S., Korrinda, M. K., & Slemmons, D. B. (1975). Active faults of Alaska. In *Developments in geotectonics* (Vol. 9, pp. 73-85). Amsterdam, Netherlands: Elsevier.
- Brothers, D. S., Elliott, J. L., Conrad, J. E., Haeussler, P. J., & Kluesner, J. W. (2018b). Strain partitioning in southeastern Alaska: is the chatham strait fault active? *Earth and Planetary Science Letters*, 481, 362–371.
- Brothers, D. S., Miller, N. C., Barrie, J. V., Haeussler, P. J., Greene, H. G., Andrews, B. D., Zielke, O., Watt, J., & Dartnell, P. (2020). Plate boundary localization, slip-rates and rupture segmentation of the Queen Charlotte Fault based on submarine tectonic geomorphology. *Earth and Planetary Science Letters*. 530(115882). <https://doi.org/10.1016/j.epsl.2019.115882>.
- Bruhn, R. L., Pavlis, T. L., Plafker, G., & Serpa, L. (2004). Deformation during terrane accretion in the Saint Elias orogen, Alaska. *Geological Society of America Bulletin*, 116(7-8), 771-787.
- Bruhn, R. L., Sauber, J., Cotton, M.M., Pavlis, T. L., Burgess, E., Ruppert, N. & Forster, R. R. (2012). Plate margin deformation and active tectonics along the northern edge of the Yakutat Terrane in the Saint Elias Orogen, Alaska, and Yukon, Canada. *Geosphere*, 8(6), 1384-1407.
- Burbank, D., Meigs, A., & Brozović, N. (1996). Interactions of growing folds and coeval depositional systems. *Basin research*, 8(3), 199-223.
- Brew, D. A., & Ford, A. B. (1978). Megalineament in southeastern Alaska marks southwest edge of Coast Range batholithic complex. *Canadian Journal of Earth Sciences*, 15(11), 1763-1772.
- Bruns, T. R. (1982). Structure and petroleum potential of the continental margin between Cross Sound and Icy Bay, northern Gulf of Alaska. *U. S. Geological Survey Open-File Report 82-929*, 64 pp.
- Bruns, T. R. (1983). Model for the origin of the Yakutat block, an accreting terrane in the northern Gulf of Alaska. *Geology*, 11(12), 718-721.
- Burkett, C. A., Bemis, S. P. and Benowitz, J. A. (2016). Along-fault migration of the Mount McKinley restraining bend of the Denali fault defined by late Quaternary fault patterns and seismicity, Denali National Park & Preserve, Alaska. *Tectonophysics*, 693, 489-506.
- Buurman, H. (2018). An improved glimpse into earthquake activity in northeastern Alaska. University of Alaska Fairbanks White paper, 8 pp. <http://hdl.handle.net/11122/9607>
- Caprio, M., Tarigan, B., Worden, C. B., Wiemer, S., & Wald, D. J. (2015). Ground motion to intensity conversion equations (GMICES): A global relationship and evaluation of regional dependency. *Bulletin of the Seismological Society of America*, 105(3), 1476-1490.

- Carlson, R. J., & Baichtal, J. F. (2015). A predictive model for locating early Holocene archaeological sites based on raised shell-bearing strata in Southeast Alaska, USA. *Geoarchaeology*, 30(2), 120-138.
- Carlson, P. R., Bruns, T. R., & Plafker, G. (1988). Late Cenozoic offsets on the offshore connection between the Fairweather and Queen Charlotte faults off southeast Alaska. *Marine Geology*, 85(1), 89-97.
- Carver, G. A., Bemis, S. P., Solie, D. N., Castonguay, S., & Obermiller, K. E. (2010). Active and potentially active faults in or near the Alaska Highway corridor, Dot Lake to Tetlin Junction, Alaska. *Alaska Division of Geological & Geophysical Surveys Preliminary Interpretive Report 2010-1*, 42.
- Carver, G., Sauber, J., Lettis, W., Witter, R., Whitney, B. (2008). Active faults on northeastern Kodiak Island, Alaska. In J. T. Freymueller, P. J. Haeussler, R. L. Wesson, and G. Ekstrom (Eds.), *Active tectonics and seismic potential of Alaska: American Geophysical Union Geophysical Monograph Series (Vol. 179, pp. 167-184)*. Washington, DC: American Geophysical Union
- Chapman, J. B., Elliott, J., Doser, D. I., & Pavlis, T. L. (2014). Slip on the Suckling Hills splay fault during the 1964 Alaska earthquake. *Tectonophysics*, 637, 191-197. <http://dx.doi.org/10.1016/j.tecto.2014.10.007>
- Chapman, J. B., Pavlis, T. L., Bruhn, R. L., Worthington, L. L., Gulick, S. P., & Berger, A. L. (2012). Structural relationships in the eastern syntaxis of the St. Elias orogen, Alaska. *Geosphere*, 8(1), 105-126. doi:10.1130/GES00677.1
- Chapman, J. B., Pavlis, T. L., Gulick, S., Berger, A., Lowe, L., Spotila, J., Bruhn, R., Vorkink, M., Koons, P., Barker, A., Picornell, C., Ridgway, K., Hallet, B., Jaeger, J., & McCalpin, J. (2008). Neotectonics of the Yakutat collision: changes in deformation driven by mass redistribution. In J. T. Freymueller, P. J. Haeussler, R. L. Wesson, and G. Ekstrom (Eds.), *Active tectonics and seismic potential of Alaska: American Geophysical Union Geophysical Monograph Series (Vol. 179, pp. 65-81)*. Washington, DC: American Geophysical Union <http://doi.org/10.1029/179GM04>
- Chapman, J. B., Worthington, L. L., Pavlis, T. L., Bruhn, R. L., & Gulick, S. P. (2011). The Suckling Hills fault, Kayak Island zone, and accretion of the Yakutat microplate, Alaska. *Tectonics*, 30(6), TC6011. doi:10.1029/2011TC002945
- Christeson, G. L., Gulick, S. P. S., van Avendonk, H. J. A., Worthington, L. L., Reece, R. S., and Pavlis, T. L. (2010). The Yakutat terrane: Dramatic change in crustal thickness across the Transition fault, Alaska. *Geology*, 38(10) 895-898. doi: 10.1130/G31170.1
- Cobbett, R., Israel, S., Mortensen, J., Joyce, N., & Crowley, J. (2017). Structure and kinematic evolution of the Duke River fault, southwestern Yukon. *Canadian Journal of Earth Sciences*, 54(3), 322-344.
- Coe, R. S., Globerman, B. R. & Thrupp, G. A. (1989). Rotation of central and southern Alaska in the early Tertiary: Oroclinal bending by megakinking?. In *Paleomagnetic rotations and continental deformation* (pp. 327-342). Dordrecht, Netherlands: Springer.
- Crone, A. J., Personius, S. F., Craw, P. A., Haeussler, P. J., & Staff, L. A. (2004). The Susitna Glacier thrust fault: Characteristics of surface ruptures on the fault that initiated the 2002

- Denali fault earthquake. *Bulletin of the Seismological Society of America*, 94(6B), S5-S22.
- Cross, R. S., & Freymueller, J. T. (2008). Evidence for and implications of a Bering plate based on geodetic measurements from the Aleutians and western Alaska. *Journal of Geophysical Research: Solid Earth*, 113(B7) B07405, doi:10.1029/2007JB005136
- Darvill, C. M., Menounos, B., Goehring, B. M., Lian, O. B., & Caffee, M. W. (2018). Retreat of the western Cordilleran Ice Sheet margin during the last deglaciation. *Geophysical Research Letters*, 45(18), 9710-9720.
- Davies, M. H., Mix, A. C., Stoner, J. S., Addison, J. A., Jaeger, J., Finney, B., & Wiest, J. (2011). The deglacial transition on the southeastern Alaska Margin: Meltwater input, sea level rise, marine productivity, and sedimentary anoxia. *Paleoceanography*, 26(2), PA2223, doi:10.1029/2010PA002051
- De Batist, M., Talling, P., Strasser, M., & Girardclos, S. (2017). Subaquatic paleoseismology: records of large Holocene earthquakes in marine and lacustrine sediments. *Marine geology*, 384, 1-3.
- DeMets, C. & Merkouriev, S. (2016). High-resolution reconstructions of Pacific–North America plate motion: 20 Ma to present. *Geophysical Journal International*, 207(2), 741-773. doi: 10.1093/gji/ggw305
- Devore, J. R., Bemis, S. P., & Walker, L. A. (2012). Evidence for post-26 ka displacement of the Northern Foothills Thrust at the Nenana River, Alaska. In *AGU Fall Meeting Abstracts* (Vol. 2012, pp. T11A-2552).
- Doser, D. I. (2010). A reevaluation of the 1958 Fairweather, Alaska, earthquake sequence. *Bulletin of the Seismological Society of America*, 100(4), 1792-1799. <https://doi.org/10.1130/GES02299.1>
- Doser, D. I. (2014). Seismicity of southwestern Yukon, Canada, and its relation to slip transfer between the Fairweather and Denali fault systems. *Tectonophysics*, 611, 121-129. <http://dx.doi.org/10.1016/j.tecto.2013.11.018>
- Doser, D. I., & Lomas, R. (2000). The transition from strike-slip to oblique subduction in southeastern Alaska from seismological studies. *Tectonophysics*, 316(1-2), 45-65.
- Doser, D. I., & Rodriguez, H. (2011). A seismotectonic study of the Southeastern Alaska Region. *Tectonophysics*, 497(1-4), 105-113.
- Eberhart-Phillips, D., Haeussler, P. J., Freymueller, J. T., Frankel, A. D., Rubin, C. M., Craw, P., Ratchkovski, N. A., Anderson, G., Carver, G. A., Crone, A. J., Dawson, T. E., Fletcher, H., Hansen, R., Harp, E. L., Harris, R. A., Hill, D. P., Hreinsdóttir, S., Jibson, R. W., Jones, L. M., Kayen, R., Keefer, D. K., Larsen, C. F., Moran, Personius, S. F., Plafker, G., Sherrod, B., Sieh, K., Sitar, N., & Wallace, W. K. (2003). The 2002 Denali fault earthquake, Alaska—A large magnitude, slip-partitioned event. *Science*, 300(5622) 1,113–1,118. <http://doi.org/10.1126/science.1082703>
- Elliott, J., Freymueller, J. T., & Larsen, C. F. (2013). Active tectonics of the St. Elias orogen, Alaska, observed with GPS measurements. *Journal of Geophysical Research: Solid Earth*, 118(10), 5625-5642.

- Elliott, J., & Freymueller, J. T. (2020). A block model of present-day kinematics of Alaska and western Canada. *Journal of Geophysical Research: Solid Earth*, *125*, e2019JB018378. doi:10.1130/10.1029/2019JB018378.
- Elliott, J. L., Larsen, C. F., Freymueller, J. T., & Motyka, R. J. (2010). Tectonic block motion and glacial isostatic adjustment in southeast Alaska and adjacent Canada constrained by GPS measurements. *Journal of Geophysical Research: Solid Earth*, *115*(B9), B09407, doi:10.1029/2009JB007139.
- Enkelmann, E., Koons, P. O., Pavlis, T. L., Hallet, B., Barker, A., Elliott, J., Garver, J. I., Gulick, S. P., Headley, R. M., Pavlis, G. L. & Ridgway, K. D. (2015b). Cooperation among tectonic and surface processes in the St. Elias Range, Earth's highest coastal mountains. *Geophysical Research Letters*, *42*(14), 5838-5846. doi:10.1002/2015GL064727.
- Enkelmann, E., Valla, P. G., & Champagnac, J. D. (2015a). Low-temperature thermochronology of the Yakutat plate corner, St. Elias Range (Alaska): bridging short-term and long-term deformation. *Quaternary Science Reviews*, *113*, 23-38, doi:10.1016/j.quascirev.2014.10.019.
- Ferguson, K. M., Armstrong, P. A., Arkle, J. C., & Haeussler, P. J. (2015). Focused rock uplift above the subduction décollement at Montague and Hinchinbrook Islands, Prince William Sound, Alaska. *Geosphere*, *11*(1), 144-159. doi:10.1130/GES01036.1
- Finn, S. P., Liberty, L. M., Haeussler, P. J., & Pratt, T. L. (2015). Landslides and Megathrust Splay Faults Captured by the Late Holocene Sediment Record of Eastern Prince William Sound, Alaska Landslides and Megathrust Splay Faults Captured by the Late Holocene Sediment Record of Eastern PWS. *Bulletin of the Seismological Society of America*, *105*(5), 2343-2353.
- Finzel, E. S., Trop, J. M., Ridgway, K. D., & Enkelmann, E. (2011). Upper plate proxies for flat-slab subduction processes in southern Alaska. *Earth and Planetary Science Letters*, *303*(3-4), 348-360.
- Fortin, D., Praet, N., McKay, N. P., Kaufman, D. S., Jensen, B. J., Haeussler, P. J., Buchanan, C. & De Batist, M. (2019). New approach to assessing age uncertainties—The 2300-year varve chronology from Eklutna Lake, Alaska (USA). *Quaternary Science Reviews*, *203*, 90-101.
- Fletcher, H. J., & Christensen, D. H. (1996). A determination of source properties of large intraplate earthquakes in Alaska. *Pure and Applied Geophysics*, *146*(1), 21–41. <https://doi.org/https://doi.org/10.1007/BF00876668>
- Freymueller, J. T., Woodard, H., Cohen, H. S., Cross, R., Elliott, J., Larsen, C., Hreinsdóttir, S., & Zweck, C. (2008). Active deformation processes in Alaska, based on 15 years of GPS measurements. In J. T. Freymueller, P. J. Haeussler, R. L. Wesson, and G. Ekstrom (Eds.), *Active tectonics and seismic potential of Alaska*: American Geophysical Union Geophysical Monograph Series (Vol. 179, pp. 1-42). Washington, DC: American Geophysical Union doi: 10.129/179GM02.

- Gaudreau, É., Nissen, E. K., Bergman, E. A., Benz, H. M., Tan, F., & Karasözen, E. (2019). The August 2018 Kaktovik earthquakes: Active tectonics in northeastern Alaska revealed with InSAR and seismology. *Geophysical Research Letters*, *46*(24), 14412-14420.
- GEBCO (2020). GEBCO\_2022 Grid [data set], doi:10.5285/e0f0bb80-ab44-2739-e053-6c86abc0289c (last access: 18 January 2023), 2022.
- Grantz, A., May, S. D., & Hart, P. E. (1994). Geology of the Arctic continental margin of Alaska. In A. Grantz, L. Johnson, and J. F. Sweeney (Eds.), *The Arctic Ocean Region*, Boulder, CO: Geological Society of America, <https://doi.org/10.1130/DNAG-GNA-L.257>
- Gulick, S. P., Lowe, L. A., Pavlis, T. L., Gardner, J. V., & Mayer, L. A. (2007). Geophysical insights into the Transition fault debate: Propagating strike slip in response to stalling Yakutat block subduction in the Gulf of Alaska. *Geology*, *35*(8), 763-766.
- Gulick, S. P., Reece, R. S., Christeson, G. L., Van Avendonk, H., Worthington, L. L., & Pavlis, T. L. (2013). Seismic images of the Transition fault and the unstable Yakutat–Pacific–North American triple junction. *Geology*, *41*(5), 571-574. doi:10.1130/G33900.1.
- Haeussler, P. J. (1998). Surficial geologic map along the Castle Mountain fault between Houston and Hatcher Pass Road, Alaska. *U. S. Geological Survey Open-File Report* 98-480.
- Haeussler, P.J. (2008). An overview of the neotectonics of interior Alaska: Far-field deformation from the Yakutat microplate collision. In J. T. Freymueller, P. J. Haeussler, R. L. Wesson, and G. Ekstrom (Eds.), *Active tectonics and seismic potential of Alaska: American Geophysical Union Geophysical Monograph Series* (Vol. 179, pp. 83-108). Washington, DC: American Geophysical Union
- Haeussler, P. J., Armstrong, P. A., Liberty, L. M., Ferguson, K. M., Finn, S. P., Arkle, J. C., & Pratt, T. L. (2015). Focused exhumation along megathrust splay faults in Prince William Sound, Alaska. *Quaternary Science Reviews*, *113*, 8-22. <https://doi.org/10.1016/j.quascirev.2014.10.013>
- Haeussler, P. J., Bruhn, R. L., & Pratt, T. L. (2000). Potential seismic hazards and tectonics of the upper Cook Inlet basin, Alaska, based on analysis of Pliocene and younger deformation. *Geological Society of America Bulletin*, *112*(9), 1414-1429.
- Haeussler, P. J., Lipovsky, P., Thoms, E., Wesson, R. (2013). The Decoeli Mountain fault – a newly identified active thrust(?) fault in the southwestern Yukon Territory. *Seismological Research Letters*, *84*(2), 378.
- Haeussler, P. J., Matmon, A., Arnold, M., Aumaitre, G., Bourles, D., & Keddadouche, K. (2022). Late Quaternary deglaciation of Prince William Sound, Alaska. *Quaternary Research*, *105*, 115-134.
- Haeussler, P. J., Matmon, A., Schwartz, D. P., and Seitz, G. G. (2017b). Neotectonics of interior Alaska and the late Quaternary slip rate along the Denali fault system. *Geosphere*, *13*(5), 1–19. doi:10.1130/GES01447.1.
- Haeussler, P. J., and Saltus, R. W. (2005). Twenty-six kilometers of offset since late Eocene time on the Lake Clark fault. In P. J. Haeussler, & J. Galloway (Eds.), *Studies by the U.S.*

- Geological Survey in Alaska, 2004: *U.S. Geological Survey Professional Paper 1709-A*, p. 1-4. <http://pubs.usgs.gov/pp/pp1709a/>
- Haeussler, P. J., & Saltus, R. W., 2011. Location and Extent of Tertiary Structures in Cook Inlet Basin, Alaska, and Mantle Dynamics that Focus Deformation and Subsidence. *U. S. Geological Survey Professional Paper 1776-D*, 26 p.
- Haeussler, P. J., Saltus, R. W., Stanley, R. G., Ruppert, N., Lewis, K., Karl, S. M., & Bender, A. (2017a). The Peters Hills basin, a Neogene wedge-top basin on the Broad Pass thrust fault, south-central Alaska. *Geosphere*, 13(5), 1464-1488.
- Haeussler, P. J., & Waythomas, C. F. (2011). Review of the Origin of the Braid Scarp Near the Pebble Prospect, Southwestern Alaska. *U.S. Geological Survey Open-File Report 2011-1028*, 14 p.
- Heinlein, S. N., Pavlis, T. L., Bruhn, R. L., & McCalpin, J. P. (2018, December). Geomorphology, high-resolution LiDAR, and aerial photography data-extracting geologic insights from 3D modeling-Ragged Mountain fault southern Alaska, USA. In *AGU Fall Meeting Abstracts* (Vol. 2018, pp. G51C-0500).
- Hoare, J. M. (1961). Geology and tectonic setting of lower Kuskokwim-Bristol Bay region, Alaska. *American Association of Petroleum Geologists Bulletin*, 45(5), 594-611.
- Jadamec, M. A., Billen, M. I., & Roeske, S. M. (2013). Three-dimensional numerical models of flat slab subduction and the Denali fault driving deformation in south-central Alaska. *Earth and Planetary Science Letters*, 376, 29-42.
- Karl, S., Miller, L., Haeussler, P., Caine, J., & Norton, J. (2023). The transition from convergence to translation on the western margin of North America: evolution of the ancestral Denali fault in southeast Alaska: Geological Society of Alaska Technical Conference abstracts. p. 20-23.  
[https://www.alaskageology.org/uploads/1/1/9/5/119566579/2023\\_tech\\_conference\\_abstracts.pdf](https://www.alaskageology.org/uploads/1/1/9/5/119566579/2023_tech_conference_abstracts.pdf) (last accessed 5/26/2023).
- Koehler, R. D. (2013). Quaternary faults and folds (QFF). *Alaska Division of Geological & Geophysical Surveys Digital Data Series 3*, <http://maps.dggs.alaska.gov/qff>.  
<http://doi.org/10.14509/24956>
- Koehler, R. D., Carver, G. A., & Alaska Seismic Hazards Safety Commission (2018). Active faults and seismic hazards in Alaska. *Alaska Division of Geological & Geophysical Surveys Miscellaneous Publication 160*, 59 p. <https://doi.org/10.14509/29705>
- Koehler, R. D., Farrell, R.-E., Burns, P. A. C., & Combellick, R. A. (2012). Quaternary faults and folds in Alaska—A digital database. in R. D. Koehler, Quaternary Faults and Folds (QFF). *Alaska Division of Geological & Geophysical Surveys Miscellaneous Publication 141*, 31 p., 1 sheet, scale 1:3,700,000. <http://doi.org/10.14509/23944>
- Koehler, R. D., & Reger, R. D. (2011). Reconnaissance Evaluation of the Lake Clark Fault, Tyonek Area, Alaska. *Alaska Division of Geological & Geophysical Surveys Preliminary Interpretive Report 2011-1*, 8 pp.
- Koehler, R. D., Reger, R. D., Carver, G. A., Spangler, E. & Gould, A. (2014, October). Castle Mountain fault southcentral Alaska: Observations on slip partitioning from lidar and

- paleoseismic trenching. In *Geological Society of America, Abstracts with Programs* (Vol. 46, No. 6, p. 273).
- Koehler, R. D., Reger, R. D., Spangler, E. R., & Gould, A. I. (2016). Investigation of potentially active tectonic faults along the route of the proposed Alaska Stand Alone Pipeline, Livengood to Cook Inlet, Alaska. *Alaska Division of Geological & Geophysical Surveys Report of Investigation 2015-4*, 71 p. <https://doi.org/10.14509/29409>
- Koehler, R. D., & Woods, R.-E. F. (2013). Paleoseismic and LiDAR investigations along the Cathedral Rapids and Dot “T” Johnson faults, interior Alaska. *Alaska Division of Geological & Geophysical Surveys Report of Investigation 2013-4*, 21 p. <http://doi.org/10.14509/26761>
- Kopczynski, S. E., Kelley, S. E., Lowell, T. V., Evenson, E. B., & Applegate, P. J. (2017). Latest Pleistocene advance and collapse of the Matanuska–Knik glacier system, Anchorage Lowland, southern Alaska. *Quaternary Science Reviews*, 156, 121-134. <https://doi.org/10.1016/j.quascirev.2016.11.026>
- Lahr, J. C., Page, R. A., Stephens, C. D., and Fogleman, K. A. (1986). Sutton, Alaska, earthquake of 1984: evidence for activity on the Talkeetna segment of the Castle Mountain fault system. *Bulletin of the Seismological Society of America*, 76, 967-983.
- Lahr, J. C., & Plafker, G. (1980). Holocene Pacific–North American plate interaction in southern Alaska: Implications for the Yakataga seismic gap. *Geology*, 8(10), 483-486.
- Leiggi, P. A. (1987). Style and age of tectonism of the Sadlerochit Mountains to Franklin Mountains, Arctic National Wildlife Refuge, Alaska. in I. Tailleux and P. Weimer (Eds.), *Alaskan North Slope geology*. Pacific Section, SEPM, and Alaska Geological Society, Book 50, p. 749-756.
- Leonard, L. J., Mazzotti, S., & Hyndman, R. D. (2008). Deformation rates estimated from earthquakes in the northern Cordillera of Canada and eastern Alaska. *Journal of Geophysical Research: Solid Earth*, 113(B8).
- Liberty, L. M., Brothers, D. S., & Haeussler, P. J. (2019). Tsunamigenic splay faults imply a long-term asperity in southern Prince William Sound, Alaska. *Geophysical Research Letters*, 46(7), 3764-3772. <https://doi.org/10.1029/2018GL081528>
- Liberty, L. M., Finn, S. P., Haeussler, P. J., Pratt, T. L., & Peterson, A. (2013). Megathrust splay faults at the focus of the Prince William Sound asperity, Alaska. *Journal of Geophysical Research: Solid Earth*, 118(10), 5428-5441. doi:10.1002/jgrb.50372
- Mackey, K. G., Fujita, K., Gunbina, L. V., Kovalev, V. N., Imaev, V. S., Koz'min, B. M., & Imaeva, L. P. (1997). Seismicity of the Bering Strait region: Evidence for a Bering block. *Geology*, 25(11), 979-982.
- Marechal, A., Mazzotti, S., Elliott, J. L., Freymueller, J. T., & Schmidt, M. (2015). Indentor-corner tectonics in the Yakutat-St. Elias collision constrained by GPS. *Journal of Geophysical Research: Solid Earth*, 120(5), 3897-3908.
- Marechal, A., Ritz, J. F., Ferry, M., Mazzotti, S., Blard, P. H., Braucher, R. & Saint-Carlier, D. (2018). Active tectonics around the Yakutat indentor: New geomorphological constraints

- on the eastern Denali, Totschunda and Duke River Faults. *Earth and Planetary Science Letters*, 482, 71-80.
- Mazzotti, S., Leonard, L. J., Hyndman, R. D. & Cassidy, J. F. (2008). Tectonics, dynamics, and seismic hazard in the Canada-Alaska Cordillera. In J. T. Freymueller, P. J. Haeussler, R. L. Wesson, and G. Ekstrom (Eds.), *Active tectonics and seismic potential of Alaska: American Geophysical Union Geophysical Monograph Series* (Vol. 179, p. 297-319). Washington, DC: American Geophysical Union
- McCalpin, J. P., Gutierrez, F., Bruhn, R. L., Guerrero, J., Pavlis, T. L. & Lucha, P. (2020). Tectonic geomorphology and late Quaternary deformation on the Ragged Mountain fault, Yakutat microplate, south coastal Alaska. *Geomorphology*, 351, 106875. <https://doi.org/10.1016/j.geomorph.2019.106875>
- Miller, D. J. (1961). Geology of the Lituya district, Gulf of Alaska Tertiary Province, Alaska: *U.S. Geological Survey Open-File Report 61-100*, 1 sheet, scale 1:96,000, <https://doi.org/10.3133/ofr61100>.
- Miller, M. S., Driscoll, L. J. O., Porritt, R. W., & Roeske, S. M. (2018). Multiscale crustal architecture of Alaska inferred from P receiver functions. *Lithosphere*, 10(2), 267–278. <https://doi.org/https://doi.org/10.1130/L701.1>
- Miller, L. D., Stowell, H. H., & Gehrels, G. E. (2000). Progressive deformation associated with mid-Cretaceous to Tertiary contractional tectonism in the Juneau gold belt, Coast Mountains, southeastern Alaska. *Geological Society of America Special Paper 343*, p. 193-212.
- Misarti, N., Finney, B. P., Jordan, J.W., Maschner, H. D. G., Addison, J. A., Shapely, M. D., Krumhardt, A., & Beget, J. (2012). Early retreat of the Alaska Peninsula Glacier Complex and the implications for coastal migrations of First Americans. *Quaternary Science Reviews* 48, 1-6.
- Moernaut, J., Daele, M. V., Heirman, K., Fontijn, K., Strasser, M., Pino, M., ... & De Batist, M. (2014). Lacustrine turbidites as a tool for quantitative earthquake reconstruction: New evidence for a variable rupture mode in south central Chile. *Journal of Geophysical Research: Solid Earth*, 119(3), 1607-1633.
- Muhs, D. R., Pigati, J. S., Budahn, J. R., Skipp, G. L., Bettis, E. A., & Jensen, B. (2018). Origin of last-glacial loess in the western Yukon-Tanana Upland, central Alaska, USA. *Quaternary Research*, 89(3), 797-819.
- Murphy, D. C. (2019). Latest Cretaceous–early Eocene Pacific-Arctic?-Atlantic connection: Co-evolution of strike-slip fault systems, oroclines, and transverse fold-and-thrust belts in the northwestern North American Cordillera. In K. Piepjohn, J. V. Strauss, L. Reinhardt, W. C. McClelland (Eds.), *Circum-Arctic Structural Events: Tectonic Evolution of the Arctic Margins and Trans-Arctic Links with Adjacent Orogens*, Geological Society of America Special Paper 541, 665-686. [https://doi.org/10.1130/2018.2541\(28\)](https://doi.org/10.1130/2018.2541(28))
- Nørgaard, J., Jansen, J. D., Neuhuber, S., Ruszkiczay-Rüdiger, Z., & Knudsen, M. F. (2022). P-PINI: A cosmogenic nuclide burial dating method for landscapes undergoing non-steady erosion. *Quaternary Geochronology*, 101420. <https://doi.org/10.1016/j.quageo.2022.101420>

- Page, R. A., Plafker, G. & Pulpan, H. (1995). Block rotation in east-central Alaska: A framework for evaluating earthquake potential? *Geology*, 23(7), 629-632.
- Pavlis, G. L., Bauer, M. A., Elliott, J. L., Koons, P., Pavlis, T. L., Ruppert, N., Ward, K. M. & Worthington, L. L. (2019). A unified three-dimensional model of the lithospheric structure at the subduction corner in southeast Alaska: Summary results from STEEP. *Geosphere*, 15(2), 382-406. doi: <https://doi.org/10.1130/GES01488.1>
- Pavlis, T. L., Chapman, J. B., Bruhn, R. L., Ridgway, K., Worthington, L. L., Gulick, S. P., & Spotila, J. (2012). Structure of the actively deforming fold-thrust belt of the St. Elias orogen with implications for glacial exhumation and three-dimensional tectonic processes. *Geosphere*, 8(5), 991-1019, doi:10.1130/GES00753.1.
- Pavlis, T. L., Picornell, C., Serpa, L., Bruhn, R. L., & Plafker, G., (2004). Tectonic processes during oblique collision: Insights from the St. Elias orogen, northern North American Cordillera. *Tectonics*, 23, TC3001. doi:10.1029/2003TC001557.
- Pegler, G. & Das, S. (1996). The 1987–1992 Gulf of Alaska earthquakes. *Tectonophysics*, 257(2–4), 111–136.
- Personius, S. F., Crone, A. J., Burns, P. A., & Reitman, N. G. (2017). Recurrent Holocene Movement on the Susitna Glacier Thrust Fault: The Structure that Initiated the  $M_w$ 7.9 Denali Fault Earthquake, Central Alaska. *Bulletin of the Seismological Society of America*, 107(4), 1593-1609. <https://doi.org/10.1785/0120160286>
- Plafker, G. (1967). Surface faults on Montague Island associated with the 1964 Alaska earthquake. *U.S. Geological Survey Professional Paper 543-G*, 42 pp.
- Plafker, G. (1969). Tectonics of the March 27, 1964 Alaska earthquake. *U.S. Geological Survey Professional Paper 543-I*, 74 pp.
- Plafker, G., Gilpin, L. M., & Lahr, J. C. (1994). Neotectonic map of Alaska. In G. Plafker, & H. C. Berg (Eds.). *The Geology of Alaska: The Geology of North America*. v. G1, Plate 12, 1 sheet with text, scale 1:2,500,000. Boulder, CO: Geological Society of America.
- Plafker, G., Hudson, T., Bruns, T., & Rubin, M. (1978). Late quaternary offsets along the fairweather fault and crustal plate interactions in southern Alaska. *Canadian Journal of Earth Sciences*, 15(5), 805–816.
- Plafker, G., and Thatcher, W. (2008). Geological and geophysical evaluation of the mechanism of the great 1899 Yakutat Bay earthquakes. In J. T. Freymueller, P. J. Haeussler, R. L. Wesson, and G. Ekstrom (Eds.), *Active tectonics and seismic potential of Alaska: American Geophysical Union Geophysical Monograph Series* (Vol. 179, pp. 215-236). Washington, DC: American Geophysical Union. <http://doi.org/10.1029/179GM12>
- Porter, C. Morin, P. Howat, I. Noh, M.-J. Bates, B. Peterman, K. Keesey, S. Schlenk, M. Gardiner, J. Tomko, K. Willis, M. Kelleher, C., Cloutier, M., Husby, E., Foga, S., Nakamura, H., Platson, M., Wethington, M., Jr., Williamson, C., Bauer, G., Enos, J., Arnold, G., Kramer, W., Becker, P., Doshi, A., D'Souza, C., Cummins, P., Laurier, F., & Bojesen, M. "ArcticDEM", <https://doi.org/10.7910/DVN/OHHUKH>, Harvard Dataverse, V1, [last access: 07 July 2023], 2018.

- Praet, N., Moernaut, J., Van Daele, M., Boes, E., Haeussler, P. J., Strupler, M., Schmidt, S., Loso, M. G., & De Batist, M. (2017). Paleoseismic potential of sublacustrine landslide records in a high-seismicity setting (south-central Alaska). *Marine Geology* 384, 103-119. <https://doi.org/10.1016/j.margeo.2016.05.004>
- Praet, N., Van Daele, M., Collart, T., Moernaut, J., Vandekerckhove, E., Kempf, P., Haeussler, P.J., & De Batist, M. (2020). Turbidite stratigraphy in proglacial lakes: Deciphering trigger mechanisms using a statistical approach. *Sedimentology*, 67(5), 2332-2359. doi: 10.1111/sed.12703
- Praet, N., Van Daele, M., Moernaut, J., Mestdagh, T., Vandorpe, T., Jensen, B. J., Witter, R. C., Haeussler, P. J. & De Batist, M. (2022). Unravelling a 2300 year long sedimentary record of megathrust and intraslab earthquakes in proglacial Skilak Lake, south-central Alaska. *Sedimentology*, 69(5), 2151-2180. doi: 10.1111/sed.12986
- Praetorius, S., Mix, A., Jensen, B., Froese, D., Milne, G., Wolhowe, M., Addison, J., & Prah, F. (2016). Interaction between climate, volcanism, and isostatic rebound in Southeast Alaska during the last deglaciation. *Earth and Planetary Science Letters*, 452, 79-89.
- Ramos, M. D., Liberty, L. M., Haeussler, P. J., & Humphreys, R. (2022). Upper-plate structure and tsunamigenic faults near the Kodiak Islands, Alaska, USA. *Geosphere*, 18(5), 1474-1491.
- Ratchkovski, N. A., & Hansen, R.A. (2002). New constraints on tectonics of interior Alaska: Earthquake locations, source mechanisms, and stress regime. *Bulletin of the Seismological Society of America*, 92(3), 998–1014, doi: 10.1785/0120010182
- Reece, R. S., Gulick, S. P. S., Christeson, G. L., Horton, B. K., van Avendonk, H., & Barth, G. (2013). The role of farfield tectonic stress in oceanic intraplate deformation, Gulf of Alaska. *Journal of Geophysical Research Solid Earth*, 118, 1862–1872, doi:10.1002/jgrb.50177
- Reifenstuhl, R. R., Dover, J. H., Newberry, R. J., Clautice, K. H., Liss, S. A., Blodgett, R. B., Bundtzen, T. K., and Weber, F. R. (1997). Interpretive geologic bedrock map of the Tanana B-1 Quadrangle, central Alaska. Alaska Division of Geological & Geophysical Surveys Report of Investigation 97- 15B, 15 p., 1 sheet, scale 1:63,360. <http://doi.org/10.14509/2552>
- Riccio, S. J., Fitzgerald, P. G., Benowitz, J. A., & Roeske, S. M. (2014). The role of thrust faulting in the formation of the eastern Alaska Range: Thermochronological constraints from the Susitna Glacier thrust fault region of the intracontinental strike-slip Denali fault system. *Tectonics*, 33(11), 2195-2217.
- Richter, D. H., Preller, C. C., Labay, K. A., I Shew, N. B. (2006). Geologic map of the Wrangell-Saint Elias National Park and Preserve. *U.S. Geological Survey Scientific Investigations Map 2877*, scale: 1:350,000.
- Ruppert, N. A., Ridgeway, K. D., Freymueller, J. T., Cross, R. C., Hansen, R. A. (2008). Active tectonics of interior Alaska-Seismology, GPS geodesy, and local geomorphology. In J. T. Freymueller, P. J. Haeussler, R. L. Wesson, and G. Ekstrom (Eds.), *Active tectonics and seismic potential of Alaska: American Geophysical Union Geophysical Monograph Series* (Vol. 179, pp. 109-133). Washington, DC: American Geophysical Union

- Saltus, R. W. (2007). Matching magnetic trends and patterns across the Tintina fault, Alaska and Canada—evidence for offset of about 490 kilometers. *U. S. Geological Survey Scientific Investigations Report 2007-5289-C*, p. C1-C7.
- Shaw, B.E., 2023. Magnitude and Slip Scaling Relations for Fault-Based Seismic Hazard. *Bulletin of the Seismological Society of America*, 113(3), p.924-947.
- Shumway, A. M. (2019). Data Release for the 2007 Alaska Seismic Hazard Model. *U.S. Geological Survey data release*, <https://doi.org/10.5066/P96AUPNO>
- Singleton, D.M., Brothers, D.S., Haeussler, P.J., Witter, R.C., Hill, J. (2022). Constraining the initiation, spatial distribution and sedimentary source of lake turbidites triggered by the 2018 Anchorage earthquake. *Seismological Research Letters*, 93(2B), 1336. <https://doi.org/10.1785/0220220087>
- St. Amand, P. (1948). The Central Alaska Earthquake Swarm of October 1947. *Transactions, American Geophysical Union*, 29(5). <https://doi.org/doi/pdf/10.1029/TR029i005p00613>
- St. Amand, P. S. (1957). Geological and geophysical synthesis of the tectonics of portions of British Columbia, the Yukon Territory, and Alaska. *Geological Society of America Bulletin*, 68(10), pp.1343-1370.
- Suleimani, E., & Freymueller, J.T. (2020). Near-field modeling of the 1964 Alaska tsunami: The role of splay faults and horizontal displacements. *Journal of Geophysical Research: Solid Earth*, 125, e2020JB019620. <https://doi.org/10.1029/2020JB019620>
- Suleimani, E., Nicolsky, D. J., Haeussler, P. J., & Hansen, R. (2011). Combined effects of tectonic and landslide-generated tsunami runup at Seward, Alaska during the Mw 9.2 1964 earthquake. *Pure and applied geophysics*, 168(6), 1053-1074. doi: 10.1007/s00024-010-0228-4
- Tape, C., Holtkamp, S., Silwal, V., Hawthorne, J., Kaneko, Y., Ampuero, J. P., Ji, C., Ruppert, N., Smith, K., & West, M. E. (2018). Earthquake nucleation and fault slip complexity in the lower crust of central Alaska. *Nature Geoscience*, 11(7), 536-541.
- Tape, C., Lomax, A., Silwal, V., Agnew, J. D., & Brettschneider, B. (2017). The 1904 Ms 7.3 earthquake in central Alaska. *Bulletin of the Seismological Society of America*, 107, 1147-1174, <https://doi.org/10.1785/0120160178>
- Tape, C., Silwal, V., Ji, C., Keyson, L., West, M. E. and Ruppert, N. (2015). Transtensional tectonics of the Minto Flats fault zone and Nenana basin, central Alaska. *Bulletin of the Seismological Society of America*, 105(4), 2081-2100.
- Tape, C. M., West, M. E., Silwal, V., and Ruppert, N. (2013). Earthquake nucleation and triggering on an optimally oriented fault. *Earth and Planetary Science Letters*, 363, 231–241. <http://doi.org/10.1016/j.epsl.2012.11.060>
- Tréhu, A. M., Scheidhauer, M., Rohr, K. M., Tikoff, B., Walton, M. A., Gulick, S. P., & Roland, E. C. (2015). An abrupt transition in the mechanical response of the upper crust to transpression along the Queen Charlotte Fault. *Bulletin of the Seismological Society of America*, 105(2B), 1114-1128.
- Thrasher, G.P. (1979). Geologic map of the Kodiak Outer Continental Shelf, western Gulf of Alaska. *U.S. Geological Survey Open-File Report 79-1267*, 2 sheets, scale 1:250,000.

- Thorson, R.M. (1979). Recurrent Late Quaternary faulting near Healy, Alaska. In Alaska Division of Geological & Geophysical Surveys, Short Notes on Alaskan Geology 1978. *Alaska Division of Geological & Geophysical Surveys Geologic Report 61C*, p. 10–14. <http://doi.org/10.14509/410>
- Trop, J. M. (2008). Latest Cretaceous forearc basin development along an accretionary convergent margin: South-central Alaska. *Geological Society of America Bulletin*, 120(1-2), 207–224. doi: <https://doi.org/10.1130/B26215.1>
- Twenhofel, W. S., & Sainsbury, C. L. (1958). Fault patterns in southeastern Alaska. *Geological Society of America Bulletin*, 69(11), 1431-1442.
- Twiss, R. J., and Moores, E. M. (1994). Structural Geology, W. H. Freeman, San Francisco, 532 p. <https://doi.org/10.1002/gj.3350290408>
- Unavco (2019), Plate motion calculator, Unavco, <https://www.unavco.org/software/geodetic-utilities/plate-motion-calculator/plate-motion-calculator.html>, last accessed 24 January 2023.
- U.S. Geological Survey [USGS] (2016). 5 meter Alaska Digital Elevation Models (DEMs), U.S. Geological Survey National Map 3DEP Downloadable Data Collection [data set], <https://earthexplorer.usgs.gov> (last access: 3 January 2023), 2016.
- U.S. Geological Survey [USGS] (2020). Quaternary Fault and Fold Database of the United States [data set], <https://www.sciencebase.gov/catalog/item/589097b1e4b072a7ac0cae23> (last access: 5 January 2023), 2020.
- Van Daele, M., Haeussler, P. J., Witter, R. C., Praet, N., & De Batist, M. (2020). The sedimentary record of the 2018 Anchorage earthquake in Eklutna Lake, Alaska: Calibrating the lacustrine seismograph. *Seismological Research Letters*, 91(1), 126-141.
- Vandekerckhove, E., Van Daele, M., Praet, N., Cnudde, V., Haeussler, P. J., & De Batist, M. (2020). Flood-triggered versus earthquake-triggered turbidites: A sedimentological study in clastic lake sediments (Eklutna Lake, Alaska). *Sedimentology*, 67(1), 364-389.
- von Huene, R., Miller, J. J., & Krabbenhoft, A. (2019). The Shumagin seismic gap structure and associated tsunami hazards, Alaska convergent margin. *Geosphere*, 15(2), 1–18. <https://doi.org/10.1130/GES01657.1>
- von Huene, R., Miller, J. J., & Krabbenhoft, A. (2021). The Alaska convergent margin backstop splay fault zone, a potential large tsunami generator between the frontal prism and continental framework. *Geochemistry, Geophysics, Geosystems*, 22, e2019GC008901. <https://doi.org/10.1029/2019GC008901>
- Wallace, W. K. (2008). Yakataga fold-and-thrust belt: Structural geometry and tectonic implications of a small continental collision zone. In J. T. Freymueller, P. J. Haeussler, R. L. Wesson, and G. Ekstrom (Eds.), *Active tectonics and seismic potential of Alaska: American Geophysical Union Geophysical Monograph Series* (Vol. 179, pp. 237-256). Washington, DC: American Geophysical Union.
- Waldien, T. S., Roeske, S. M., Benowitz, J. A., Allen, W. K., Ridgway, K. D., & O’Sullivan, P. B. (2018). Late Miocene to Quaternary evolution of the McCallum Creek thrust system,

- Alaska: Insights for range-boundary thrusts in transpressional orogens. *Geosphere*, 14(6), 2379–2406, <https://doi.org/10.1130/GES01676.1>.
- Walton, M. A., Gulick, S. P., Haeussler, P. J., Roland, E. C., & Tréhu, A. M. (2015). Basement and regional structure along strike of the Queen Charlotte fault in the context of modern and historical earthquake ruptures. *Bulletin of the Seismological Society of America*, 105(2B), 1090-1105.
- Walton, M. A. L., Gulick, S. P. S., & Haeussler, P. J. (2022). Revisiting the 1899 earthquake series using integrative geophysical analysis in Yakutat Bay, Alaska, USA. *Geosphere*, 18(5) 1453-1473. <https://doi.org/10.1130/GES02423.1>
- Weber, F. R., Wheeler, K. L., Rinehart, C. D., Chapman, R. M., and Blodgett, R. B. (1992). Geologic map of the Livengood Quadrangle, Alaska. *U.S. Geological Survey Open-File Report 92-562*, 20 p., 1 sheet, scale 1:250,000.
- Wesson, R. L., Boyd, O. S., Mueller, C. S., Bufe, C. G., Frankel, A. D., & Petersen, M. D. (2007). Revision of time-independent probabilistic seismic hazard maps for Alaska. *U.S. Geological Survey Open- File Report 2007-1043*. <http://pubs.usgs.gov/of/2007/1043/>
- Wesson, R. L., Frankel, A. D., Mueller, C. S., and Harmsen, S. C. (1999). Probabilistic seismic hazard maps of Alaska. *U.S. Geological Survey Open-File Report 99-36*, 43 p.
- West, M. E., Bender, A., Gardine, M., Gardine, L., Gately, K., Haeussler, P., Hassan, W., Meyer, F., Richards, C., Ruppert, N. and Tape, C., 2020. The 30 November 2018  $M_w$ 7.1 Anchorage earthquake. *Seismological Research Letters*, 91(1), 66-84.
- Winkler, G. R., & Plafker, G. (1993). Geologic map of the Cordova and Middleton Island quadrangles, Southern Alaska. *U.S. Geological Survey Miscellaneous Investigations Series Map 1984*, 1 sheet, scale 1:250,000.
- Wilson, F. H. (2006). Digital data for the reconnaissance geologic map of the lower Yukon River region, Alaska (geologic map by Patton, W. W., Jr., Wilson, F. H., and Labay, K. A.)—Preliminary integrated geologic map databases for the United States. *U. S. Geological Survey Open-File Report 1292*.
- Wilson, F. H., Hults, C. P., Mull, C. G, & Karl, S. M, compilers, (2015). Geologic map of Alaska. *U.S. Geological Survey Scientific Investigations Map 3340*, pamphlet 196 p., 2 sheets, scale 1:1,584,000, <http://dx.doi.org/10.3133/sim3340>
- Witter, R. C., Bender, A. M., Scharer, K. M., DuRoss, C. B., Haeussler, P. J., & Lease, R. O. (2021). Geomorphic expression and slip rate of the Fairweather fault, southeast Alaska, and evidence for predecessors of the 1958 rupture. *Geosphere*, 17(3), 711–738, <https://doi.org/10.1130/GES02299.1>
- Witter, R. C., Briggs, R. W., Dura, T., Englehart, S. E., Nelson, A., Koehler, R. D., Haeussler, P. J., 2022, Paleoseismological perspectives on megathrust locking, rupture and tsunami hazard in Alaska. *Seismological Research Letters*, 93(2B), 1195-1196, <https://doi.org/10.1785/0220220087>
- Witter, R. C., Kelsey, H.M., Lease, R. O., Bender, A. M., Scharer, K. M., Haeussler, P. J., & Brothers, D. S. (2023, this volume). Transpression along the fastest ocean-continent transform plate boundary causes extreme uplift rates on the Fairweather fault, southeast

- Alaska. In N. A. Ruppert, M. Jadamec, and J. T. Freymueller (Eds.), *Tectonics and seismicity of Alaska and western Canada: Earthscope and beyond*. American Geophysical Union Geophysical Monograph Series (Vol. XXX, pp. XX-XX). Washington, DC: American Geophysical Union
- Worthington, L. L., Daigle, H., Clary, W. A., Gulick, S. P., & Montelli, A. (2018). High sedimentation rates and thrust fault modulation: Insights from ocean drilling offshore the St. Elias Mountains, southern Alaska. *Earth and Planetary Science Letters*, 483, 1-12.
- Worthington, L. L., Gulick, S. P. S., & Pavlis, T. L. (2008). Identifying active structures in the Kayak Island and Pamplona zones: Implications for offshore tectonics of the Yakutat Microplate, Gulf of Alaska. In J. T. Freymueller, P. J. Haeussler, R. L. Wesson, and G. Ekstrom (Eds.), *Active tectonics and seismic potential of Alaska*: American Geophysical Union Geophysical Monograph Series (Vol. 179, pp. 257-268). Washington, DC: American Geophysical Union. doi:10.1029/179GM14.
- Worthington, L. L., Gulick, S. P. S., & Pavlis, T. L. (2010). Coupled stratigraphic and structural evolution of a glaciated orogenic wedge, offshore St. Elias orogen, Alaska. *Tectonics*, 29, TC6013, doi:10.1029/2010TC002723.
- Worthington, L.L., van Avendonk, H. J. A., Gulick, S. P. S., Christeson, G. L., & Pavlis, T. L. (2012). Crustal structure of the Yakutat terrane and the evolution of subduction and collision in southern Alaska. *J. Geophys. Res.*, 117, B01102, doi:10.1029/2011JB008493
- Xu, G., Xu, C., Wen, Y., Xiong, W., & Valkaniotis, S. (2020). The complexity of the 2018 Kaktovik earthquake sequence in the northeast of the Brooks Range, Alaska. *Geophysical Research Letters*, 47(19), e2020GL088012.
- Yue, H., Lay, T., Freymueller, J. T., Ding, K., Rivera, L., Ruppert, N. A., & Koper, K. D. (2013). Supershear rupture of the 5 January 2013 Craig, Alaska (MW 7.5) earthquake. *Journal of Geophysical Research: Solid Earth*, 118(11), 5903-5919
- Yukon Geological Survey (2020). Yukon digital bedrock geology. Yukon Geological Survey, <https://data.geology.gov.yk.ca/Compilation/3> [accessed 25 January 2023].
- Ziwu, F. D., Doser, D. I. and Schinagel, S. M. (2020). A geophysical study of the Castle Mountain Fault, southcentral Alaska. *Tectonophysics*, 789, 228567.